

RD-A140 290

PRESSURE DISTRIBUTION ON MODELS OF THE SL-7  
CONTAINERSHIP AND GREAT LAKES. (U) MICHIGAN UNIV ANN  
ARBOR DEPT OF NAVAL ARCHITECTURE AND MARINE.

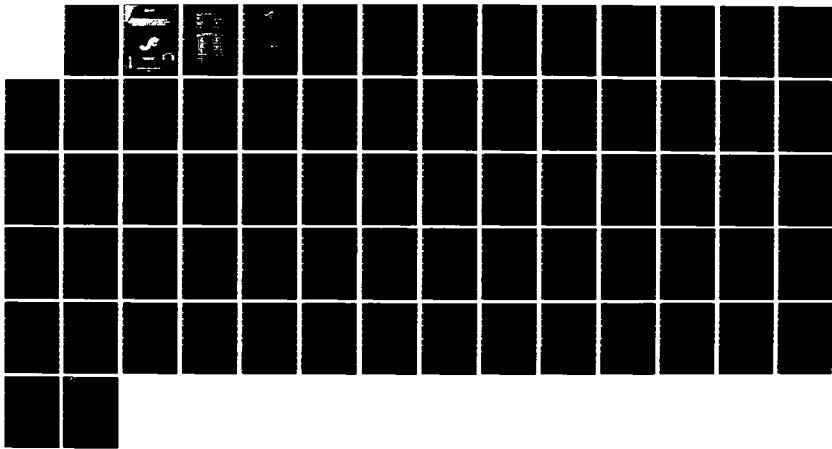
1/1

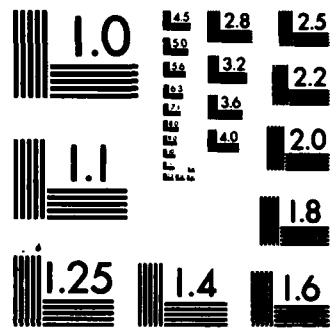
UNCLASSIFIED

A W TROESCH ET AL. 1982 SR-1271 SSC-314

F/G 13/10

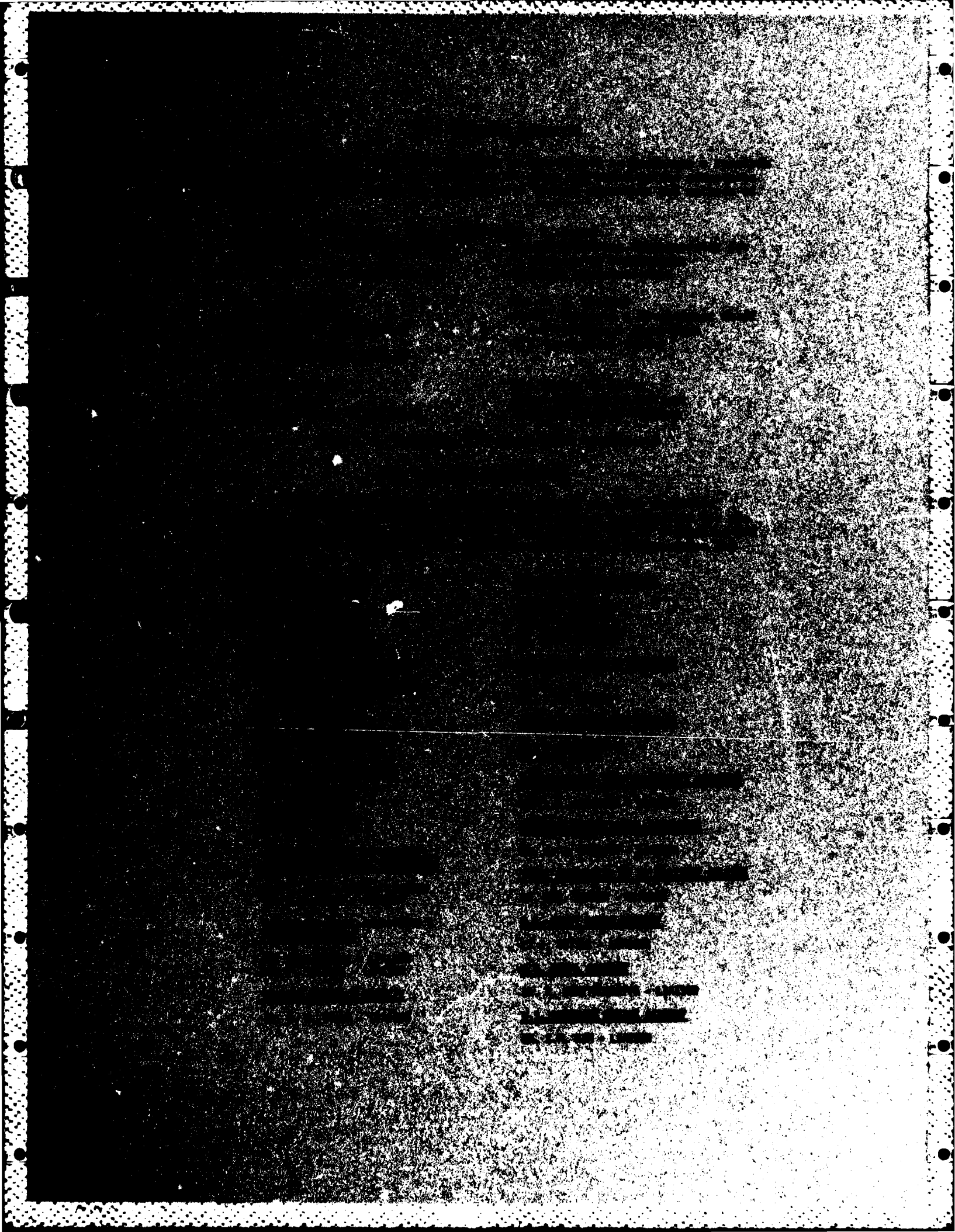
NL





MICROCOPY RESOLUTION TEST CHART  
NATIONAL BUREAU OF STANDARDS-1963-A

ADA140290



Member Agencies:

United States Coast Guard  
Naval Sea Systems Command  
Military Sealift Command  
Maritime Administration  
United States Geological Survey  
American Bureau of Shipping



An Interagency Advisory Committee  
Dedicated to Improving the Structure of Ships

Address Correspondence to:

Secretary, Ship Structure Committee  
U.S. Coast Guard Headquarters, (G-M/TP 13)  
Washington, D.C. 20593

SR-1271

Many Ship Structure Committee programs have dealt with sea loads imposed on the hull girder. However, knowledge of pressures on the hull surface is also needed to determine the required strength of local structures to withstand maximum anticipated pressures in a seaway.

Computer programs for calculating pressure distributions are available. Sea conditions can be simulated in the wave tank. Model motions can be accurately measured and pressure distributions can be simultaneously recorded. The Committee therefore sponsored a model experiment project to gather data for comparison with calculated pressures.

This report presents the model testing results. A report is subsequently being prepared by the American Bureau of Shipping to compare some of these selected test data with their computer results.

  
Clyde T. Lusk Jr.  
Rear Admiral, U.S. Coast Guard  
Chairman, Ship Structure Committee

Accession For	
MFIS	GRA&I
DFIC TAB	<input type="checkbox"/>
Unpublished	<input type="checkbox"/>
Justification	
By	
Distribution	
Availability Copies	
Distr	Aval. &/or Special
A1	



## Technical Report Documentation Page

1. Report No. SSC-314	2. Government Accession No. <i>AD-A140 290</i>	3. Recipient's Catalog No.	
4. Title and Subtitle  Pressure Distribution on Models of the SL-7 Containership and Great Lakes Bulk Carrier S.J. Cort in Waves.		5. Report Date 1982	
6. Performing Organization Code SR-1271		7. Author(s) A.W. Troesch and S. Slocum	
8. Performing Organization Report No.		9. Performing Organization Name and Address  Department of Naval Architecture and Marine Engineering University of Michigan Ann Arbor, MI 48109	
10. Work Unit No. (TRAIS)		11. Contract or Grant No. DOT-CG-91 3367-A	
12. Sponsoring Agency Name and Address  U.S. Department of Transportation United State Coast Guard Office of Research and Development Washington, DC 20590		13. Type of Report and Period Covered  Final Report	
14. Sponsoring Agency Code G-M			
15. Supplementary Notes  This is a Ship Structure Committee sponsored project.			
16. Abstract  Scale models of the SL-7 Containership and Great Lakes bulk carrier S.J. Cort were tested in head seas for a variety of speeds and wave lengths. Both models were free to heave and pitch. Pressures at various locations over the hull were measured and the results presented. The model of the SL-7 was also tested in conditions which measured the separate components of pressure. The diffraction pressures were measured by restraining the model and the radiation pressures were measured by forcing the model to oscillate in heave and pitch.			
17. Key Words  Motions Head Seas Pressures Forced Oscillation Diffraction	18. Distribution Statement  Document is available to the U.S. Public through the National Technical Information Service, Springfield, VA 22161		
19. Security Classif. (of this report)  Unclassified	20. Security Classif. (of this page)  Unclassified	21. No. of Pages 54 + xiii	22. Price

## METRIC CONVERSION FACTORS

### Approximate Conversions to Metric Measures

Symbol	When You Know	Multiply by	To Find	Symbol	When You Know	Multiply by	To Find	Symbol
			<u>LENGTH</u>				<u>LENGTH</u>	
			millimeters	mm			inches	"
			centimeters	cm			inches	"
			meters	m			feet	'
			kilometers	km			yards	'"
							miles	mi
			<u>AREA</u>				<u>AREA</u>	
			square centimeters	cm <sup>2</sup>			square inches	in. <sup>2</sup>
			square meters	m <sup>2</sup>			square yards	yd. <sup>2</sup>
			square kilometers	km <sup>2</sup>			square miles	mi. <sup>2</sup>
							<u>MASS (weight)</u>	
			grams	g			ounces	oz.
			kilograms	kg			pounds	lb.
			tonnes (1,000 kg)	t			short tons	sh.t.
			<u>VOLUME</u>				<u>VOLUME</u>	
			milliliters	ml			fluid ounces	fl.oz.
			liters	l			pints	pt.
			milliliters	ml			quarts	qt.
			liters	l			gallons	gal.
			cubic meters	m <sup>3</sup>			cubic feet	cu. ft.
			cubic meters	m <sup>3</sup>			cubic yards	cu. yd.
			<u>TEMPERATURE (exact)</u>				<u>TEMPERATURE (exact)</u>	
			°C				°C	
			Celsius temperature				Celsius temperature	
			9/5 (times and 32)				9/5 (times and 32)	
			°F				°F	
			32				32	
			°C				°C	
			0				0	
			5/9 (either subtracting 32)				5/9 (either subtracting 32)	
			°F				°F	
			100				100	
			22				22	

\* 1 m = 3.281 ft exactly. For other exact conversions and more detailed tables, see NBS Spec. Publ. C13 (1958).

Units of Weights and Measures, Price \$2.25, 50 Catalog No. C13 (1958).

C O N T E N T S

I.	INTRODUCTION	1
II.	BACKGROUND	2
III.	EXPERIMENTAL APPARATUS AND TECHNIQUES	3
A.	Towing Tank and Wavemaker	3
B.	Forced-Oscillation Mechanism	3
C.	Models	3
D.	Instrumentation	5
1.	Pressure Transducers	5
2.	Heave and Pitch Measurements	5
3.	Wave Probe	5
4.	Data Recording	5
E.	Test Procedure	6
IV.	DATA REDUCTION TECHNIQUES	8
V.	EXPERIMENTAL RESULTS	9
VI.	CONCLUDING REMARKS	12
	ACKNOWLEDGMENTS	13
	REFERENCES	13
	APPENDIX	14

## LIST OF FIGURES

<b>Figure 1:</b>	S.J. Cort Body Plan (with frame numbers)	16
<b>Figure 2:</b>	SL-7 Body Plan (with station numbers)	16
<b>Figure 3:</b>	SL-7 Heave RAO, $F_n=0.15$	17
<b>Figure 4:</b>	SL-7 Heave RAO, $F_n=0.23$	17
<b>Figure 5:</b>	SL-7 Heave RAO, $F_n=0.32$	17
<b>Figure 6:</b>	SL-7 Pitch RAO, $F_n=0.15$	17
<b>Figure 7:</b>	SL-7 Pitch RAO, $F_n=0.23$	17
<b>Figure 8:</b>	SL-7 Pitch RAO, $F_n=0.32$	17
<b>Figure 9:</b>	S.J. Cort Heave RAO, Full Load Condition, $F_n=.100$	18
<b>Figure 10:</b>	S.J. Cort Heave RAO, Full Load Condition, $F_n=.132$	18
<b>Figure 11:</b>	S.J. Cort Heave RAO, Ballast Condition, $F_n=.100$	18
<b>Figure 12:</b>	S.J. Cort Heave RAO, Ballast Condition, $F_n=.132$	18
<b>Figure 13:</b>	S.J. Cort Pitch RAO, Full Load Condition, $F_n=.100$	19
<b>Figure 14:</b>	S.J. Cort Pitch RAO, Full Load Condition, $F_n=.132$	19
<b>Figure 15:</b>	S.J. Cort Pitch RAO, Ballast Condition, $F_n=.100$	19
<b>Figure 16:</b>	S.J. Cort Pitch RAO, Ballast Condition, $F_n=.132$	19
<b>Figure 17:</b>	SL-7 Pressure RAO, $F_n=0.15$ , Tap No. 1	20
<b>Figure 18:</b>	SL-7 Pressure RAO, $F_n=0.15$ , Tap No. 2	20
<b>Figure 19:</b>	SL-7 Pressure RAO, $F_n=0.15$ , Tap No. 3	20
<b>Figure 20:</b>	SL-7 Pressure RAO, $F_n=0.15$ , Tap No. 4	20
<b>Figure 21:</b>	SL-7 Pressure RAO, $F_n=0.15$ , Tap No. 5	20
<b>Figure 22:</b>	SL-7 Pressure RAO, $F_n=0.15$ , Tap No. 6	20
<b>Figure 23:</b>	SL-7 Pressure RAO, $F_n=0.15$ , Tap No. 7	21
<b>Figure 24:</b>	SL-7 Pressure RAO, $F_n=0.15$ , Tap No. 8	21
<b>Figure 25:</b>	SL-7 Pressure RAO, $F_n=0.15$ , Tap No. 9	21
<b>Figure 26:</b>	SL-7 Pressure RAO, $F_n=0.15$ , Tap No. 10	21
<b>Figure 27:</b>	SL-7 Pressure RAO, $F_n=0.15$ , Tap No. 11	21
<b>Figure 28:</b>	SL-7 Pressure RAO, $F_n=0.15$ , Tap No. 12	21
<b>Figure 29:</b>	SL-7 Pressure RAO, $F_n=0.15$ , Tap No. 13	22
<b>Figure 30:</b>	SL-7 Pressure RAO, $F_n=0.15$ , Tap No. 14	22
<b>Figure 31:</b>	SL-7 Pressure RAO, $F_n=0.15$ , Tap No. 15	22
<b>Figure 32:</b>	SL-7 Pressure RAO, $F_n=0.15$ , Tap No. 16	22
<b>Figure 33:</b>	SL-7 Pressure RAO, $F_n=0.15$ , Tap No. 17	22
<b>Figure 34:</b>	SL-7 Pressure RAO, $F_n=0.15$ , Tap No. 18	22
<b>Figure 35:</b>	SL-7 Pressure RAO, $F_n=0.15$ , Tap No. 19	23

Figure 36:	SL-7 Pressure RAO, $F_n=0.15$ , Tap No. 20	23
Figure 37:	SL-7 Pressure RAO, $F_n=0.15$ , Tap No. 21	23
Figure 38:	SL-7 Pressure RAO, $F_n=0.15$ , Tap No. 22	23
Figure 39:	SL-7 Pressure RAO, $F_n=0.15$ , Tap No. 23	23
Figure 40:	SL-7 Pressure RAO, $F_n=0.15$ , Tap No. 24	23
Figure 41:	SL-7 Pressure RAO, $F_n=0.15$ , Tap No. 25	24
Figure 42:	SL-7 Pressure RAO, $F_n=0.15$ , Tap No. 26	24
Figure 43:	SL-7 Pressure RAO, $F_n=0.23$ , Tap No. 1	24
Figure 44:	SL-7 Pressure RAO, $F_n=0.23$ , Tap No. 2	24
Figure 45:	SL-7 Pressure RAO, $F_n=0.23$ , Tap No. 3	24
Figure 46:	SL-7 Pressure RAO, $F_n=0.23$ , Tap No. 4	24
Figure 47:	SL-7 Pressure RAO, $F_n=0.23$ , Tap No. 5	25
Figure 48:	SL-7 Pressure RAO, $F_n=0.23$ , Tap No. 6	25
Figure 49:	SL-7 Pressure RAO, $F_n=0.23$ , Tap No. 7	25
Figure 50:	SL-7 Pressure RAO, $F_n=0.23$ , Tap No. 8	25
Figure 51:	SL-7 Pressure RAO, $F_n=0.23$ , Tap No. 9	25
Figure 52:	SL-7 Pressure RAO, $F_n=0.23$ , Tap No. 10	25
Figure 53:	SL-7 Pressure RAO, $F_n=0.23$ , Tap No. 11	26
Figure 54:	SL-7 Pressure RAO, $F_n=0.23$ , Tap No. 12	26
Figure 55:	SL-7 Pressure RAO, $F_n=0.23$ , Tap No. 13	26
Figure 56:	SL-7 Pressure RAO, $F_n=0.23$ , Tap No. 14	26
Figure 57:	SL-7 Pressure RAO, $F_n=0.23$ , Tap No. 15	26
Figure 58:	SL-7 Pressure RAO, $F_n=0.23$ , Tap No. 16	26
Figure 59:	SL-7 Pressure RAO, $F_n=0.23$ , Tap No. 17	27
Figure 60:	SL-7 Pressure RAO, $F_n=0.23$ , Tap No. 18	27
Figure 61:	SL-7 Pressure RAO, $F_n=0.23$ , Tap No. 19	27
Figure 62:	SL-7 Pressure RAO, $F_n=0.23$ , Tap No. 20	27
Figure 63:	SL-7 Pressure RAO, $F_n=0.23$ , Tap No. 21	27
Figure 64:	SL-7 Pressure RAO, $F_n=0.23$ , Tap No. 22	27
Figure 65:	SL-7 Pressure RAO, $F_n=0.23$ , Tap No. 23	28
Figure 66:	SL-7 Pressure RAO, $F_n=0.23$ , Tap No. 24	28
Figure 67:	SL-7 Pressure RAO, $F_n=0.23$ , Tap No. 25	28
Figure 68:	SL-7 Pressure RAO, $F_n=0.23$ , Tap No. 26	28
Figure 69:	SL-7 Pressure RAO, $F_n=0.32$ , Tap No. 1	29
Figure 70:	SL-7 Pressure RAO, $F_n=0.32$ , Tap No. 2	29
Figure 71:	SL-7 Pressure RAO, $F_n=0.32$ , Tap No. 3	29

<b>Figure 72:</b>	SL-7 Pressure RAO, $F_n=0.32$ , Tap No. 4	29
<b>Figure 73:</b>	SL-7 Pressure RAO, $F_n=0.32$ , Tap No. 5	29
<b>Figure 74:</b>	SL-7 Pressure RAO, $F_n=0.32$ , Tap No. 6	29
<b>Figure 75:</b>	SL-7 Pressure RAO, $F_n=0.32$ , Tap No. 7	30
<b>Figure 76:</b>	SL-7 Pressure RAO, $F_n=0.32$ , Tap No. 8	30
<b>Figure 77:</b>	SL-7 Pressure RAO, $F_n=0.32$ , Tap No. 9	30
<b>Figure 78:</b>	SL-7 Pressure RAO, $F_n=0.32$ , Tap No. 10	30
<b>Figure 79:</b>	SL-7 Pressure RAO, $F_n=0.32$ , Tap No. 11	30
<b>Figure 80:</b>	SL-7 Pressure RAO, $F_n=0.32$ , Tap No. 12	30
<b>Figure 81:</b>	SL-7 Pressure RAO, $F_n=0.32$ , Tap No. 13	31
<b>Figure 82:</b>	SL-7 Pressure RAO, $F_n=0.32$ , Tap No. 14	31
<b>Figure 83:</b>	SL-7 Pressure RAO, $F_n=0.32$ , Tap No. 15	31
<b>Figure 84:</b>	SL-7 Pressure RAO, $F_n=0.32$ , Tap No. 16	31
<b>Figure 85:</b>	SL-7 Pressure RAO, $F_n=0.32$ , Tap No. 17	31
<b>Figure 86:</b>	SL-7 Pressure RAO, $F_n=0.32$ , Tap No. 18	31
<b>Figure 87:</b>	SL-7 Pressure RAO, $F_n=0.32$ , Tap No. 19	32
<b>Figure 88:</b>	SL-7 Pressure RAO, $F_n=0.32$ , Tap No. 20	32
<b>Figure 89:</b>	SL-7 Pressure RAO, $F_n=0.32$ , Tap No. 21	32
<b>Figure 90:</b>	SL-7 Pressure RAO, $F_n=0.32$ , Tap No. 22	32
<b>Figure 91:</b>	SL-7 Pressure RAO, $F_n=0.32$ , Tap No. 23	32
<b>Figure 92:</b>	SL-7 Pressure RAO, $F_n=0.32$ , Tap No. 24	32
<b>Figure 93:</b>	SL-7 Pressure RAO, $F_n=0.32$ , Tap No. 25	33
<b>Figure 94:</b>	SL-7 Pressure RAO, $F_n=0.32$ , Tap No. 26	33
<b>Figure 95:</b>	S.J. Cort Pressure RAO, Full Load Condition, $F_n=.100$ , Tap No. 1	33
<b>Figure 96:</b>	S.J. Cort Pressure RAO, Full Load Condition, $F_n=.100$ , Tap No. 2	33
<b>Figure 97:</b>	S.J. Cort Pressure RAO, Full Load Condition, $F_n=.100$ , Tap No. 3	33
<b>Figure 98:</b>	S.J. Cort Pressure RAO, Full Load Condition, $F_n=.100$ , Tap No. 4	33
<b>Figure 99:</b>	S.J. Cort Pressure RAO, Full Load Condition, $F_n=.100$ , Tap No. 5	34
<b>Figure 100:</b>	S.J. Cort Pressure RAO, Full Load Condition, $F_n=.100$ , Tap No. 6	34
<b>Figure 101:</b>	S.J. Cort Pressure RAO, Full Load Condition, $F_n=.100$ , Tap No. 7	34
<b>Figure 102:</b>	S.J. Cort Pressure RAO, Full Load Condition, $F_n=.100$ , Tap No. 8	34
<b>Figure 103:</b>	S.J. Cort Pressure RAO, Full Load Condition, $F_n=.100$ , Tap No. 9	34

<b>Figure 104:</b>	S.J. Cort Pressure RAO, Full Load Condition, $F_n = .100$ , Tap No. 10	34
<b>Figure 105:</b>	S.J. Cort Pressure RAO, Full Load Condition, $F_n = .100$ , Tap No. 11	35
<b>Figure 106:</b>	S.J. Cort Pressure RAO, Full Load Condition, $F_n = .100$ , Tap No. 12	35
<b>Figure 107:</b>	S.J. Cort Pressure RAO, Full Load Condition, $F_n = .100$ , Tap No. 13	35
<b>Figure 108:</b>	S.J. Cort Pressure RAO, Full Load Condition, $F_n = .100$ , Tap No. 14	35
<b>Figure 109:</b>	S.J. Cort Pressure RAO, Full Load Condition, $F_n = .100$ , Tap No. 15	35
<b>Figure 110:</b>	S.J. Cort Pressure RAO, Full Load Condition, $F_n = .100$ , Tap No. 16	35
<b>Figure 111:</b>	S.J. Cort Pressure RAO, Full Load Condition, $F_n = .100$ , Tap No. 17	36
<b>Figure 112:</b>	S.J. Cort Pressure RAO, Full Load Condition, $F_n = .100$ , Tap No. 18	36
<b>Figure 113:</b>	S.J. Cort Pressure RAO, Full Load Condition, $F_n = .100$ , Tap No. 19	36
<b>Figure 114:</b>	S.J. Cort Pressure RAO, Full Load Condition, $F_n = .100$ , Tap No. 20	36
<b>Figure 115:</b>	S.J. Cort Pressure RAO, Full Load Condition, $F_n = .100$ , Tap No. 21	36
<b>Figure 116:</b>	S.J. Cort Pressure RAO, Full Load Condition, $F_n = .100$ , Tap No. 22	36
<b>Figure 117:</b>	S.J. Cort Pressure RAO, Full Load Condition, $F_n = .100$ , Tap No. 23	37
<b>Figure 118:</b>	S.J. Cort Pressure RAO, Full Load Condition, $F_n = .100$ , Tap No. 24	37
<b>Figure 119:</b>	S.J. Cort Pressure RAO, Full Load Condition, $F_n = .132$ , Tap No. 1	37
<b>Figure 120:</b>	S.J. Cort Pressure RAO, Full Load Condition, $F_n = .132$ , Tap No. 2	37
<b>Figure 121:</b>	S.J. Cort Pressure RAO, Full Load Condition, $F_n = .132$ , Tap No. 3	37
<b>Figure 122:</b>	S.J. Cort Pressure RAO, Full Load Condition, $F_n = .132$ , Tap No. 4	37
<b>Figure 123:</b>	S.J. Cort Pressure RAO, Full Load Condition, $F_n = .132$ , Tap No. 5	38
<b>Figure 124:</b>	S.J. Cort Pressure RAO, Full Load Condition, $F_n = .132$ , Tap No. 6	38
<b>Figure 125:</b>	S.J. Cort Pressure RAO, Full Load Condition, $F_n = .132$ , Tap No. 7	38
<b>Figure 126:</b>	S.J. Cort Pressure RAO, Full Load Condition, $F_n = .132$ , Tap No. 8	38
<b>Figure 127:</b>	S.J. Cort Pressure RAO, Full Load Condition, $F_n = .132$ , Tap No. 9	38

Figure 128:	S.J. Cort Pressure RAO, Full Load Condition, $F_n = .132$ , Tap No. 10	38
Figure 129:	S.J. Cort Pressure RAO, Full Load Condition, $F_n = .132$ , Tap No. 11	39
Figure 130:	S.J. Cort Pressure RAO, Full Load Condition, $F_n = .132$ , Tap No. 12	39
Figure 131:	S.J. Cort Pressure RAO, Full Load Condition, $F_n = .132$ , Tap No. 13	39
Figure 132:	S.J. Cort Pressure RAO, Full Load Condition, $F_n = .132$ , Tap No. 14	39
Figure 133:	S.J. Cort Pressure RAO, Full Load Condition, $F_n = .132$ , Tap No. 15	39
Figure 134:	S.J. Cort Pressure RAO, Full Load Condition, $F_n = .132$ , Tap No. 16	39
Figure 135:	S.J. Cort Pressure RAO, Full Load Condition, $F_n = .132$ , Tap No. 17	40
Figure 136:	S.J. Cort Pressure RAO, Full Load Condition, $F_n = .132$ , Tap No. 18	40
Figure 137:	S.J. Cort Pressure RAO, Full Load Condition, $F_n = .132$ , Tap No. 19	40
Figure 138:	S.J. Cort Pressure RAO, Full Load Condition, $F_n = .132$ , Tap No. 20	40
Figure 139:	S.J. Cort Pressure RAO, Full Load Condition, $F_n = .132$ , Tap No. 21	40
Figure 140:	S.J. Cort Pressure RAO, Full Load Condition, $F_n = .132$ , Tap No. 22	40
Figure 141:	S.J. Cort Pressure RAO, Full Load Condition, $F_n = .132$ , Tap No. 23	41
Figure 142:	S.J. Cort Pressure RAO, Full Load Condition, $F_n = .132$ , Tap No. 24	41
Figure 143:	S.J. Cort Pressure RAO, Ballast Condition, $F_n = .100$ , Tap No. 1	41
Figure 144:	S.J. Cort Pressure RAO, Ballast Condition, $F_n = .100$ , Tap No. 4	41
Figure 145:	S.J. Cort Pressure RAO, Ballast Condition, $F_n = .100$ , Tap No. 8	41
Figure 146:	S.J. Cort Pressure RAO, Ballast Condition, $F_n = .100$ , Tap No. 12	41
Figure 147:	S.J. Cort Pressure RAO, Ballast Condition, $F_n = .100$ , Tap No. 13	42
Figure 148:	S.J. Cort Pressure RAO, Ballast Condition, $F_n = .100$ , Tap No. 14	42
Figure 149:	S.J. Cort Pressure RAO, Ballast Condition, $F_n = .100$ , Tap No. 17	42
Figure 150:	S.J. Cort Pressure RAO, Ballast Condition, $F_n = .100$ , Tap No. 18	42
Figure 151:	S.J. Cort Pressure RAO, Ballast Condition, $F_n = .100$ , Tap No. 21	42

<b>Figure 152:</b>	S.J. Cort Pressure RAO, Ballast Condition, $F_n=.100$ , Tap No. 22	42
<b>Figure 153:</b>	S.J. Cort Pressure RAO, Ballast Condition, $F_n=.132$ , Tap No. 1	43
<b>Figure 154:</b>	S.J. Cort Pressure RAO, Ballast Condition, $F_n=.132$ , Tap No. 4	43
<b>Figure 155:</b>	S.J. Cort Pressure RAO, Ballast Condition, $F_n=.132$ , Tap No. 8	43
<b>Figure 156:</b>	S.J. Cort Pressure RAO, Ballast Condition, $F_n=.132$ , Tap No. 12	43
<b>Figure 157:</b>	S.J. Cort Pressure RAO, Ballast Condition, $F_n=.132$ , Tap No. 13	43
<b>Figure 158:</b>	S.J. Cort Pressure RAO, Ballast Condition, $F_n=.132$ , Tap No. 14	43
<b>Figure 159:</b>	S.J. Cort Pressure RAO, Ballast Condition, $F_n=.132$ , Tap No. 17	44
<b>Figure 160:</b>	S.J. Cort Pressure RAO, Ballast Condition, $F_n=.132$ , Tap No. 18	44
<b>Figure 161:</b>	S.J. Cort Pressure RAO, Ballast Condition, $F_n=.132$ , Tap No. 21	44
<b>Figure 162:</b>	S.J. Cort Pressure RAO, Ballast Condition, $F_n=.132$ , Tap No. 22	44
<b>Figure 163:</b>	SL-7 Pressure RAO, Restrained from motion, $F_n=0.23$ , Tap No. 1	44
<b>Figure 164:</b>	SL-7 Pressure RAO, Restrained from motion, $F_n=0.23$ , Tap No. 2	44
<b>Figure 165:</b>	SL-7 Pressure RAO, Restrained from motion, $F_n=0.23$ , Tap No. 3	45
<b>Figure 166:</b>	SL-7 Pressure RAO, Restrained from motion, $F_n=0.23$ , Tap No. 4	45
<b>Figure 167:</b>	SL-7 Pressure RAO, Restrained from motion, $F_n=0.23$ , Tap No. 6	45
<b>Figure 168:</b>	SL-7 Pressure RAO, Restrained from motion, $F_n=0.23$ , Tap No. 7	45
<b>Figure 169:</b>	SL-7 Pressure RAO, Restrained from motion, $F_n=0.23$ , Tap No. 8	45
<b>Figure 170:</b>	SL-7 Pressure RAO, Restrained from motion, $F_n=0.23$ , Tap No. 9	45
<b>Figure 171:</b>	SL-7 Pressure RAO, Restrained from motion, $F_n=0.23$ , Tap No. 10	46
<b>Figure 172:</b>	SL-7 Pressure RAO, Restrained from motion, $F_n=0.23$ , Tap No. 11	46
<b>Figure 173:</b>	SL-7 Pressure RAO, Restrained from motion, $F_n=0.23$ , Tap No. 12	46
<b>Figure 174:</b>	SL-7 Pressure RAO, Restrained from motion, $F_n=0.23$ , Tap No. 13	46
<b>Figure 175:</b>	SL-7 Pressure RAO, Restrained from motion, $F_n=0.23$ , Tap No. 14	46

Figure 176:	SL-7 Pressure RAO, Restrained from motion, $F_n=0.23$ , Tap No. 19	46
Figure 177:	SL-7 Pressure RAO, Restrained from motion, $F_n=0.23$ , Tap No. 21	47
Figure 178:	SL-7 Pressure RAO, Forced Heave motion, $F_n=0.23$ , Tap No. 2	47
Figure 179:	SL-7 Pressure RAO, Forced Heave motion, $F_n=0.23$ , Tap No. 3	47
Figure 180:	SL-7 Pressure RAO, Forced Heave motion, $F_n=0.23$ , Tap No. 4	47
Figure 181:	SL-7 Pressure RAO, Forced Heave motion, $F_n=0.23$ , Tap No. 6	47
Figure 182:	SL-7 Pressure RAO, Forced Heave motion, $F_n=0.23$ , Tap No. 7	47
Figure 183:	SL-7 Pressure RAO, Forced Heave motion, $F_n=0.23$ , Tap No. 9	48
Figure 184:	SL-7 Pressure RAO, Forced Heave motion, $F_n=0.23$ , Tap No. 10	48
Figure 185:	SL-7 Pressure RAO, Forced Heave motion, $F_n=0.23$ , Tap No. 11	48
Figure 186:	SL-7 Pressure RAO, Forced Heave motion, $F_n=0.23$ , Tap No. 12	48
Figure 187:	SL-7 Pressure RAO, Forced Heave motion, $F_n=0.23$ , Tap No. 14	48
Figure 188:	SL-7 Pressure RAO, Forced Heave motion, $F_n=0.23$ , Tap No. 19	48
Figure 189:	SL-7 Pressure RAO, Forced Pitch Motion, $F_n=0.23$ , Tap No. 1	49
Figure 190:	SL-7 Pressure RAO, Forced Pitch Motion, $F_n=0.23$ , Tap No. 2	49
Figure 191:	SL-7 Pressure RAO, Forced Pitch Motion, $F_n=0.23$ , Tap No. 3	49
Figure 192:	SL-7 Pressure RAO, Forced Pitch Motion, $F_n=0.23$ , Tap No. 4	49
Figure 193:	SL-7 Pressure RAO, Forced Pitch Motion, $F_n=0.23$ , Tap No. 6	49
Figure 194:	SL-7 Pressure RAO, Forced Pitch Motion, $F_n=0.23$ , Tap No. 7	49
Figure 195:	SL-7 Pressure RAO, Forced Pitch Motion, $F_n=0.23$ , Tap No. 9	50
Figure 196:	SL-7 Pressure RAO, Forced Pitch Motion, $F_n=0.23$ , Tap No. 11	50
Figure 197:	SL-7 Pressure RAO, Forced Pitch Motion, $F_n=0.23$ , Tap No. 12	50
Figure 198:	SL-7 Pressure RAO, Forced Pitch Motion, $F_n=0.23$ , Tap No. 14	50
Figure 199:	SL-7 Pressure RAO, Forced Pitch Motion, $F_n=0.23$ , Tap No. 19	50

<b>Figure 200:</b>	<b>SL-7 Pressure RAO, Forced Pitch Motion, <math>F_n=0.23</math>, Tap No. 21</b>	<b>50</b>
<b>Figure 201:</b>	<b>SL-7 Linearity Check, Pressure RAO, <math>F_n=0.23</math>, Tap No. 8</b>	<b>51</b>
<b>Figure 202:</b>	<b>SL-7 Linearity Check, Pressure RAO, <math>F_n=0.23</math>, Tap No. 14</b>	<b>51</b>
<b>Figure 203:</b>	<b>SL-7 Linearity Check, Pressure RAO, <math>F_n=0.23</math>, Tap No. 18</b>	<b>51</b>
<b>Figure 204:</b>	<b>SL-7 Linearity Check, Pressure RAO, <math>F_n=0.23</math>, Tap No. 24</b>	<b>51</b>
<b>Figure 205:</b>	<b>S.J. Cort Linearity Check, Pressure RAO, <math>F_n=.132</math>, Tap No. 1</b>	<b>52</b>
<b>Figure 206:</b>	<b>S.J. Cort Linearity Check, Pressure RAO, <math>F_n=.132</math>, Tap No. 4</b>	<b>52</b>
<b>Figure 207:</b>	<b>S.J. Cort Linearity Check, Pressure RAO, <math>F_n=.132</math>, Tap No. 10</b>	<b>52</b>
<b>Figure 208:</b>	<b>S.J. Cort Linearity Check, Pressure RAO, <math>F_n=.132</math>, Tap No. 16</b>	<b>52</b>
<b>Figure 209:</b>	<b>Pressure Tap Locations on SL-7 (Forebody)</b>	<b>53</b>
<b>Figure 210:</b>	<b>Pressure Tap Locations on SL-7 (Afterbody)</b>	<b>53</b>
<b>Figure 211:</b>	<b>Pressure Tap Locations on S.J. Cort (Forebody)</b>	<b>54</b>
<b>Figure 212:</b>	<b>Pressure Tap Locations on S.J. Cort (Afterbody)</b>	<b>54</b>

## I. INTRODUCTION

The prediction of the total dynamic pressure acting on the hull of a ship operating in waves is of practical importance in the design of ship structures and, by extension, in the setting of design standards and rules for building and classification. Local dynamic pressures on a ship's hull in waves can far exceed the static head. As a result, these loads can determine the safety of the hull against local plating damage, or failure of shell panels between web frames. Ultimately, rational structural design and effective design rules should include an accurate estimation of the dynamic pressure at various locations on the ship's hull.

This report deals with the results of an experimental study of dynamic pressures. The principal task of the work described here was to obtain experimental pressure data from model tests on two vessels, namely, the SL-7 class containership, and the Great Lakes self-unloader Stewart J. Cort.

## II. BACKGROUND

Generally, the total pressure acting at any point on the hull of a ship moving through waves may be attributed to a number of components. Under a linear hypothesis, the following components are assumed to be additive:

1. Static head.
2. Pressure due to steady forward motion.
3. Pressures due to the incident and diffracted waves.
4. Pressure due to the vessel's motions in response to the waves.

In the experiments described here, measurements were confined to the time-dependent components of pressure, namely, the latter two components listed above. (The last component, the pressure due to the resultant motions, normally include slamming and impact pressures. These often are substantial. However, for the tests described in this report, the motions were purposely kept small so that the results could be compared with linear theory predictions.)

It is possible, of course, to measure the total pressure in a single experiment, by running the model in waves, free to heave and pitch. In fact, this straightforward procedure allows the most direct comparison with certain computed results. It also permits direct comparison with full-scale experimental data, if this is available. This particular configuration, where the model is free to heave and pitch, accounted for approximately 80% of the test runs described in this report.

For purposes of developing predictive techniques that would be useful for design standards over a wider range of vessel types, speeds, and hull forms, it might be most valuable to separate the components of dynamic pressure at the experimental level. In this way, the separate components could be estimated for a particular location on the hull, and for a particular wave-length and amplitude, and then added according to linear theory. Static head, of course, is calculated trivially, while the steady dynamic pressure due to forward speed can be estimated using slender-body theory. In general, however, these steady components are smaller than the time-dependent pressures. Pressures due to the incident and diffracted waves can be independently addressed by using such methods as described by Faltinsen (1971), Troesch (1976), and Beck and Troesch (1980).

Finally, with relevant information on ship motions, together with experimental determinations of pressure distributions resulting from forced motions in the absence of incident waves, the components of dynamic pressure due to heave and pitch could be estimated.

A limited number of tests were conducted using the SL-7 model with the primary goal being to investigate the different parts of the time-dependent pressure. Typical experiments aimed at separating the components of total dynamic pressure can be briefly summarized as follows:

1. Pressures due to the incident and diffracted waves can be measured by holding the model fixed in both heave and pitch while operating in waves. Ideally, this experiment can be performed over a range of heading angles, frequencies, and speeds (including zero speed). In the case of experiments conducted in a normal towing tank, however, the experiment is limited for practical reasons to the consideration of head seas with some minimum forward speed necessitated by the desire to avoid tank reflections. Such a test, with the model restrained from heave and pitch, is commonly referred to as the "diffraction" or "scattering" experiment.

2. The pressure component arising from ship motions can be separately investigated by forcibly oscillating the model in either heave or pitch while running at steady forward speed in the absence of incident waves. This procedure, in which the only waves present are those radiated by the oscillating ship, is usually referred to as a "forced oscillation" or, more informally, a "shaker" test.

Experiments of both these types, together with tests of the model free to heave and pitch with incident waves, in head seas, have been conducted in the course of this work. These test techniques have been used successfully in the past, principally by Japanese researchers, as described in Fujii and Takahashi (1974), Nakamura, Saito, and Asai (1974), and Matsuyama (1975). Abstracts of these Japanese works are included in an appendix. The work reported here constitutes an extension of these methods to higher Froude numbers (in the case of the SL-7), and to higher values of ship length/wave length and block coefficient (for the Cort).

As a secondary objective of this work, consideration was given to the need for further experimental work aimed at extending these methods to oblique seas. To a certain extent, this work has already been done. A comparison between theoretical predictions and experimental results for oblique seas, drawn from Japanese work, is presented in Matseyama (1975), Sugai, et. al. (1972), and Caretti (1980). Summaries of these and other relevant works are included in the Appendix. The next sections deal primarily with the experimental apparatus, test procedures, data-reduction techniques, and results of the head-sea, diffraction, and forced-oscillation test conducted in the tank.

### III. EXPERIMENTAL APPARATUS AND TECHNIQUES

#### A. Towing Tank and Wavemaker

The University of Michigan Department of Naval Architecture and Marine Engineering maintains a towing tank of 190.7m (360 ft) in length, approximately 6.7m (22 ft) wide at the normal waterline, and 4.3m (14 ft) deep. The towing carriage is capable of speeds up to 4.88m (16 ft/sec), and models up to 9.1m (30 ft) in length have been tested.

A vertically oscillating wedge-shaped steel tank is installed as a wavemaker. It is hydraulically actuated, and gives acceptably linear response over a wavelength band from 0.9 to 5.5m (3 to 18 ft), with wave heights up to approximately 0.15m (0.5 ft), depending somewhat on the wavelength involved. Input to the hydraulic control system is from an oscillator, for nominally sinusoidal regular waves. Alternatively, random waves can be generated using prerecorded input derived from a given sea spectrum. In the tests described here, regular seas were generated.

#### B. Forced-Oscillation Mechanism

The forced-oscillation device was developed in connection with recent ABS-supported experimental work. The device is capable of forcing oscillation in either pitch or heave. The mechanism is electrically actuated, with frequency controlled by varying the speed of the electric drive. The amplitude of the impressed motion could be varied by discrete increments, using a scotch yoke mechanism.

#### C. Models

The models used in this study were those of the SL-7 class containership and the Great Lakes bulk carrier Stewart J. Cort. These vessels represent almost diametrically opposite combinations of hull-form characteristics and speed. Dimensions, weights, hull-form coefficients, and pitch gyradii for the two ships and their models are shown in Tables I and II for the SL-7 and Cort, respectively. Body plans of the two ships are shown in Figs. 1 and 2. The frame spacing of the Cort is listed in Table III.

TABLE I: SL-7 Hull Particulars

	<u>SHIP</u>	<u>MODEL</u>
LOA m(ft)	288.5(946.6)	3.607(11.83)
LBP m(ft)	268.4(880.5)	3.355(11.01)
Beam m(ft)	32.16(105.5)	0.402(1.319)
Draft @ LCF m(ft)	9.94(32.6)	0.124(.408)
Trim by stern mm(ft)	43.0(0.14)	0.53(0.0018)
LCG Aft of % m(ft)	11.7(38.4)	0.146(.480)
Displacement MT(LT)	48364(47500)	0.0945(.0928)
Pitch Radius of Gyration	0.21 LBP	0.21 LBP

TABLE II: S.J. CORT Hull Particulars

	<u>SHIP</u>	
	<u>FULL LOAD</u>	<u>LIGHT BALLAST</u>
LOA m(ft)	304.8 (1000)	304.8 (1000)
LBP m(ft)	301.4 (989)	301.4 (989)
Beam m(ft)	31.9 (104.6)	31.9 (104.6)
Displacement MT(LT)	69,500(68,259)	38,981(38,285)
LCG( <del>X</del> @ LOA/2)m(ft)	1.4.9(4.9)fwd <del>X</del>	12.7(41.8)aft <del>X</del>
Draft (@ <del>X</del> ) m(ft)	7.85(25.75)	4.52(14.82)
Trim m(ft)	0.0	3.5(11.4) by stern
Pitch Radius of Gyration	0.249 LOA	0.266 LOA

	<u>MODEL</u>	
	<u>FULL LOAD</u>	<u>LIGHT BALLAST</u>
LOA m(ft)	4.57 (15.00)	4.57 (15.00)
LBP m(ft)	4.52 (14.83)	4.52 (14.83)
Beam m(ft)	0.478 (1.57)	0.478 (1.57)
Displacement MT(LT)	0.2346(.2304)	0.1316(.1292)
LCG( <del>X</del> @ LOA/2) m(ft)	0.022(0.074)fwd <del>X</del>	0.191(0.627)aft <del>X</del>
Draft (@ <del>X</del> ) m(ft)	0.188(0.386)	0.068(0.222)
Trim m(ft)	0.0	0.052(0.171) by stern
Pitch Radius of Gyration	0.249 LOA	0.266 LOA

TABLE III: S.J. CORT Frame Spacing

<u>FRAMES</u>	<u>SPACING m(ft)</u>
FWD Stem to Station 0	0.610 (2.0)
FP(0) - 13	0.610 (2.0)
13 - 18	0.914 (3.0)
18 - 20	1.067 (3.5)
20 - 21	1.219 (4.0)
21 - 128	2.438 (8.0)
128 - 129	1.219 (4.0)
129 - 153	0.914 (3.0)
153 - 154	0.762 (2.5)
154 - 159	0.610 (2.0)
159 - 160 (Transom)	0.457 (1.5)
AP is at Fr. 155	

Pressure tap locations for the SL-7 and Cort models are given in Tables IV and V, respectively. Invoking the symmetry associated with the hull form and head sea conditions, pressure tap locations were not duplicated on both sides; 26 taps were fitted on the SL-7 model, 24 on the Cort.

#### D. Instrumentation

##### 1. Pressure Transducers

Normally, on each run only 6 to 8 of the available pressure taps were active. This limitation was imposed by the number of available channels for data recording and the number of working pressure transducers. As a result, each speed and wave length condition was repeated three times in order to get a complete set of data from all taps. The pressure transducers were of the standard semi-conductor type, Kulite Semi-conductor model XCS-190. The pressure tap diaphragm diameter was 3.86 mm (0.152 in). Signal conditioning of the pressure tap output was performed by Honeywell Accudata 218 gauge/control amplifiers.

##### 2. Heave and Pitch Measurements

For the free running tests, the heave displacement was measured by a linear voltage differential transformer (LVDT) attached to the heave staff. The pitch rotation was measured by a rotary VDT at the model attachment point. For the forced-oscillation tests, both heave and pitch were measured by LVDT's attached to the driving mechanism.

##### 3. Wave Probe

A sonic wave probe, Wesmar Ultrasonic Level Monitor Model LM 4000, was fitted under the forward end of the towing carriage, approximately 1.83 m (6 ft) ahead of the model.

##### 4. Data Recording

An analog tape recording system (Honeywell 5600 C) was fitted on the towing carriage for these tests. For free heave and pitch tests, the data channels re-

**TABLE IV: Pressure Tap Locations on SL-7**  
(Dimensions are for full-scale)  
(See Figures 209 and 210)

<u>Tap No.</u>	<u>Station (Sta. 20 = FP)</u>	<u>WL m(ft) (Dist. above B)</u>	<u>Butt m(ft) (Dist. off C)</u>
1	18	0.0	0.0
2	17	0.0	0.0
3	16	0.0	0.0
4	15	0.0	0.0
5	15	2.03(6.67)	-
6	15	4.07(13.37)	-
7	15	7.11(23.33)	-
8	14	0.0	0.0
9	14	4.07(13.33)	-
10	13	0.0	0.0
11	13	1.00(3.30)	-
12	13	4.06(13.33)	-
13	13	7.11(23.33)	-
14	12	0.0	0.0
15	10	0.0	0.0
16	10	-	8.12(26.67)
17	10	4.06(13.33)	-
18	10	7.11(23.33)	-
19	7	0.0	0.0
20	7	4.06(13.33)	-
21	5	0.0	0.0
22	5	-	8.12(26.67)
23	5	4.06(13.33)	-
24	5	7.11(23.33)	-
25	3	0.0	0.0
26	3	4.06(13.33)	-

corded included heave, pitch, incident wave, and a maximum of 7 pressure readings. For diffraction tests, only the incident wave was required, leaving 8 channels free for pressure records. Similarly, in the forced-oscillation tests, the impressed motion was recorded, leaving 8 channels for pressure.

In addition to the analog tape, oscilloscope displays of all recorded tracks and a strip chart of the incident wave were taken during each run in order to facilitate preliminary analysis of the data, spot experimental or system problems, and provide guidance for further runs.

#### E. Test Procedure

Each run consisted of three phases: a mechanical calibration, voltage calibration, and the actual wave, pressure and motion responses. In the mechanical calibration, the model was displaced vertically by 2.54 cm (1 in). This displacement provided output calibration signals for both the pressure transducers and the LVDT's. For free running tests the model was also trimmed 5.08 cm (2 in) to calibrate the RVDT.

Table V: Pressure Tap Locations of S.J. CORT  
 (Dimensions are for full scale)  
 (See Figures 211 and 212)

<u>Tap No.</u>	<u>Longitudinal Location m(ft) (Dist. aft F.P.)</u>	<u>WL m(ft) (Dist. above B)</u>	<u>Butt. m(ft) (Dist. off C)</u>
1	6.1(20)	0.0	0.0
2	6.1(20)	2.49(8.16)	-
3	6.1(20)	5.50(18.06)	-
4	14.6(48)	0.0	0.0
5	14.6(48)	0.0	7.42(24.33)
6	14.6(48)	2.49(8.16)	-
7	14.6(48)	5.50(18.06)	-
8	36.6(120)	0.0	0.0
9	36.6(120)	2.49(8.16)	-
10	36.6(120)	4.02(13.19)	-
11	36.6(120)	5.50(18.06)	-
12	76.2(250)	0.0	0.0
13	76.2(250)	0.0	13.55(44.44)
14	76.2(250)	2.49(8.16)	-
15	76.2(250)	5.50(18.06)	-
16	115.8(380)	5.50(18.06)	-
17	158.5(520)	0.0	0.0
18	158.5(520)	2.49(8.16)	-
19	158.5(520)	5.50(18.06)	-
20	195.1(640)	5.50(18.06)	-
21	234.7(770)	0.0	0.0
22	234.7(770)	2.38(7.81)	-
23	234.7(770)	5.50(18.06)	-
24	274.3(900)	5.50(18.06)	-

The voltage calibration consisted simply of the recording of a known input voltage direct from a power supply.

The motion and fixed tests were conducted in regular waves. The forced oscillation tests were run with the shaker mechanism operating at a number of frequencies simultaneously. This sort of transient test technique is described by Takezawa and Hirayama (1976).

#### IV. DATA REDUCTION TECHNIQUES

The basic methods used to analyze the experimental data are given by Troesch (1980). A brief explanation, together with some details of the application of these methods to the present experiments, will be given here.

Typically, model tests of vessel motions or other related responses are conducted over a range of frequencies, the wave input for each run being assumed sinusoidal. By measuring the amplitudes of the input and response, the ordinate of the response amplitude operator at the nominal frequency can be determined. This method is based on an idealized ability to generate regular sinusoidal waves in the laboratory.

In fact, it is not possible, even in principle, to generate finite-amplitude sinusoidal waves. The presence of higher harmonics is unavoidable, due to the nonlinear free surface boundary condition. Then, too, any noise or mechanical nonlinearity in the wavemaker itself will obviously introduce further frequency content. To circumvent the problems associated with the nearly sinusoidal waves, the wave maker was turned on for only a short period. A period long enough to generate a packet of ten to twelve crests. In the case of this finite record, it is possible to apply a Fast "Fourier frequency decomposition," which is a discrete Fourier transform. In effect, the frequency decomposition is analogous to an extremely narrow-banded spectrum.

With such frequency decompositions of both the response and input for a single run, the result is information on the transfer function over a certain narrow frequency band around the nominal frequency. The obvious advantage of this method is that the over-all shape of the transfer function can be determined with fewer runs. In addition, in the neighborhood of resonance, where the transfer function may be quite sharply peaked, this method reduces the possibility of missing the actual peak, and thereby underestimating the maximum value of the transfer function. This procedure was used in the analysis of both the scattering tests and the free heave and pitch tests. An example of the type of data produced from this technique is shown in Figures 119 and 120. The side band frequency points are denoted by "□".

Similar Fourier transform methods were employed in the forced oscillation test. On each run, a slow frequency sweep was made with the shaker device's motor control, thus providing an effective wide band input. The success of this type of testing has been demonstrated by Takezawa and Takekawa (1976). Signal-conditioning techniques and the Fast Fourier Transform algorithm were the same as used in the wave tests described above.

## V. EXPERIMENTAL RESULTS

The test matrix for the two models is shown in Table VI. For the motions test where the model was free to heave and pitch, the Cort was tested at full load and ballast conditions, at two speeds, and at eight wave lengths. The SL-7 was tested at only the full load condition, but ran at three speeds in eight wave lengths.

TABLE VI: Model Test Conditions

### SL-7

$V/\sqrt{g \cdot LBP}$	0.15, 0.23, 0.32
Ship Length/Wave Length	0.60, 0.75, 0.90, 1.05, 1.20, 1.35, 1.50, 1.65

### S.J. Cort (Ballast and Full Load)

$V/\sqrt{g \cdot LBP}$	0.100, 0.132
Ship Length/Wave Length	1.00, 1.28, 1.88, 2.58, 3.49, 4.41, 5.55, 6.54

The forced oscillation and diffracted tests were conducted on the SL-7 at one speed and the various wave lengths. Due to budgetary restrictions, only the pressure taps in the forward half of the model were fitted with pressure transducers. The remainder of the taps were plugged to avoid problems associated with leakage.

The values of model speeds and encounter wave lengths were selected to reflect the operating environment of the full-scale vessel. For the Cort, this implied low speeds and short waves. Typical wave lengths on the Great Lakes seldom exceed 152m (500 ft). Consequently, most of the ship length to wave length ratios that are of interest are greater than 2.0. The SL-7 represents a class of ocean-going vessels that travel at relatively higher speeds and encounter relatively larger waves.

The actual test results are presented in the following figures. In all cases, except where noted, the points represent unfaired data. (The points are connected by straight line segments for visual effect). The normalized quantities displayed are the pitch, heave, and pressure amplitudes, all plotted as functions of ship length to incident wave length. Heave is defined as the vertical displacement of the model measured at midship, and pitch as the angular rotation about an axis located at the intersection of the water plane and the midship station.

The following non-dimensional scheme was used:

- i) Heave response amplitude operator (RAO)

$$\text{Heave coef.} = \frac{\text{heave amplitude}}{\text{incident wave amplitude}}$$

- ii) Pitch response amplitude operator (RAO)

$$\text{Pitch coef.} = \frac{(\text{amplitude of pitch rotation in radians}) \times (\text{LBP}/2)}{\text{incident wave amplitude}}$$

- iii) Pressure response amplitude operator (RAO) resulting from motions in incident waves

$$\text{Pressure coef.} = \frac{\text{pressure amplitude}}{(\text{water density}) \times (\text{gravitation constant}) \times (\text{incident wave amplitude})}$$

- iv) Pressure response amplitude operator (RAO) for the model fixed in incident waves. The pressure coefficient is the same as that described in iii)

- v) Pressure response amplitude operator (RAO) for the model in forced heave

$$\text{Pressure coef.} = \frac{\text{pressure amplitude}}{(\text{water density}) \times (\text{gravitation constant}) \times (\text{heave amplitude})}$$

- vi) Pressure response amplitude operator (RAO) for the model in forced pitch

$$\text{Pressure coef.} = \frac{\text{pressure amplitude}}{(\text{water density}) \times (\text{gravitation constant}) \times (\text{vertical displacement})}$$

The vertical displacement is the vertical amplitude of motion of the particular pressure tap in question when the model is forced to pitch. It is equal to the pitch rotation in radians multiplied by the longitudinal distance from the pressure tap to midship.

- vii) Froude number

$$F_n = \frac{\text{ship velocity}}{\sqrt{\text{LBP} \times \text{gravitation constant}}}$$

All of the length, mass, and time quantities in the above coefficients should be expressed in consistent units. For example, if the heave amplitude is given in meters, then the incident wave amplitude should also be given in meters.

Figures 3 through 8 show the heave and pitch RAO's for the SL-7. Figures 9 through 16 show the heave and pitch RAO's for the Cort. For most of the ship length to wave length ratios of interest, the Cort experiences very little heave or pitch motions.

Figures 17 through 94 display the pressure RAO's for the various pressure taps on the SL-7 model. Table IV lists the various tap locations. The trends shown in the graphs generally agree with those published by Nakamura, et. al. (1974).

Figures 95 through 162 show the pressure RAO's for the pressure taps on the Cort. Table V lists the tap numbers and their corresponding locations. As mentioned in the section on data reduction techniques, Figures 119 and 120 include the points that represent the side band frequencies. These points are denoted as squares. The light ballast condition for the Cort exposed a number of taps to the air, either in still water or during the runs in waves. This resulted in pressure records that were of questionable use. Only the taps that remained submerged throughout a particular run are presented here.

Figures 163 through 177 show the pressure RAO's for the set of experiments where the SL-7 was fixed. This test measures the effect of the incident and diffracted wave pressures.

Figures 178 through 200 show the pressure RAO's resulting from forced heave and pitch motions of the SL-7. The oscillator drive mechanism started from rest and swept through the frequency range during a single run. This transient test technique has been described in detail by Takezawa and Hirayama (1976) and Takezawa and Takekawa (1976). Because of the irregular nature of the input signal, and the corresponding scatter of the output signal, the test results were faired before plotted. The level of variation of the test results over the ship length to wave length range was less than 10%.

Figures 201 through 204 show representative linearity checks on the SL-7 pressure RAO's. Figures 205 through 208 show similar checks for the Cort. The nominal wave height used during the regular tests was 2.54 cm (1 inch). For the linearity checks, the wave height was increased to approximately 5.08 cm (2 inches). These points are represented as squares. From the tests it appears that pressures on or near the keel or pressures on after stations follow a linear scaling law. However, the linearity checks for forward stations near the free surface indicate an amplitude dependence on the pressures.

While it is difficult to precisely identify the source of scatter that is apparent in most of the plots, certain general statements may be made. On the average, the pressure and motion transducers were linear and repeatable to within 1%. This was verified through bench tests in the electronics shop which is adjacent to the towing tank. The transducers were recalibrated before every run by the mechanical calibration procedure as described earlier in the section labeled, "Test Procedure." In the later stages of the forced oscillation tests on the SL-7 it was discovered that there was a standing wave in the tank with a period of approximately 40 seconds. (These were the last series of tests run in the project.) The amplitude of the standing wave varied over the length of the day but never seemed to exceed 2.0mm (0.08 in) in amplitude. Since the mechanical calibration before each run provided the gain factor for that particular run,

the experimental results reflect a bias introduced by the standing wave. The level and sign of the bias depends upon the amplitude of the standing wave and the location of the wave crest during the actual calibration. As a consequence, the standing wave was responsible for introducing a  $\pm$  scatter in the data. The sonic wave probe was calibrated three times during the day - in the morning, at mid-day, and in the evening. Over this period, there was a slight zero drift, on the order of an equivalent 1.3 mm (.05 in) of water, but virtually no gain change. (Since the experiments were designed to investigate time dependent phenomenon during a run of approximately 30 seconds, this small zero shift had no effect on the results.) The heave staff that provided the tow force for the model has linear roller bearings that introduced some frictional damping. However, this will only influence the heave motions around heave resonance. This could have been a problem for some of the longer wavelengths that the SL-7 was tested in, but should not have effected the Cort since that model saw little heave excitation. In summary then, the largest apparent source of scatter could be the variability of the calibrated gain.

## VI. CONCLUDING REMARKS

The results presented in this paper should provide a basis by which different theoretical calculations may be evaluated. While there are no published results that allow for a direct comparison between these experiments and theory, certain observations are possible. The closest theoretical results that can be compared to the particular model types shown here are given in the list of references. The reader is referred to the references for more details. Since the model types did differ, care must be taken in the comparisons. However, the following general statements may be made:

- i) When comparing similar test conditions, the experimental results shown in Figures 3 through 200 yield results that appear to be consistent with pressure/motions experiments conducted by Japanese researchers. See the Appendix for a summary of these papers. By testing the SL-7 at higher speeds and the Cort in shorter waves, the effect of the motions and incident waves on pressure response amplitude operators has been extended.
- ii) Theoretical and experimental comparisons of hydrodynamic pressures on a hull have been done by a number of researchers. See, for example, Sugai, et. al. (1972), Nakamura, et. al. (1974), Fujii and Takahashi (1974), and Caretti (1980). The test conditions included head and oblique seas. The general conclusion based upon these papers, is that most theories appear adequate for predicting pressures away from the free surface for long waves in head and bow quartering seas. In beam seas where the roll motion is generally not predicted well due to viscous effects, these references note that the comparison is less satisfactory. As the wave length becomes shorter, theory and experiment begin to diverge at all headings. This could be significant for Great Lakes vessels.
- iii) As the free surface is approached, especially in the bow region, the theories as given in the references appear to give questionable results. It is in this area that future efforts in both theory and experiments should be directed.

#### ACKNOWLEDGMENTS

The authors wish to thank Dr. Kimio Saito, Visiting Research Scientist, (University of Michigan, on leave from Osaka University) for his suggestions during the setup of the experiments and also Mr. Robert Scher for his help in the preparation of this report.

#### REFERENCES

- Beck, R.F., and Troesch, A.W., "Wave Diffraction Effects in Head Seas," International Shipbuilding Progress, Vol. 27, December 1980.
- Caretti, F., "A Comparison Between Theoretical and Experimental Response Amplitude Operators of Wave Pressure on Hulls," Congresso NAV '80, 1980.
- Faltinsen, O.M., "A Rational Strip Theory of Ship Motions: Part 2," Report No. 113, Department of Naval Architecture and Marine Engineering, The University of Michigan, Ann Arbor, Michigan, 1971.
- Fujii, H., and Takehashi, T., "Experimental Study on the Ship Motion and Hydrodynamic Pressure in Regular Oblique Waves," Trans. West Japan Society of Naval Architects, No. 49, 1974.
- Matsuyama, M., "Model Tests on Hydrodynamic Pressures Acting on the Hull Surface," Journal Society of Naval Architects Japan, No. 137, 1975.
- Nakamura, S., Saito, K., Asai, S., "Hydrodynamic Pressure Acting on a Ship Hull in Waves (1st Report)," Journal Kansai Society Naval Architects Japan, No. 155, 1974.
- Sugai, K., et. al., "Model Tests on Hydrodynamic Pressures Acting on the Hull of an Ore-Carrier in Oblique Waves," Journal Society of Naval Architects Japan, No. 133, 1972.
- Takezawa, S., and Takekawa, M., "Advanced Experimental Techniques for Testing Ship Models in Transient Water Waves, Part I," 11th Symposium on Naval Hydrodynamics, London, 1976.
- Takezawa, S., and Hirayama, T., "Advanced Experimental Techniques for Testing Ship Models in Transient Water Waves, Part II," 11th Symposium on Naval Hydrodynamics, London, 1976.
- Troesch, A.W., "The Diffraction Potential For a Slender Ship Moving Through Oblique Waves," Report No. 176, Department of Naval Architecture and Marine Engineering, The University of Michigan, Ann Arbor, Michigan.
- Troesch, A.W., "Measurement of Short Wave, Springing Excitation," 19th ATTC, Ann Arbor, Michigan, 1980.

## APPENDIX

### EXPERIMENTAL STUDY ON THE SHIP MOTION AND HYDRODYNAMIC PRESSURE IN REGULAR OBLIQUE WAVES

Fujii, Hitoshi  
Takahashi, Takeshi

#### PUBLICATION:

Transactions of the West-Japan Society of Naval Architects; #49; 1974

#### ABSTRACT

In order to apply the theoretical calculation of ship motion and hydrodynamic pressure to the practical ship design, it is necessary to confirm the agreement between prediction and experiments. In the present study, three kinds of test were carried out in connection with the terms in the equations of ship motion, using models of a container ship and an oil tanker.

- (1) Forced oscillation model test in calm water to check the coefficients of the equation of ship motion and the radiation pressure acting on hull surface,
- (2) Restrained model test in oblique waves to check the terms of wave excitation and the wave pressure,
- (3) Free-running model test in oblique waves to check the amplitude of motion and the total pressure,

Experimental results were compared with the computed ones.

It was clarified that the present approach is effective to find out the key point for the improvement of the calculation method.

### FUNDAMENTAL STUDY OF WAVE IMPACT LOADS ON SHIP BOW (2nd Report) - EFFECT ON THE SCALE OF THE MODEL ON MAXIMUM IMPACT PRESSURE AND EQUIVALENT STATIC PRESSURE.

Hagiware, Koichi  
Yuhara, Tetsuo

#### PUBLICATION:

Journal of Society of Naval Architects of Japan; #140; 1976

#### ABSTRACT

As part of their studies conducted regarding the wave impact loads acting on the ship bow and the structural responses thereto by a series of drop tests, the authors analyzed the scale effect, or the influence of the scale of bow models therein used on the results of the drop tests.

It is often claimed that the estimated impulsive pressure determined by a model test varies with the scale of the model. To see if such a claim was well-founded or not, the authors carried out the drop test using a 1/15 scale model and compared the results with those obtained using the 1/3 scale model in the previous tests. The results of this comparative study may be summarized as follows:

At first, the maximum impulsive pressure obtained using the 1/15 scale model was considerably smaller than that determined using the 1/3 scale model. This difference became small with large relative impact angle  $\alpha$ . Such a difference must have come from the difference in relative size of the pressure gauges fitted to these two models. On the other hand, the equivalent static pressure  $P_{eq}$  obtained using the 1/15 scale model and that obtained using the 1/3 scale model remained the same, if the size of the panel was proportioned to the size of the model. That is,  $P_{eq}$  didn't vary with the scale of the model.

Further, investigation was made of the effects of the size and the location of the panel of  $P_{eq}$ .  $P_{eq}$  indicated a considerable change according to the size and location of the panel when the impact angle  $\alpha$  was  $0^\circ$ , but the change became smaller with large  $\alpha$  of, say  $\alpha = 5^\circ$ .

## MODEL TESTS ON HYDRODYNAMIC PRESSURES ACTING ON THE HULL SURFACE

Matsuyama, Michi

### PUBLICATION:

Journal of Society of Naval Architects of Japan; #137; 1975

### ABSTRACT

In obtaining the hydrodynamic pressure exerted on the ship's hull running in regular waves, the Ordinary Strip Method has been used so far. However, the Strict Method has recently been proposed by Nakamura and Takagi. In this new method, unlike the O.S.M., the wave-induced hydrodynamic pressure can be obtained from the direct solution of the diffraction problem by satisfying the boundary condition on the surface of the ship.

In the present paper, descriptions are made on the experiments which were conducted to see what is the practical accuracy of estimation of the hydrodynamic pressure in the above two calculation methods. Measurements were made not only for the total hydrodynamic pressure, but also for two kinds of pressure components; wave-induced and radiation pressure, and comparisons of these pressures were made between the calculated values and the experimental ones. From the present study, it is shown that the above two strip methods are useful and they give the accuracy of estimation with almost the same order. Both methods, however, will be much more useful for obtaining the hydrodynamic pressure, if the ship's rolling motion could be estimated more accurately.

## HYDRODYNAMIC PRESSURE ACTING ON A SHIP HULL IN WAVES (1st Report)

Nakamura, Shoichi  
Saito, Kimio  
Asai, Shigeru

### PUBLICATION:

Journal of Society of Naval Architects of Japan; #155; 1974

### ABSTRACT

In order to study the hydrodynamic pressure on ship's hull travelling in regular head waves, model experiments have been carried out with two models of a container ship and an ore carrier.

The following three kinds of experiments have been performed to investigate the components of the hydrodynamic pressure:

- (1) Experiment I: Measurement of the hydrodynamic pressure acting on a free running model in regular head waves.
- (2) Experiment II: Measurement of the hydrodynamic pressure acting on a restrained model in regular head waves.
- (3) Experiment III: Measurement of the hydrodynamic pressure acting on a model which is forced to oscillate sinusoidally in calm water.

The results of each experiment are compared with those of theoretical calculation based upon the ordinary strip method and the validity of the calculation method to estimate the hydrodynamic pressure is discussed.

## MODEL TESTS ON HYDRODYNAMIC PRESSURES ACTING ON THE HULL OF AN ORE-CARRIER IN OBLIQUE WAVES

Sugai, Kazuo	Godai, Kunio
Kitagawa, Hiromitsu	Takesi, Yukio
Kam, Makoto	Miyamoto, Takeshi
Oomatsu, Shigeo	Okamoto, Michio

### PUBLICATION:

Journal of Society of Naval Architects of Japan; #133; 1972

### ABSTRACT

Test results on a free running model of a gigantic ore-carrier are described, in which the hydrodynamic pressures on the hull in oblique waves together with the ship behaviors were measured in order to present the useful materials for the method of wave loads estimation.

The behaviors of the gigantic ore-carrier in rough seas, namely speed loss, ship motions and relative water elevations are shown. The distributions of hydrodynamic pressure amplitudes are shown for various wave length and heading angle. In addition to amplitude distributions, phase relations of the hydrodynamic pressures are also shown. Characteristics of the hydrodynamic pressures are explained in connection with the relative wave elevations. Comparison between the experimental data and the calculated results obtained by the strip method are made and the usefulness of the strip method for the estimation of the hydrodynamic pressures is discussed.

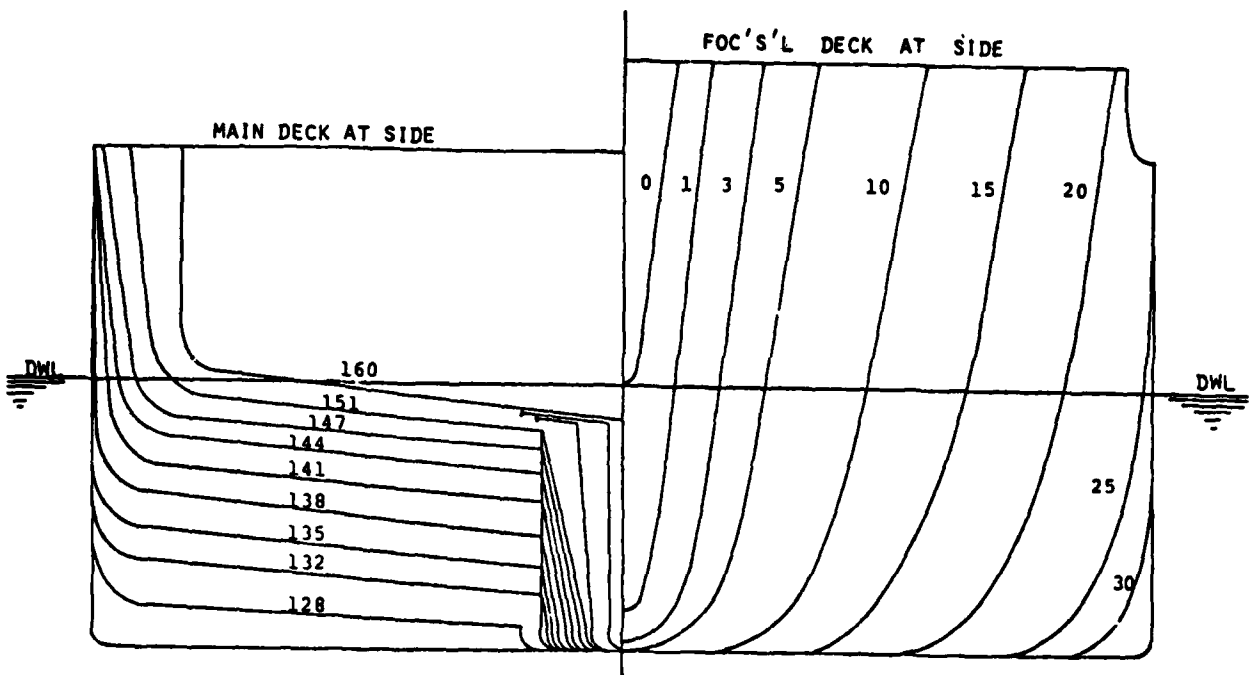


FIGURE 1: CORT BODY PLAN (WITH FRAME NUMBERS)

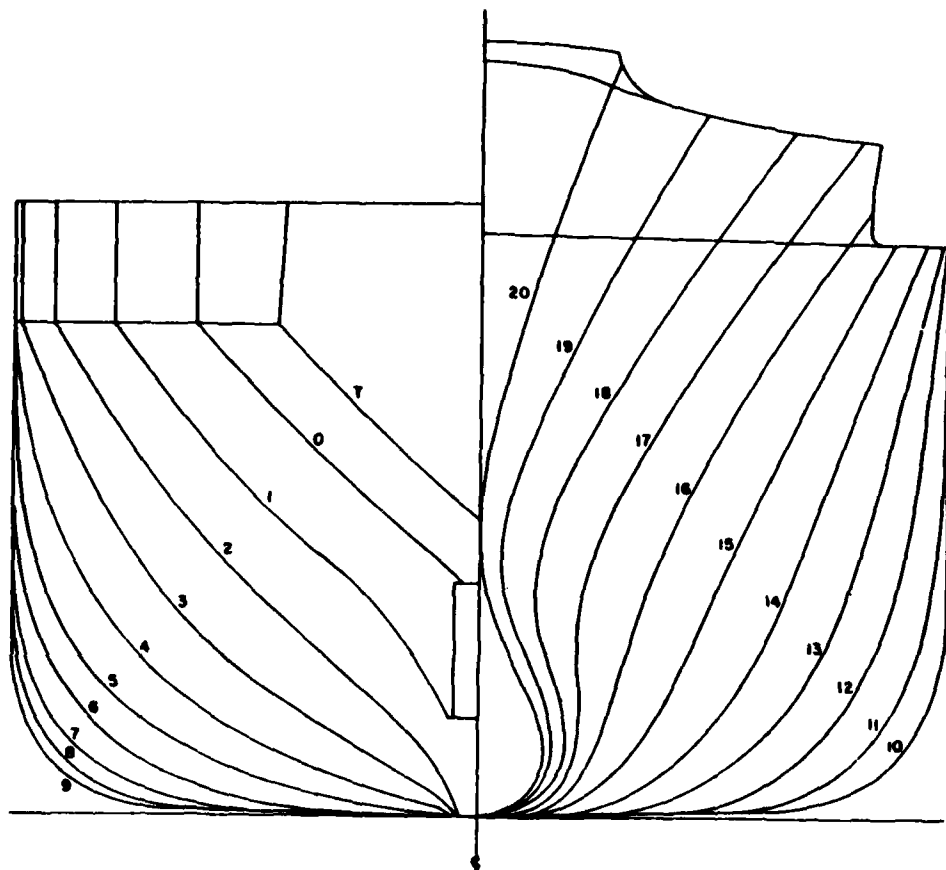


FIGURE 2: SL-7 BODY PLAN (WITH STATION NUMBERS)

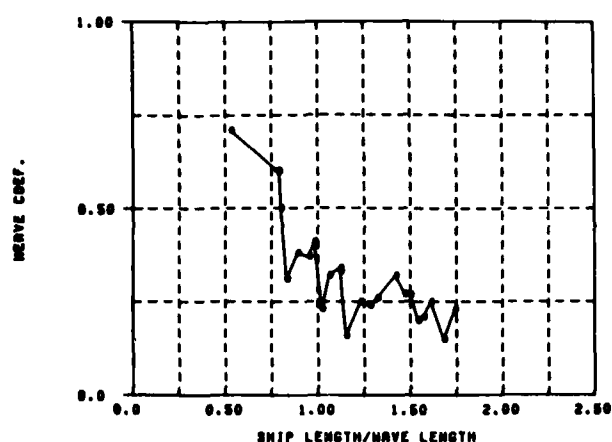


FIGURE 3: SL-7 HEAVE RAO,  $F_R=0.15$

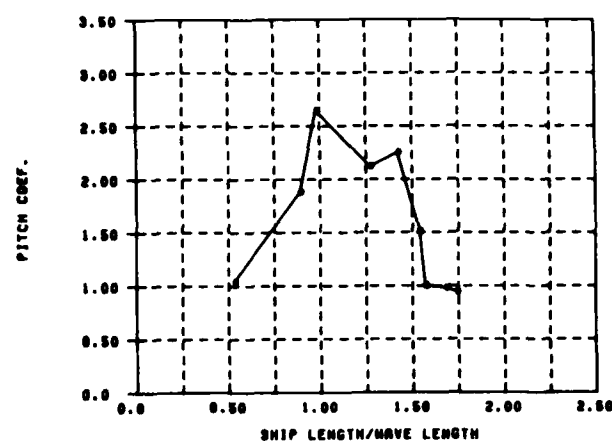


FIGURE 6: SL-7 PITCH RAO,  $F_R=0.15$

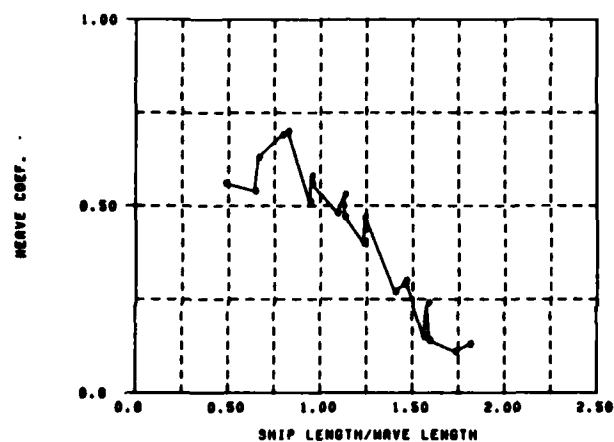


FIGURE 4: SL-7 HEAVE RAO,  $F_R=0.25$

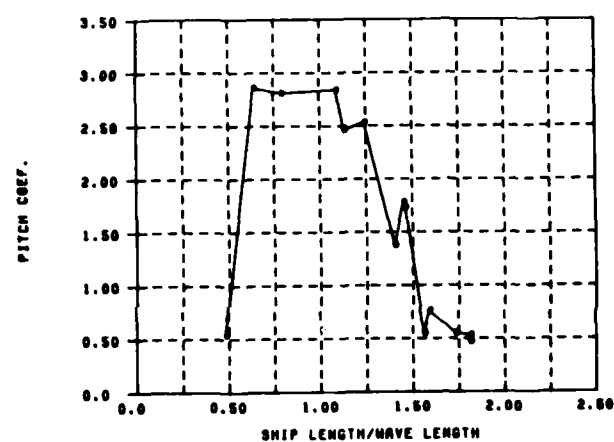


FIGURE 7: SL-7 PITCH RAO,  $F_R=0.25$

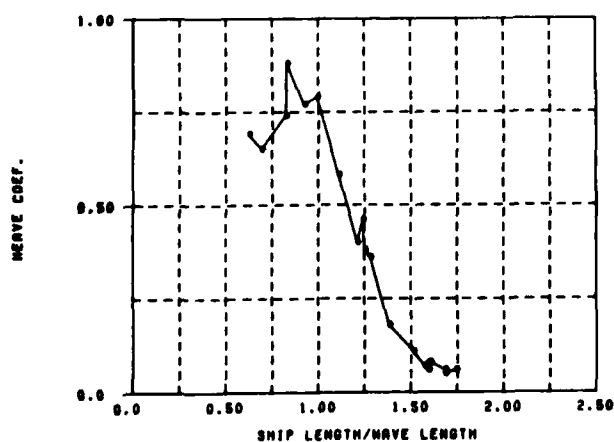


FIGURE 5: SL-7 HEAVE RAO,  $F_R=0.32$

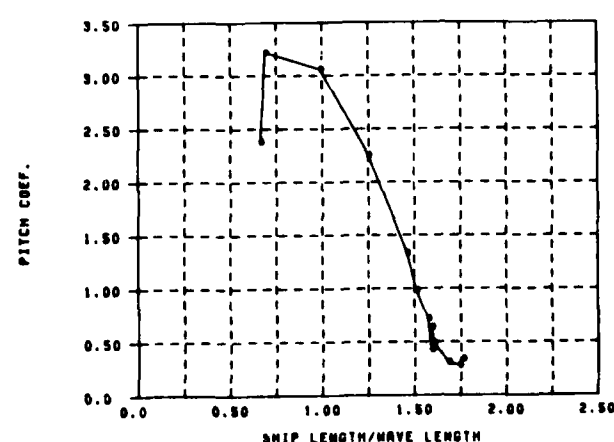


FIGURE 8: SL-7 PITCH RAO,  $F_R=0.32$

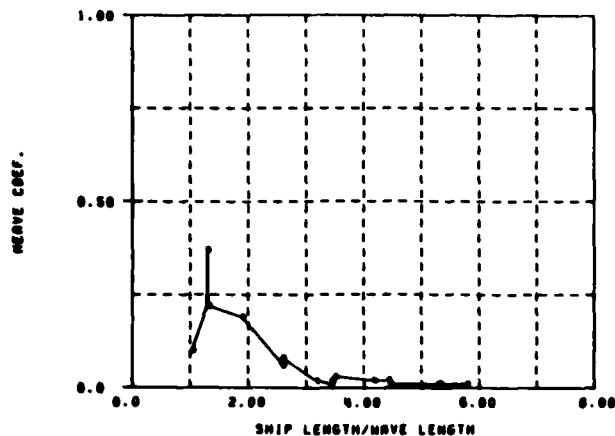


FIGURE 9: S.J. CORT HEAVE RAO, FULL LOAD CONDITION,  $F_B=100$

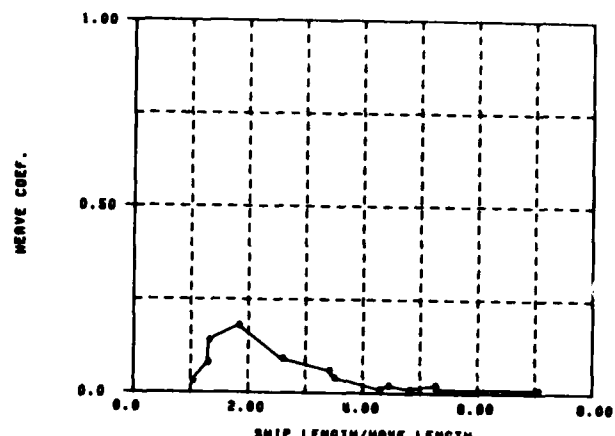


FIGURE 11: S.J. CORT HEAVE RAO, BALLAST CONDITION,  $F_B=100$

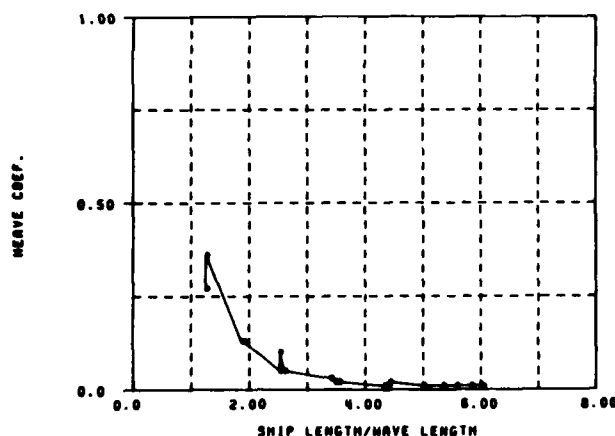


FIGURE 10: S.J. CORT HEAVE RAO, FULL LOAD CONDITION,  $F_B=132$

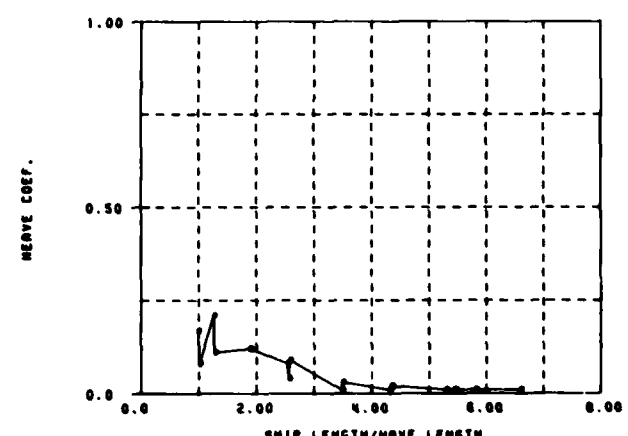


FIGURE 12: S.J. CORT HEAVE RAO, BALLAST CONDITION,  $F_B=132$

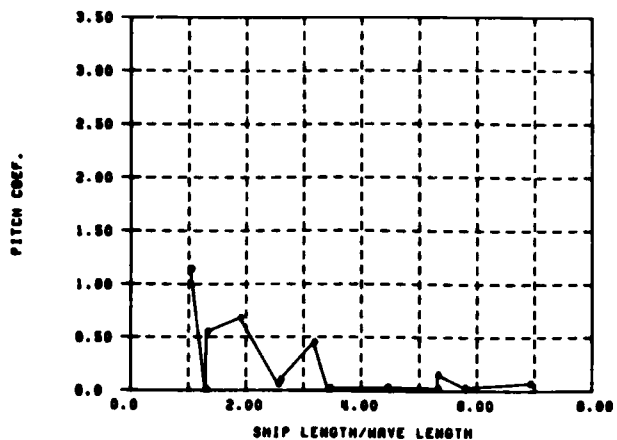


Figure 13: S.J. Corp Pitch RAO, Full Load Condition,  $F_R=100$

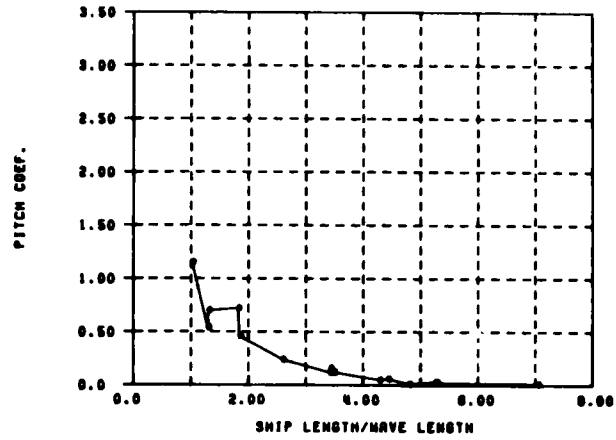


Figure 15: S.J. Corp Pitch RAO, Ballast Condition,  $F_R=100$

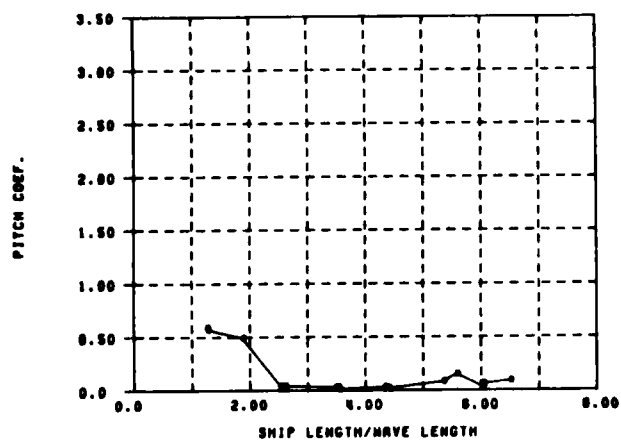


Figure 14: S.J. Corp Pitch RAO, Full Load Condition,  $F_R=132$

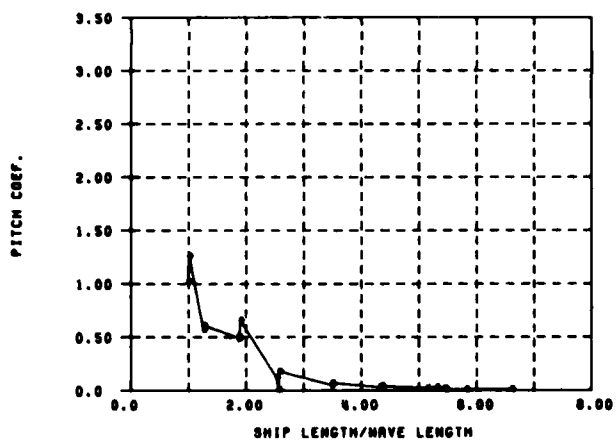


Figure 16: S.J. Corp Pitch RAO, Ballast Condition,  $F_R=132$

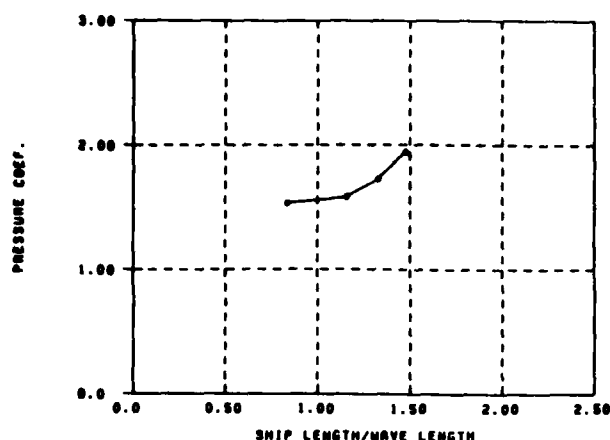


FIGURE 17: SL-7 PRESSURE RAO,  $F_h=0.15$ , TAP NO. 1

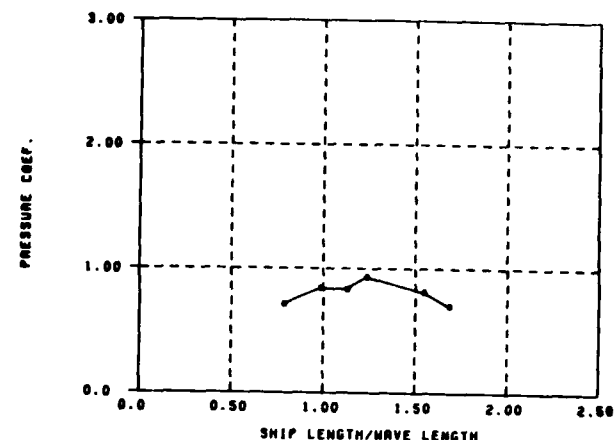


FIGURE 20: SL-7 PRESSURE RAO,  $F_h=0.15$ , TAP NO. 4

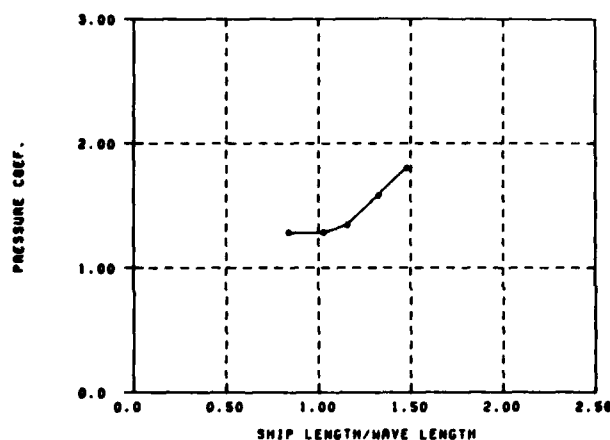


FIGURE 18: SL-7 PRESSURE RAO,  $F_h=0.15$ , TAP NO. 2

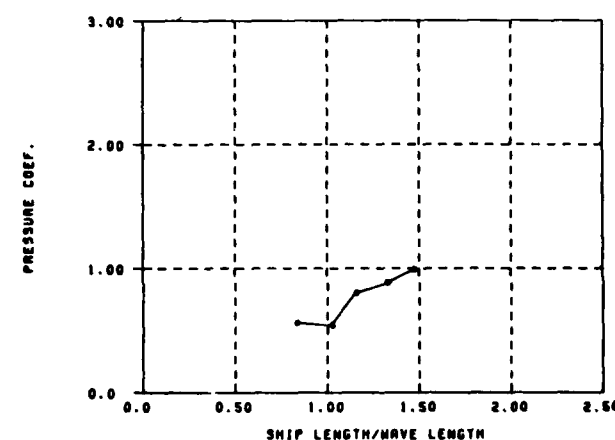


FIGURE 21: SL-7 PRESSURE RAO,  $F_h=0.15$ , TAP NO. 5

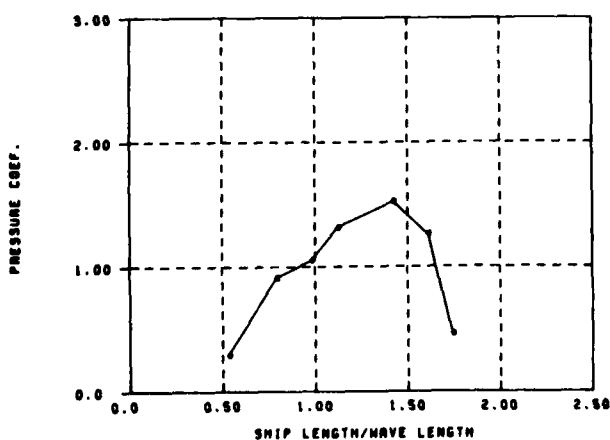


FIGURE 19: SL-7 PRESSURE RAO,  $F_h=0.15$ , TAP NO. 3

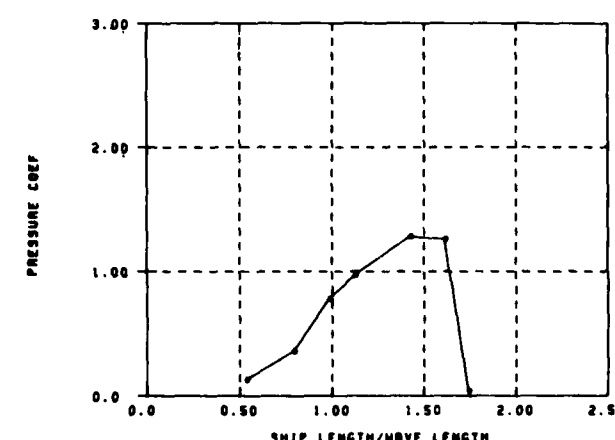


FIGURE 22: SL-7 PRESSURE RAO,  $F_h=0.15$ , TAP NO. 6

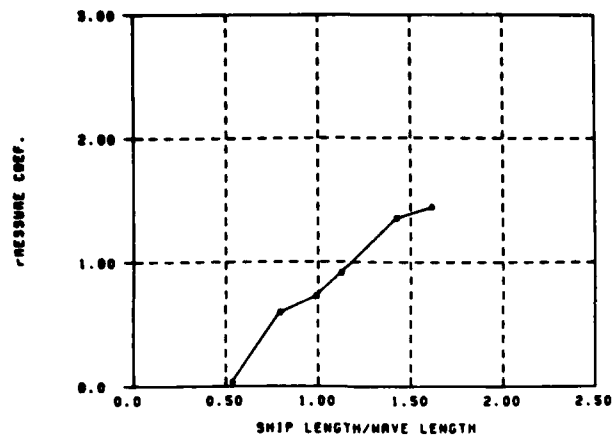


FIGURE 25: SL-7 PRESSURE RAO,  $F_n=0.15$ , TAP NO. 7

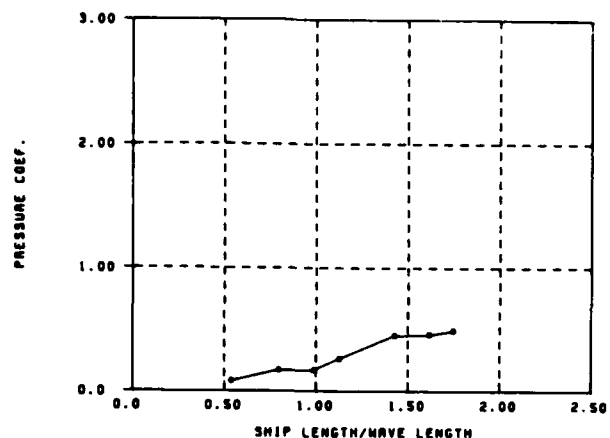


FIGURE 26: SL-7 PRESSURE RAO,  $F_n=0.15$ , TAP NO. 10

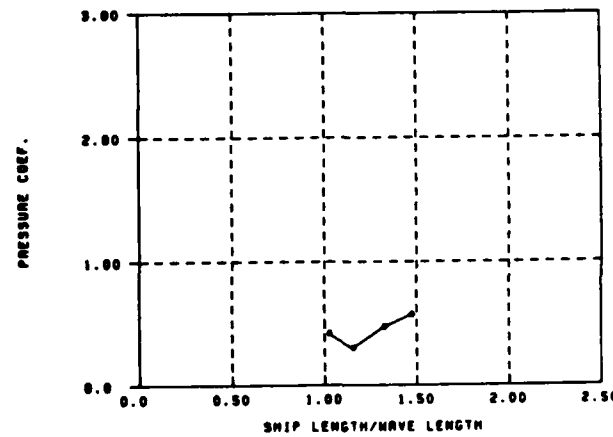


FIGURE 24: SL-7 PRESSURE RAO,  $F_n=0.15$ , TAP NO. 8

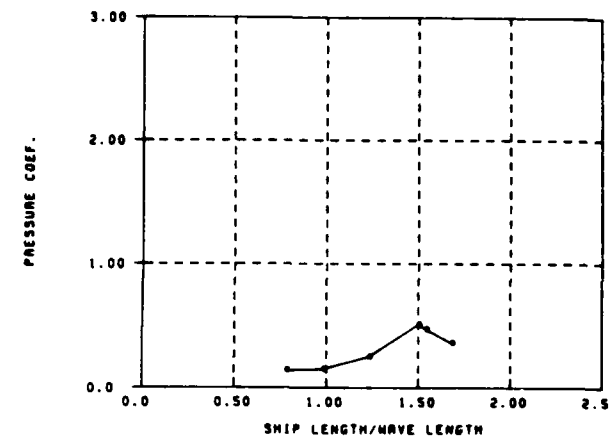


FIGURE 27: SL-7 PRESSURE RAO,  $F_n=0.15$ , TAP NO. 11

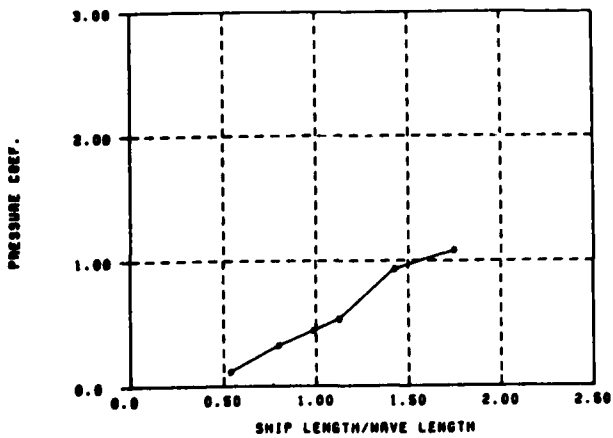


FIGURE 25: SL-7 PRESSURE RAO,  $F_n=0.15$ , TAP NO. 9

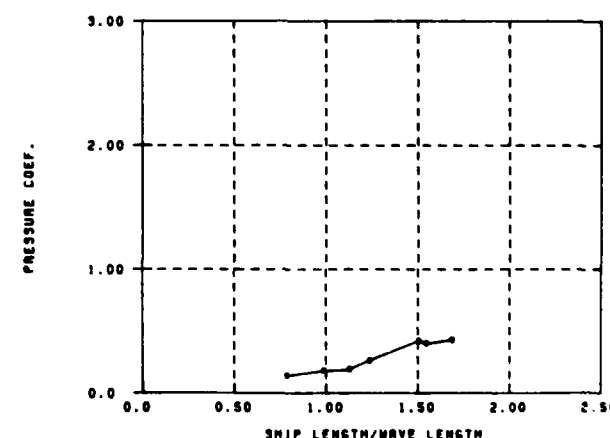


FIGURE 28: SL-7 PRESSURE RAO,  $F_n=0.15$ , TAP NO. 12

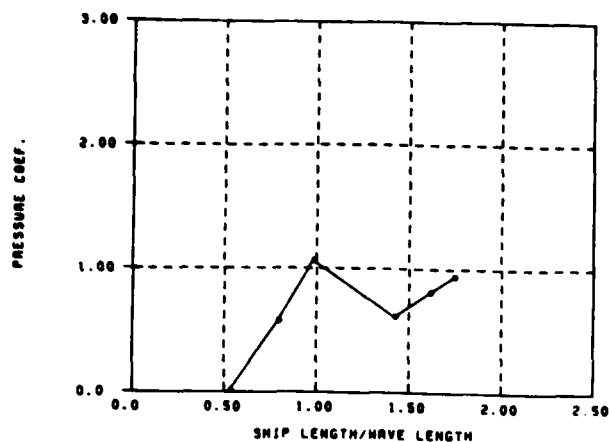


FIGURE 29: SL-7 PRESSURE RAO,  $F_p=0.15$ , TAP NO. 13

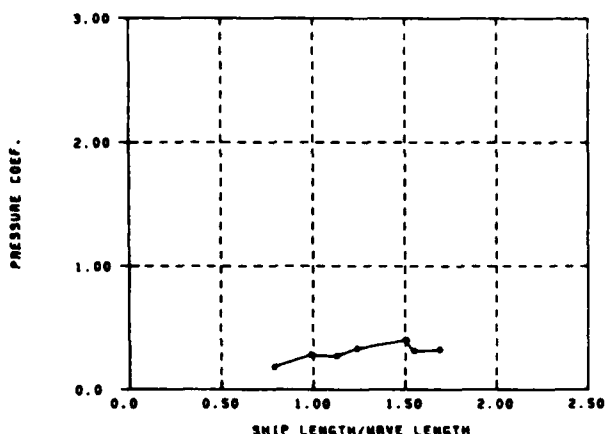


FIGURE 32: SL-7 PRESSURE RAO,  $F_p=0.15$ , TAP NO. 16

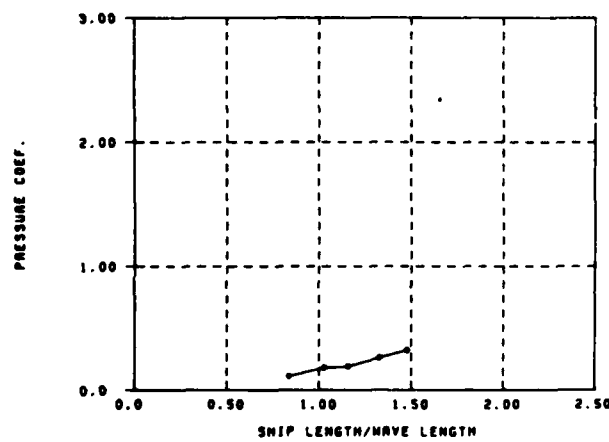


FIGURE 30: SL-7 PRESSURE RAO,  $F_p=0.15$ , TAP NO. 18

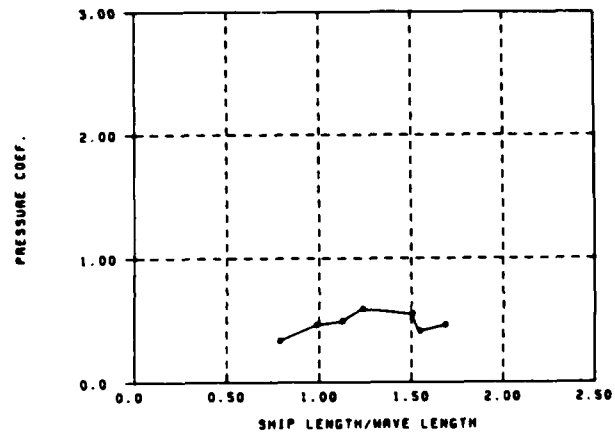


FIGURE 33: SL-7 PRESSURE RAO,  $F_p=0.15$ , TAP NO. 17

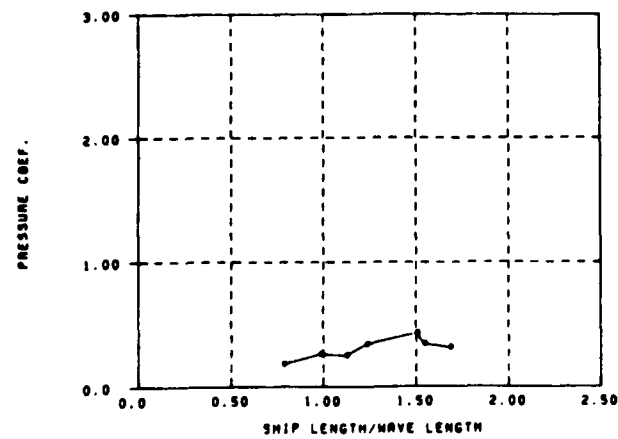


FIGURE 31: SL-7 PRESSURE RAO,  $F_p=0.15$ , TAP NO. 15

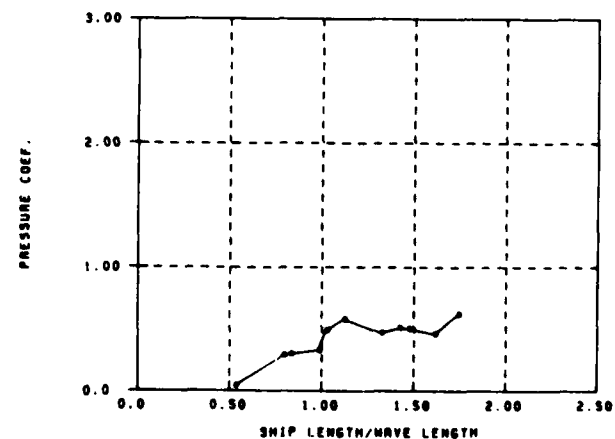


FIGURE 34: SL-7 PRESSURE RAO,  $F_p=0.15$ , TAP NO. 19

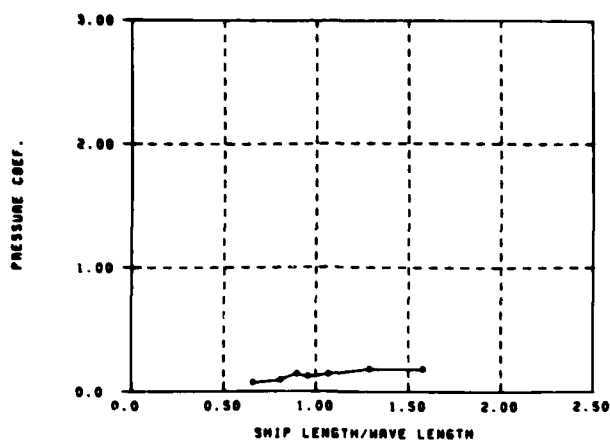


Figure 35: SL-7 Pressure RAO,  $F_n=0.15$ , Tap No. 19

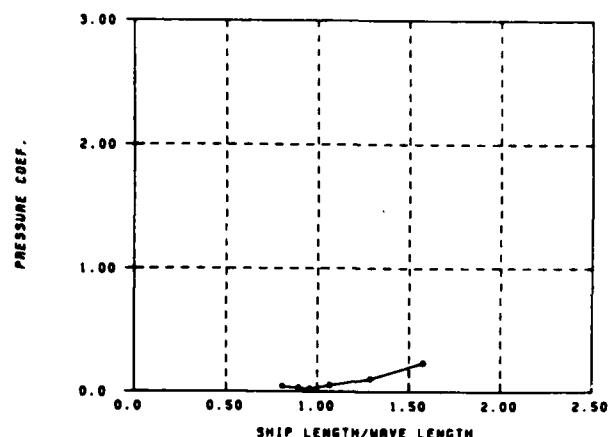


Figure 36: SL-7 Pressure RAO,  $F_n=0.15$ , Tap No. 22

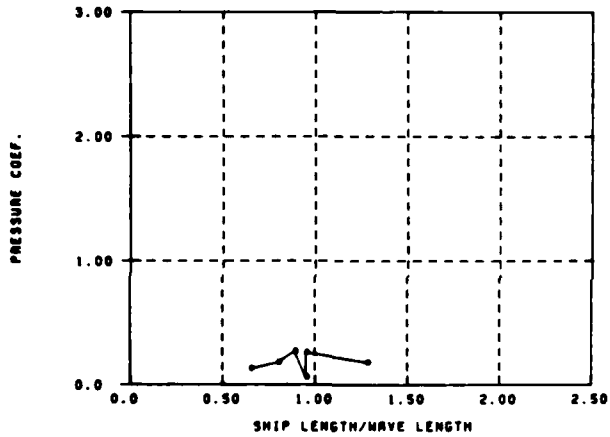


Figure 37: SL-7 Pressure RAO,  $F_n=0.15$ , Tap No. 20

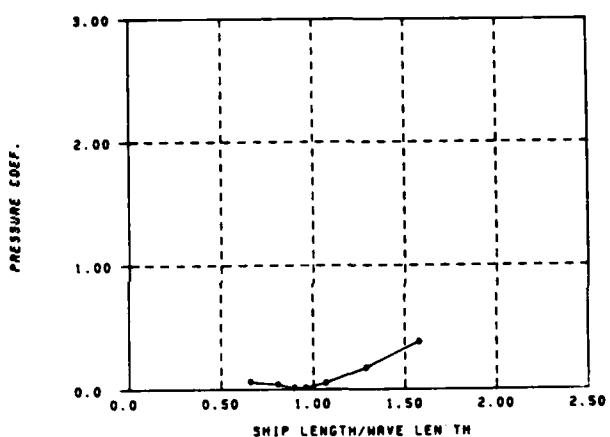


Figure 38: SL-7 Pressure RAO,  $F_n=0.15$ , Tap No. 23

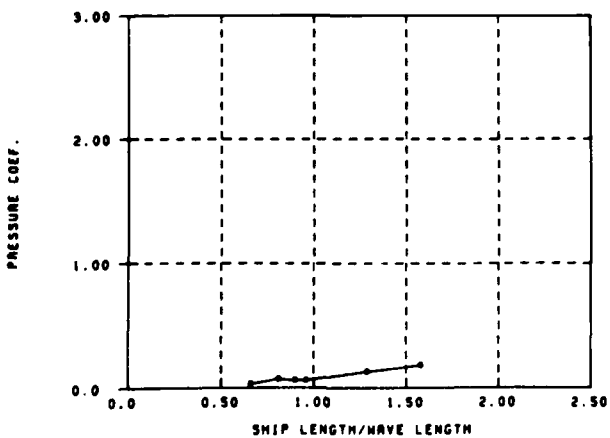


Figure 39: SL-7 Pressure RAO,  $F_n=0.15$ , Tap No. 21

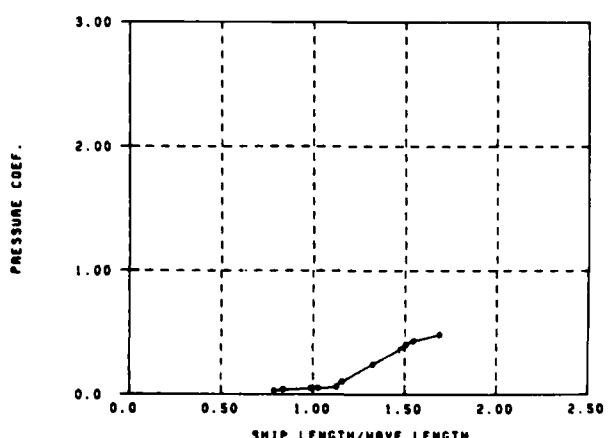


Figure 40: SL-7 Pressure RAO,  $F_n=0.15$ , Tap No. 24

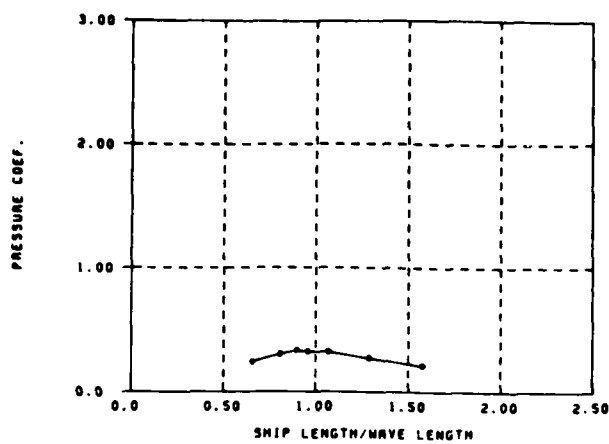


FIGURE 41: SL-7 PRESSURE RAO,  $F_n=0.15$ , TAP NO. 25

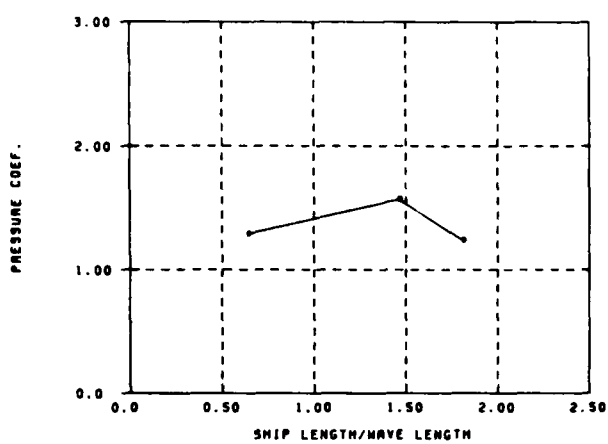


FIGURE 44: SL-7 PRESSURE RAO,  $F_n=0.23$ , TAP NO. 2

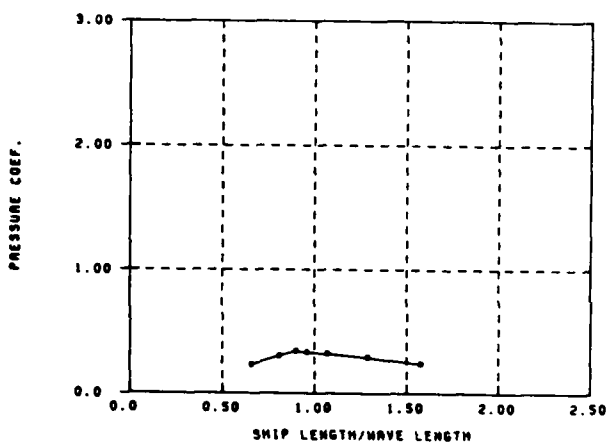


FIGURE 42: SL-7 PRESSURE RAO,  $F_n=0.15$ , TAP NO. 26

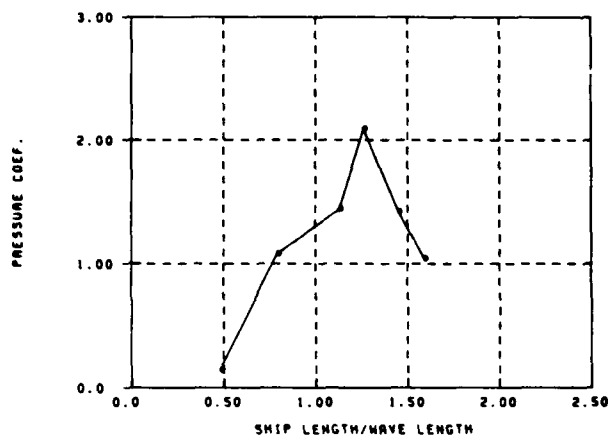


FIGURE 45: SL-7 PRESSURE RAO,  $F_n=0.23$ , TAP NO. 3

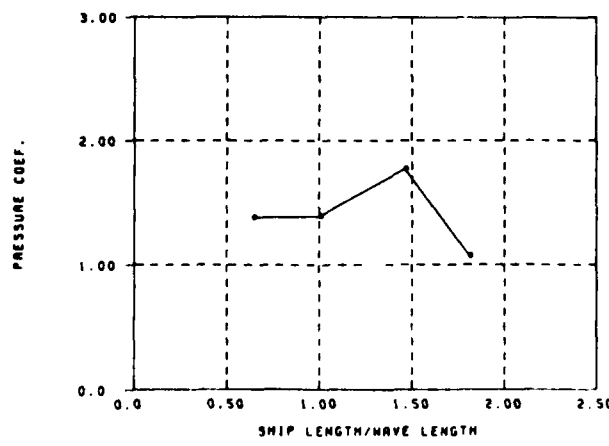


FIGURE 43: SL-7 PRESSURE RAO,  $F_n=0.23$ , TAP NO. 1

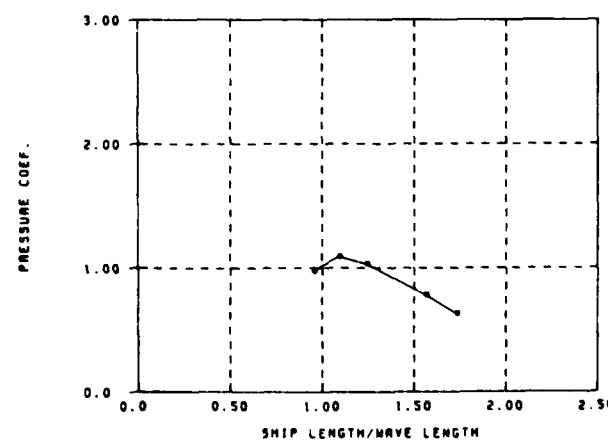


FIGURE 46: SL-7 PRESSURE RAO,  $F_n=0.23$ , TAP NO. 4

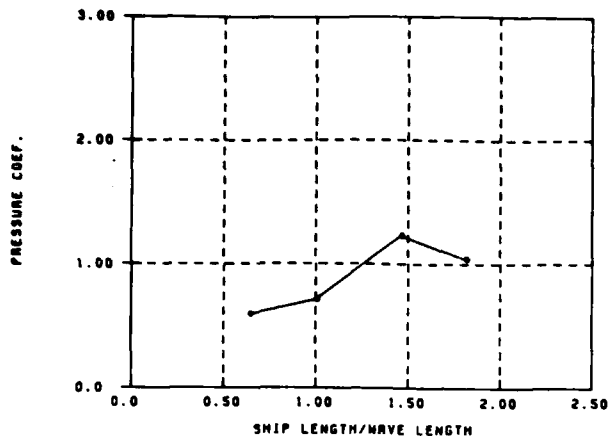


FIGURE 47: SL-7 PRESSURE RAO,  $F_n=0.23$ , TAP NO. 5

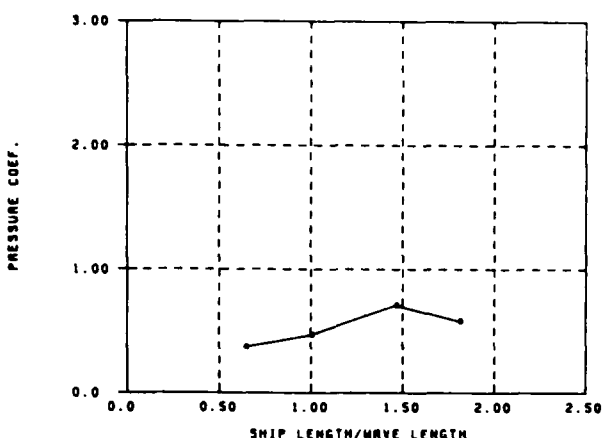


FIGURE 50: SL-7 PRESSURE RAO,  $F_n=0.23$ , TAP NO. 8

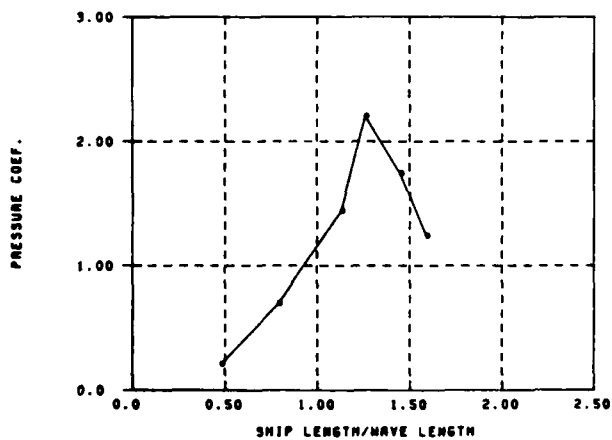


FIGURE 48: SL-7 PRESSURE RAO,  $F_n=0.23$ , TAP NO. 6

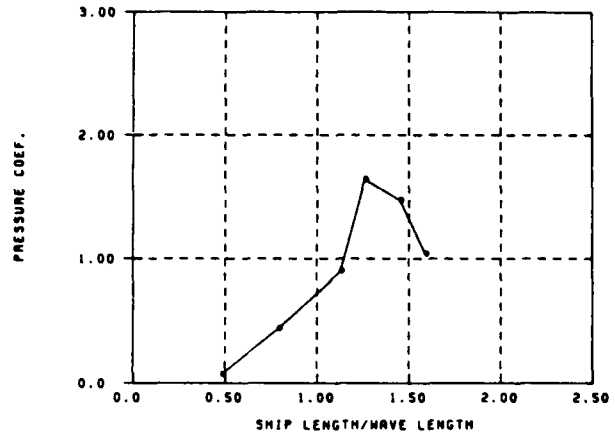


FIGURE 51: SL-7 PRESSURE RAO,  $F_n=0.23$ , TAP NO. 9

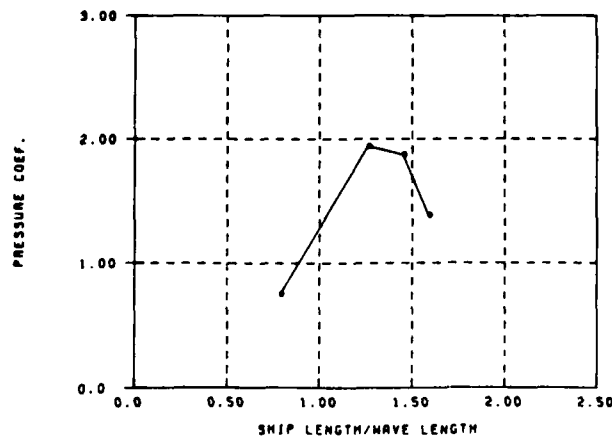


FIGURE 49: SL-7 PRESSURE RAO,  $F_n=0.23$ , TAP NO. 7

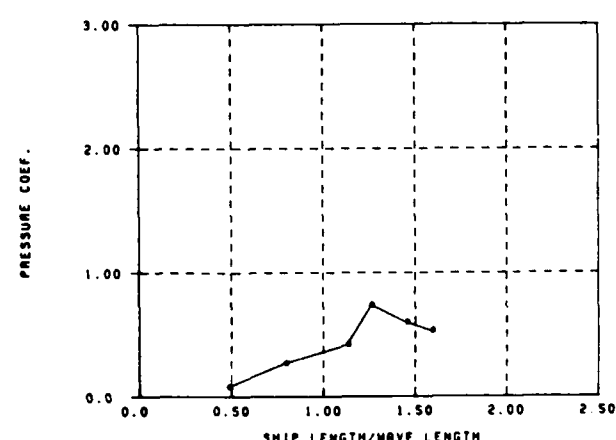


FIGURE 52: SL-7 PRESSURE RAO,  $F_n=0.23$ , TAP NO. 10

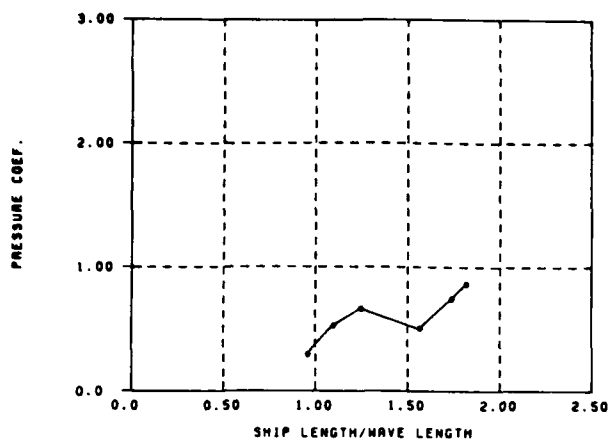


FIGURE 53: SL-7 PRESSURE RAO,  $F_n=0.23$ , TAP NO. 11

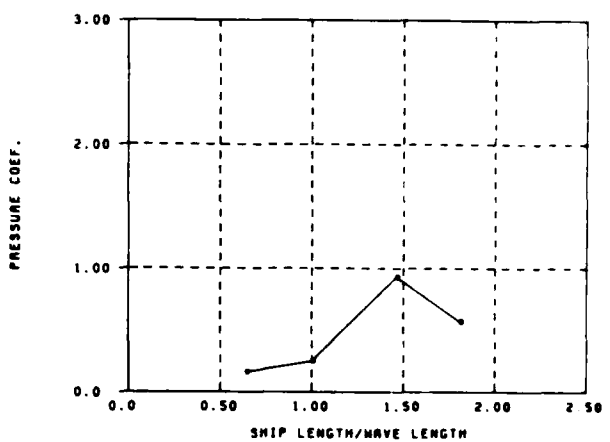


FIGURE 54: SL-7 PRESSURE RAO,  $F_n=0.23$ , TAP NO. 14

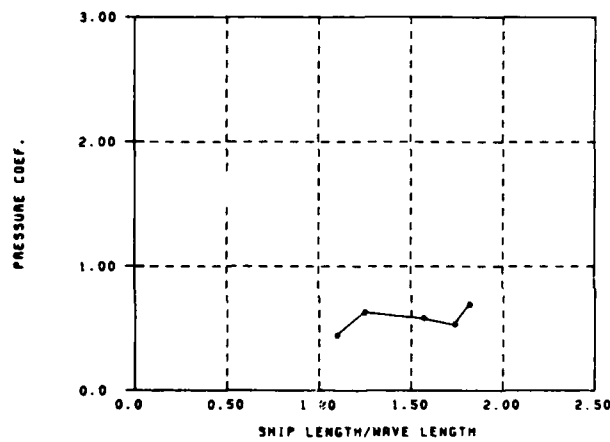


FIGURE 55: SL-7 PRESSURE RAO,  $F_n=0.23$ , TAP NO. 12

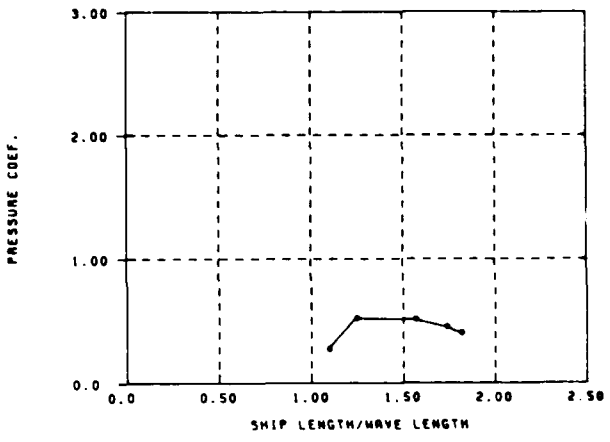


FIGURE 56: SL-7 PRESSURE RAO,  $F_n=0.23$ , TAP NO. 15

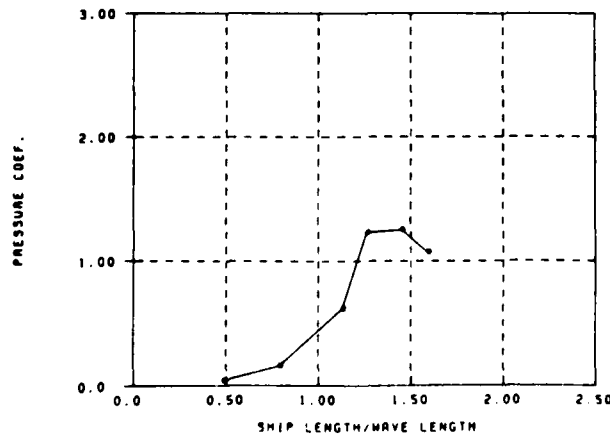


FIGURE 57: SL-7 PRESSURE RAO,  $F_n=0.23$ , TAP NO. 13

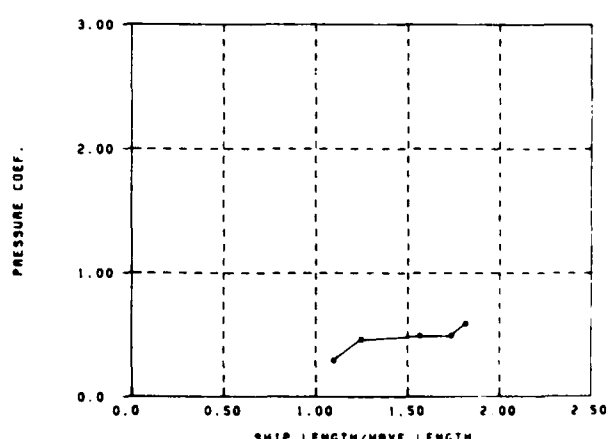


FIGURE 58: SL-7 PRESSURE RAO,  $F_n=0.23$ , TAP NO. 16

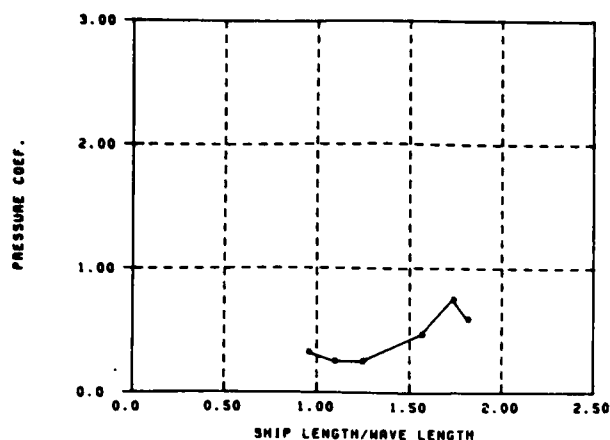


FIGURE 59: SL-7 PRESSURE RAO,  $F_n=0.23$ , TAP NO. 17

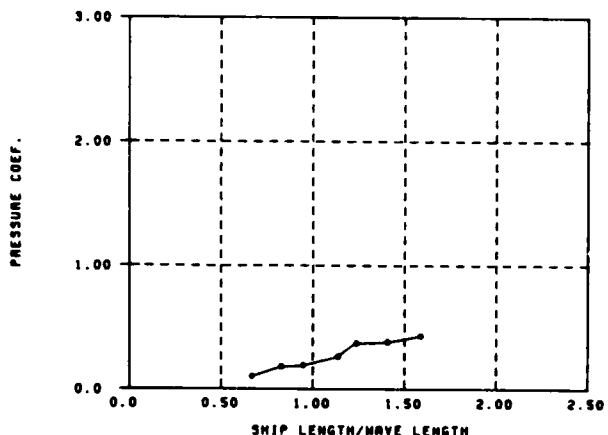


FIGURE 62: SL-7 PRESSURE RAO,  $F_n=0.23$ , TAP NO. 20

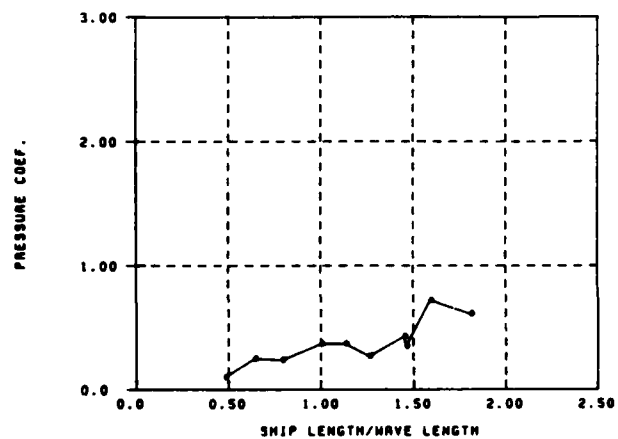


FIGURE 60: SL-7 PRESSURE RAO,  $F_n=0.23$ , TAP NO. 18

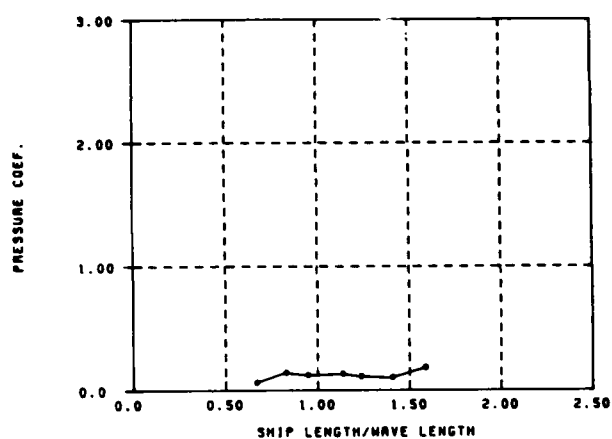


FIGURE 63: SL-7 PRESSURE RAO,  $F_n=0.23$ , TAP NO. 21

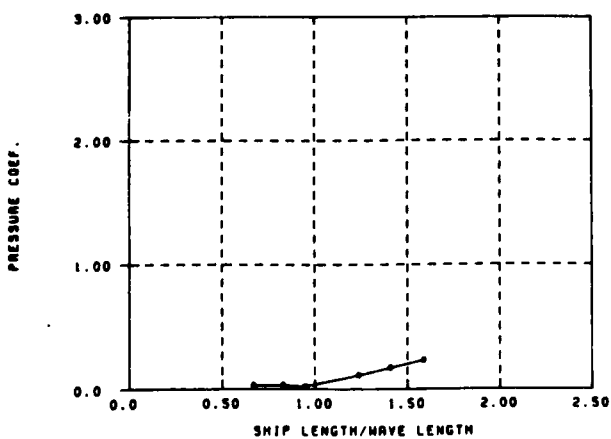


FIGURE 61: SL-7 PRESSURE RAO,  $F_n=0.23$ , TAP NO. 19

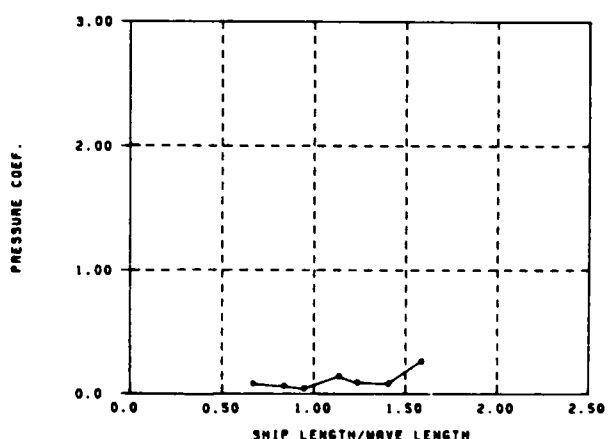


FIGURE 64: SL-7 PRESSURE RAO,  $F_n=0.23$ , TAP NO. 22

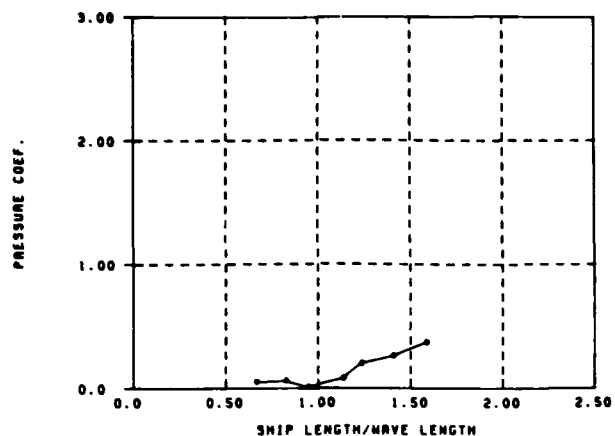


FIGURE 65: SL-7 Pressure RAO,  $F_n=0.23$ , Tap No. 23

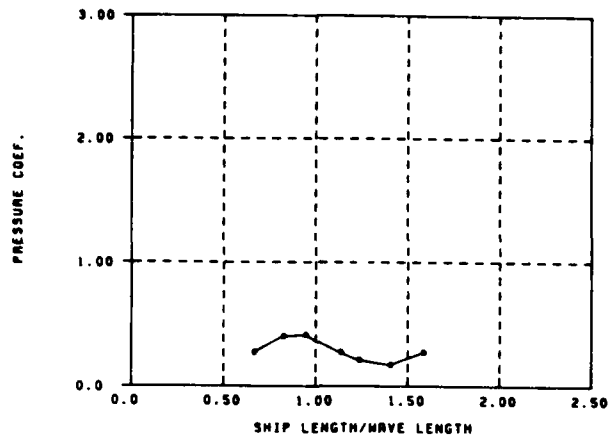


FIGURE 67: SL-7 Pressure RAO,  $F_n=0.23$ , Tap No. 25

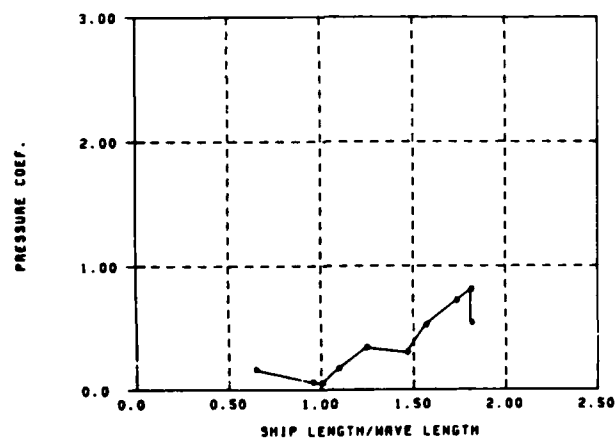


FIGURE 66: SL-7 Pressure RAO,  $F_n=0.23$ , Tap No. 24

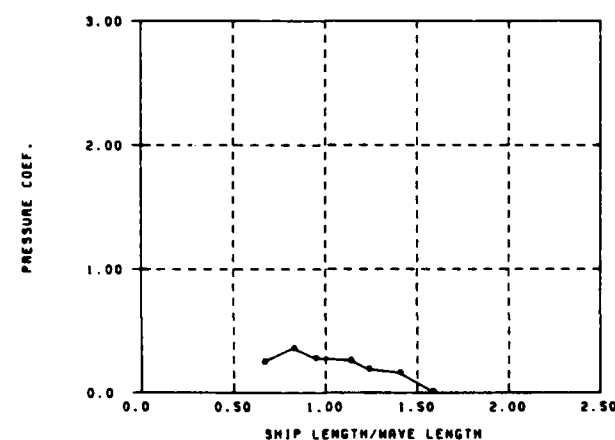


FIGURE 68: SL-7 Pressure RAO,  $F_n=0.23$ , Tap No. 26

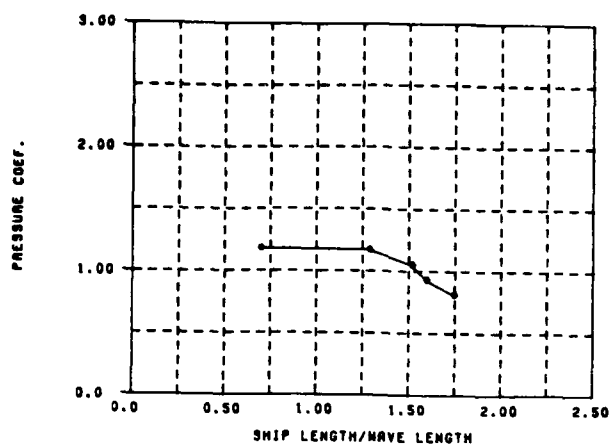


FIGURE 69: SL-7 PRESSURE RAO,  $F_n=0.32$ , TAP NO. 1

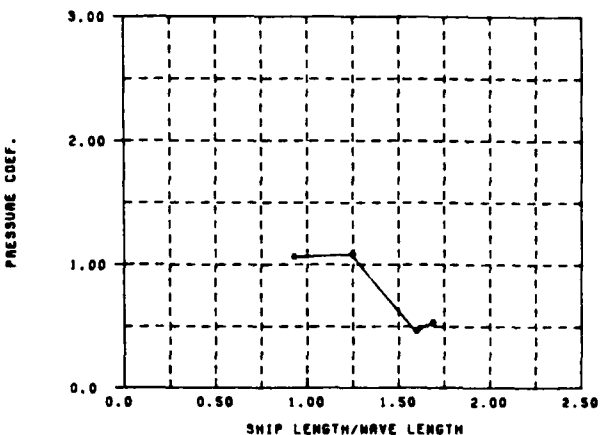


FIGURE 72: SL-7 PRESSURE RAO,  $F_n=0.32$ , TAP NO. 4

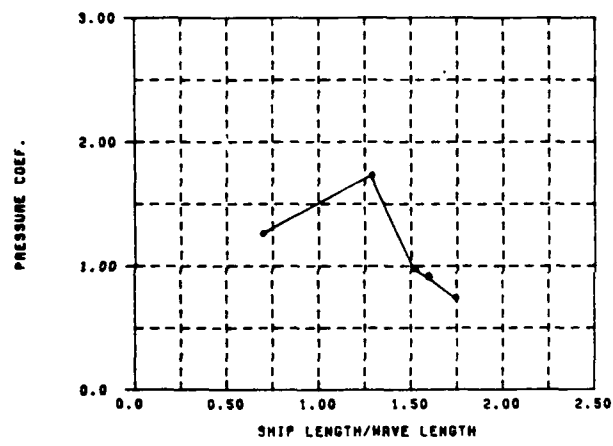


FIGURE 70: SL-7 PRESSURE RAO,  $F_n=0.32$ , TAP NO. 2

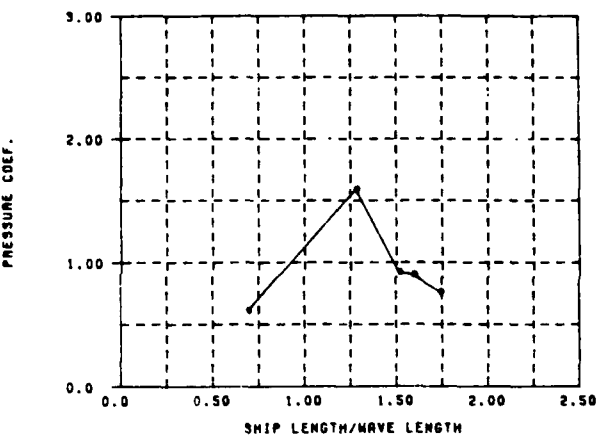


FIGURE 73: SL-7 PRESSURE RAO,  $F_n=0.32$ , TAP NO. 5

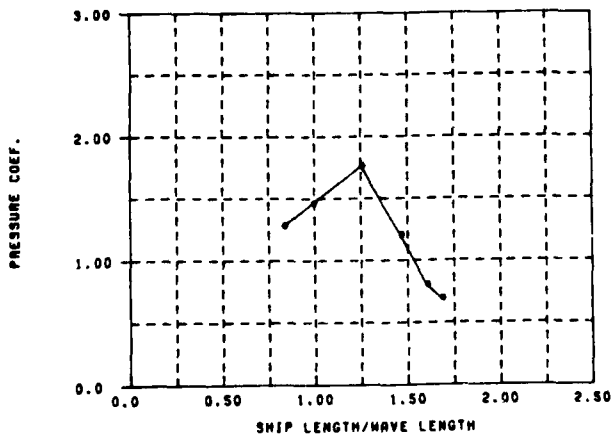


FIGURE 71: SL-7 PRESSURE RAO,  $F_n=0.32$ , TAP NO. 3

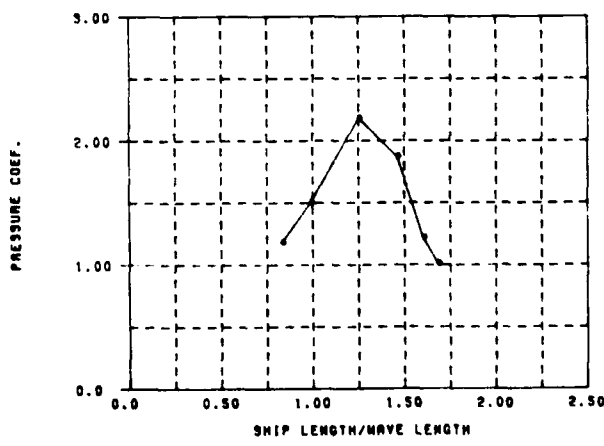


FIGURE 74: SL-7 PRESSURE RAO,  $F_n=0.32$ , TAP NO. 6

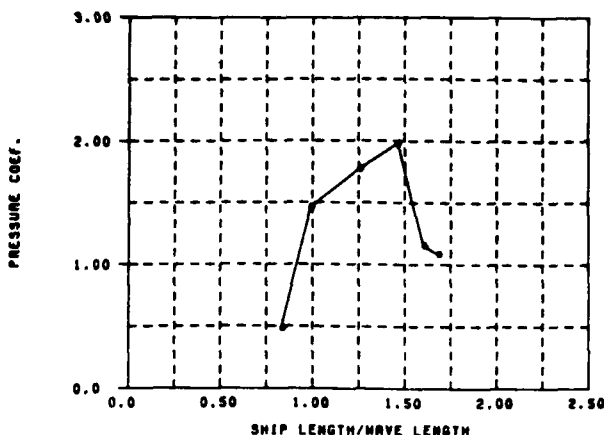


Figure 75: SL-7 Pressure RAO,  $F_R=0.32$ , Tap No. 7

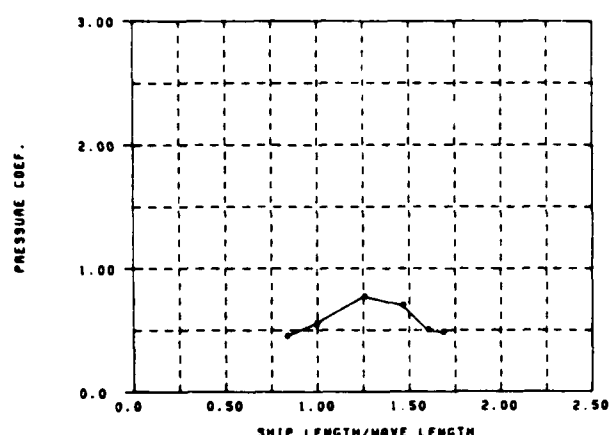


Figure 76: SL-7 Pressure RAO,  $F_R=0.32$ , Tap No. 10

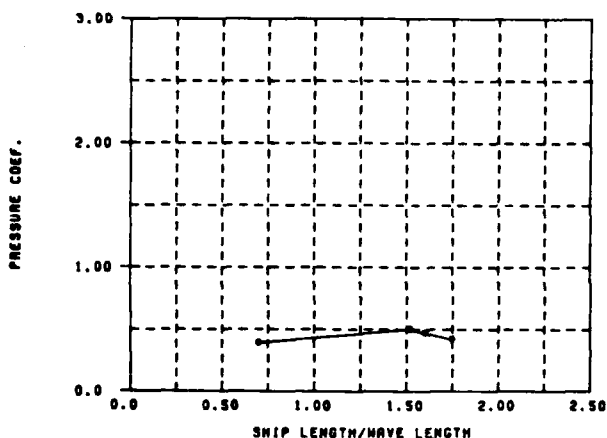


Figure 76: SL-7 Pressure RAO,  $F_R=0.32$ , Tap No. 8

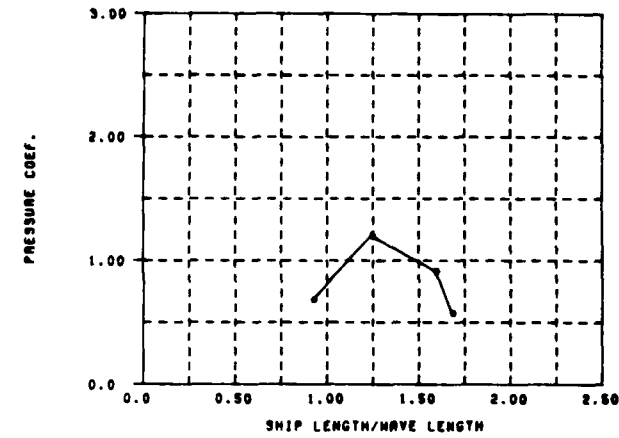


Figure 77: SL-7 Pressure RAO,  $F_R=0.32$ , Tap No. 11

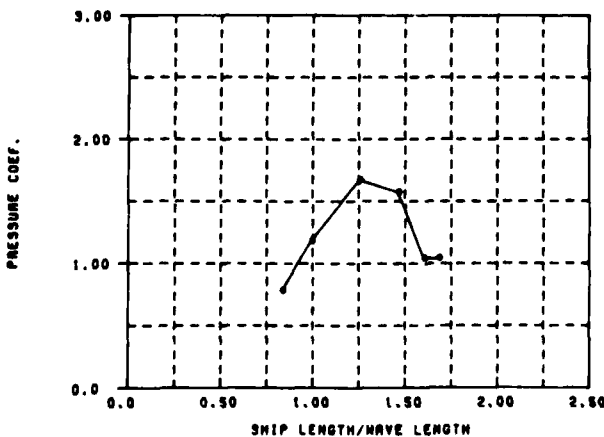


Figure 77: SL-7 Pressure RAO,  $F_R=0.32$ , Tap No. 9

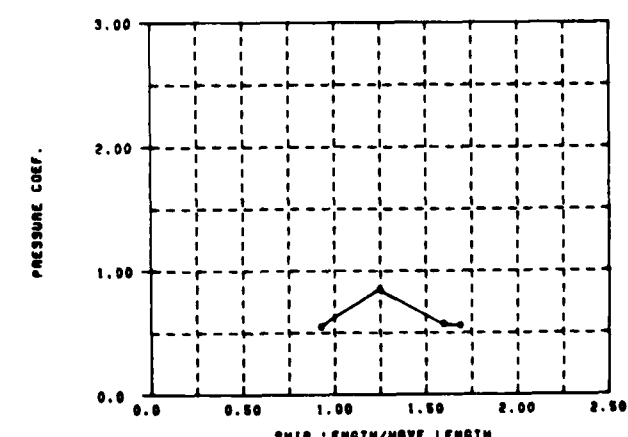


Figure 78: SL-7 Pressure RAO,  $F_R=0.32$ , Tap No. 12

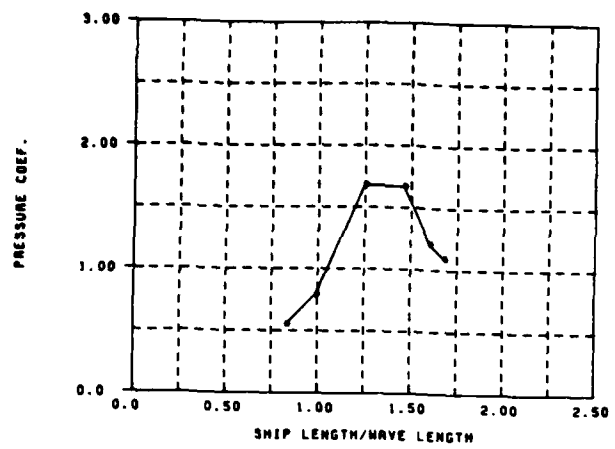


FIGURE 81: SL-7 PRESSURE RAO,  $F_n=0.32$ , TAP NO. 13

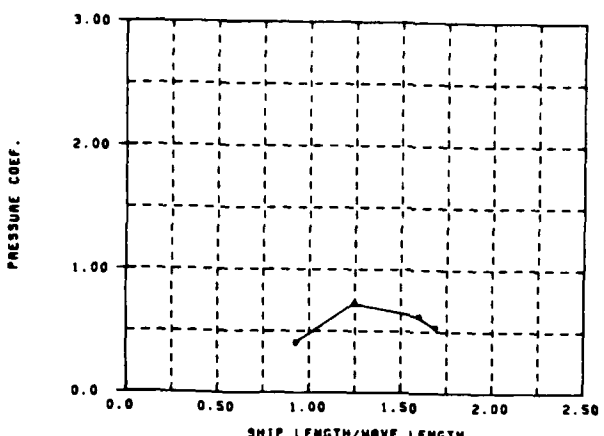


FIGURE 84: SL-7 PRESSURE RAO,  $F_n=0.32$ , TAP NO. 16

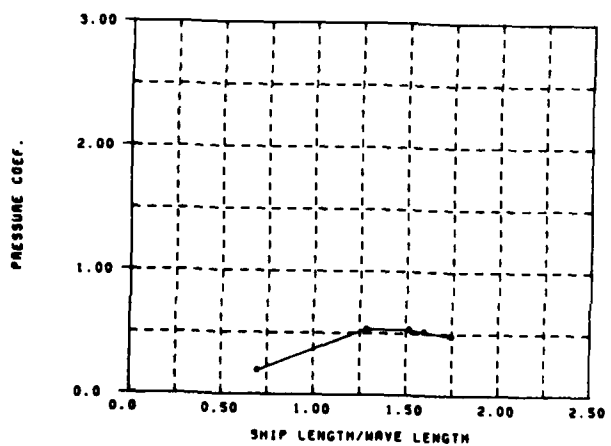


FIGURE 82: SL-7 PRESSURE RAO,  $F_n=0.32$ , TAP NO. 14

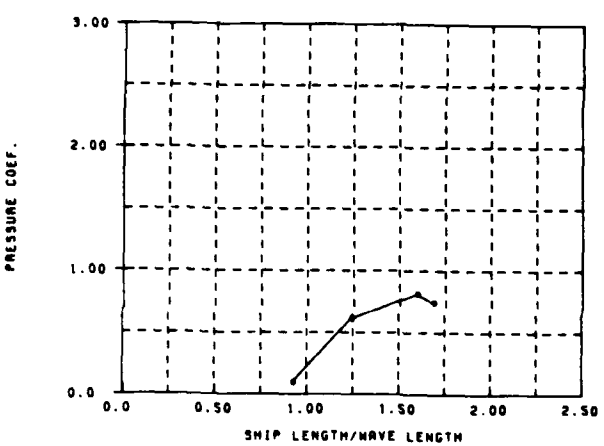


FIGURE 85: SL-7 PRESSURE RAO,  $F_n=0.32$ , TAP NO. 17

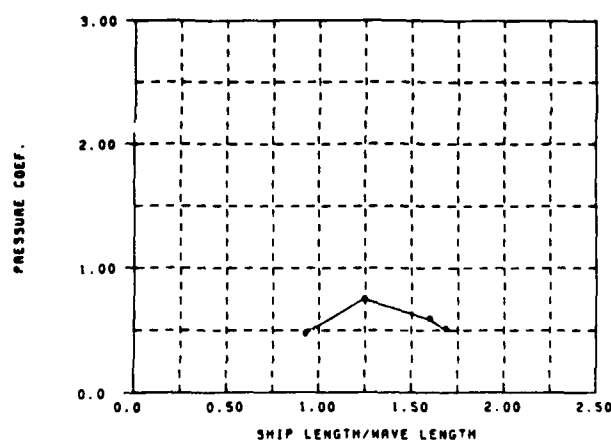


FIGURE 83: SL-7 PRESSURE RAO,  $F_n=0.32$ , TAP NO. 15

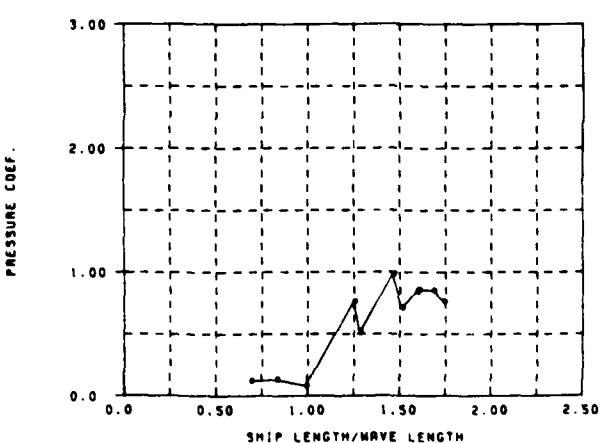


FIGURE 86: SL-7 PRESSURE RAO,  $F_n=0.32$ , TAP NO. 19

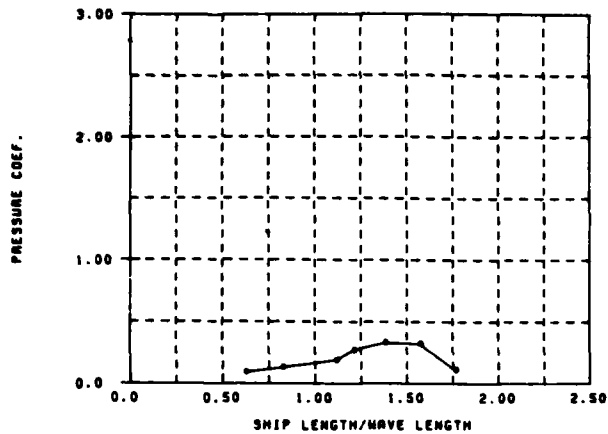


FIGURE 87: SL-7 PRESSURE RAO,  $F_n=0.32$ , TAP NO. 19

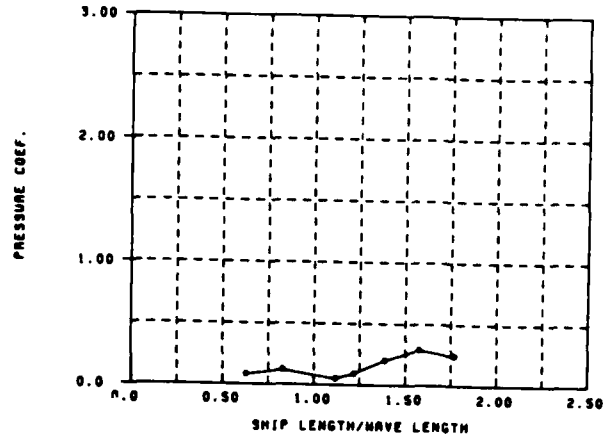


FIGURE 90: SL-7 PRESSURE RAO,  $F_n=0.32$ , TAP NO. 22

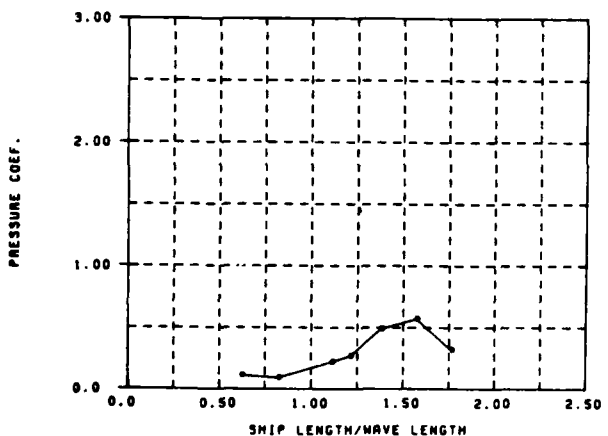


FIGURE 88: SL-7 PRESSURE RAO,  $F_n=0.32$ , TAP NO. 20

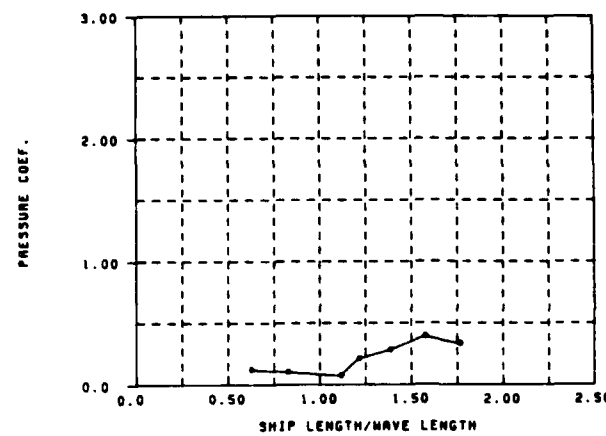


FIGURE 91: SL-7 PRESSURE RAO,  $F_n=0.32$ , TAP NO. 23

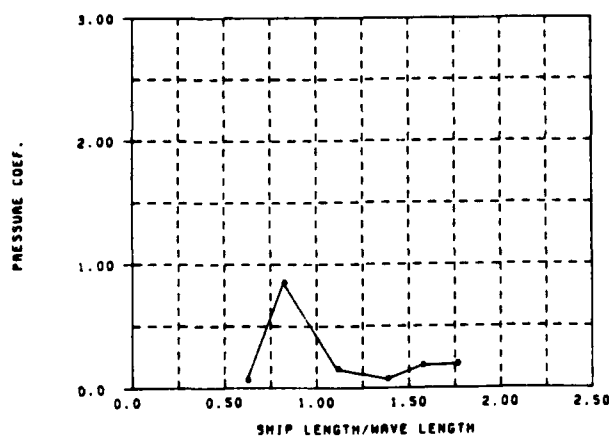


FIGURE 89: SL-7 PRESSURE RAO,  $F_n=0.32$ , TAP NO. 21

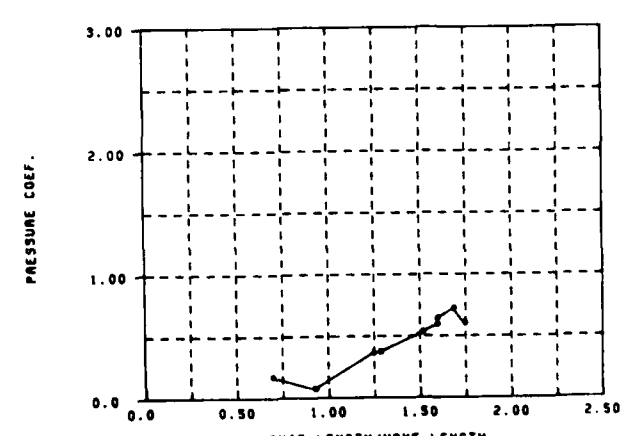


FIGURE 92: SL-7 PRESSURE RAO,  $F_n=0.32$ , TAP NO. 24

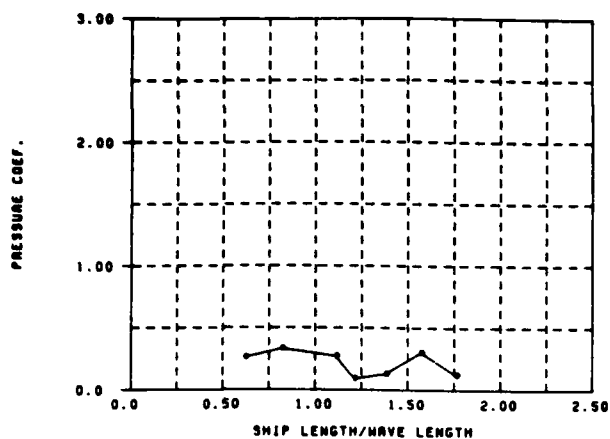


FIGURE 93: SL-7 PRESSURE RAO,  $F_n=0.32$ , TAP NO. 25

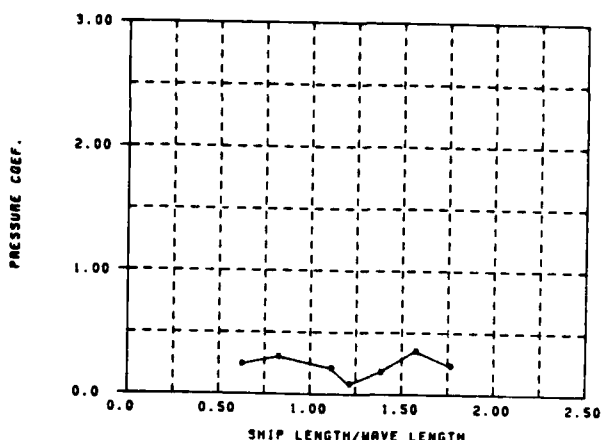


FIGURE 94: SL-7 PRESSURE RAO,  $F_n=0.32$ , TAP NO. 26

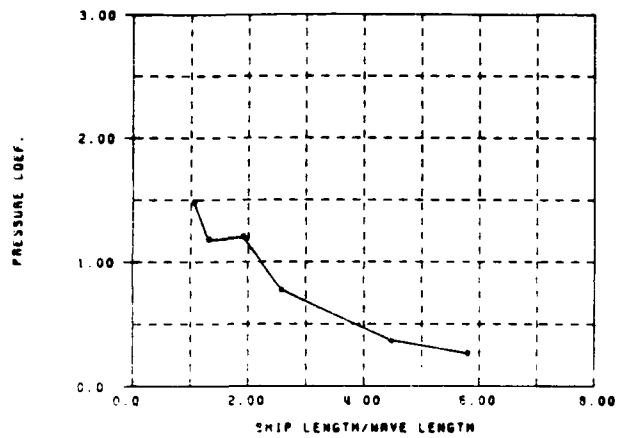


FIGURE 95: S.J. COAT PRESSURE RAO, FULL LOAD CONDITION,  $F_n=100$ , TAP NO. 1

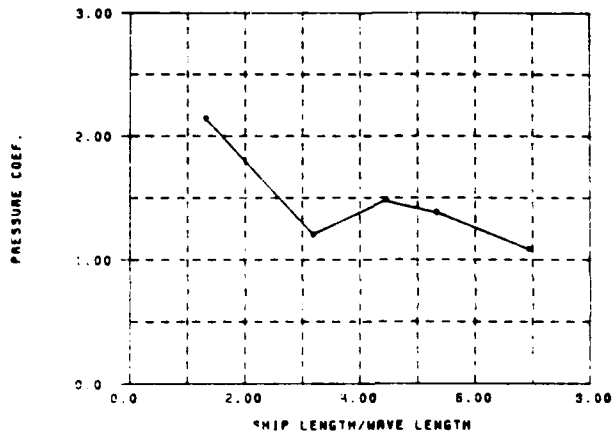


FIGURE 97: S.J. COAT PRESSURE RAO, FULL LOAD CONDITION,  $F_n=100$ , TAP NO. 3

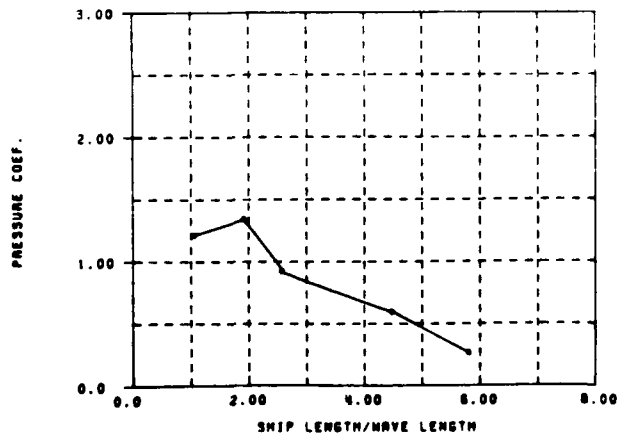


FIGURE 96: S.J. COAT PRESSURE RAO, FULL LOAD CONDITION,  $F_n=100$ , TAP NO. 2

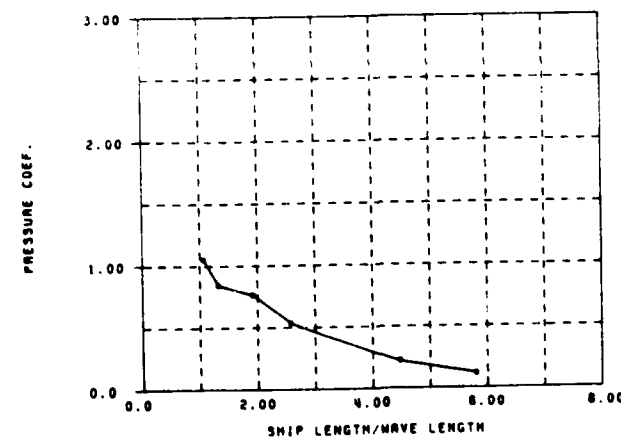


FIGURE 98: S.J. COAT PRESSURE RAO, FULL LOAD CONDITION,  $F_n=100$ , TAP NO. 4

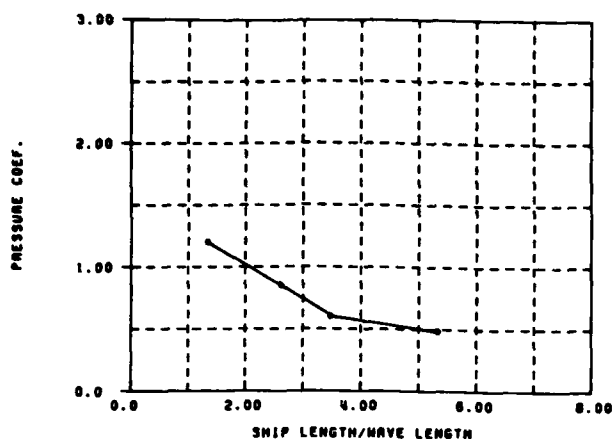


FIGURE 99: S-J. CORY PRESSURE RAO, FULL LOAD CONDITION,  $F_R=-100$ , TAP NO. 5

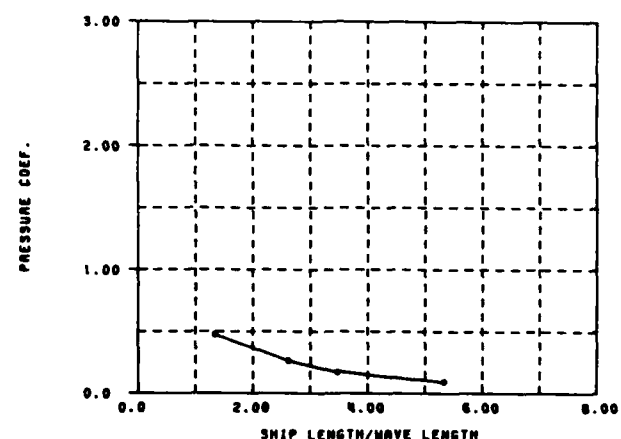


FIGURE 102: S-J. CORY PRESSURE RAO, FULL LOAD CONDITION,  $F_R=-100$ , TAP NO. 8

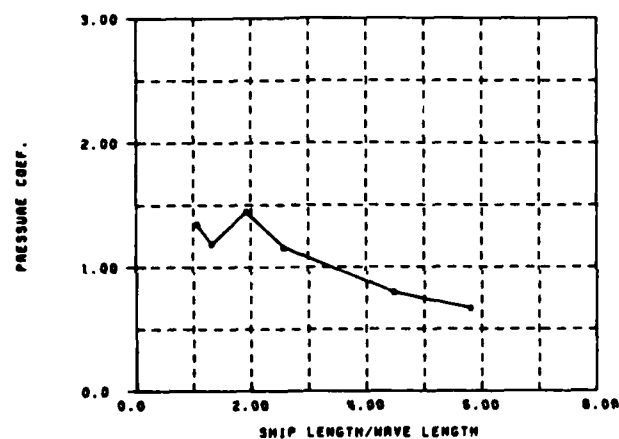


FIGURE 100: S-J. CORY PRESSURE RAO, FULL LOAD CONDITION,  $F_R=-100$ , TAP NO. 6

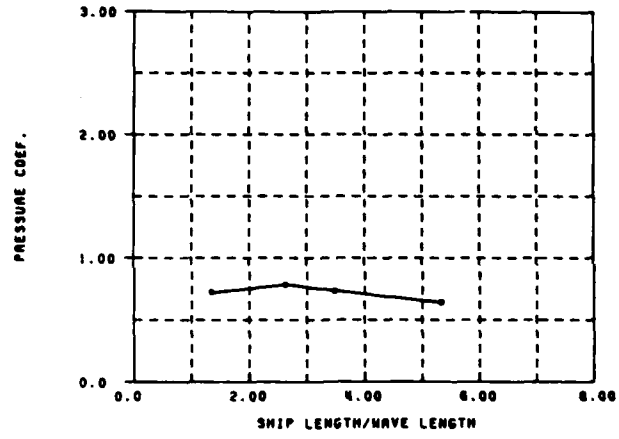


FIGURE 103: S-J. CORY PRESSURE RAO, FULL LOAD CONDITION,  $F_R=-100$ , TAP NO. 9

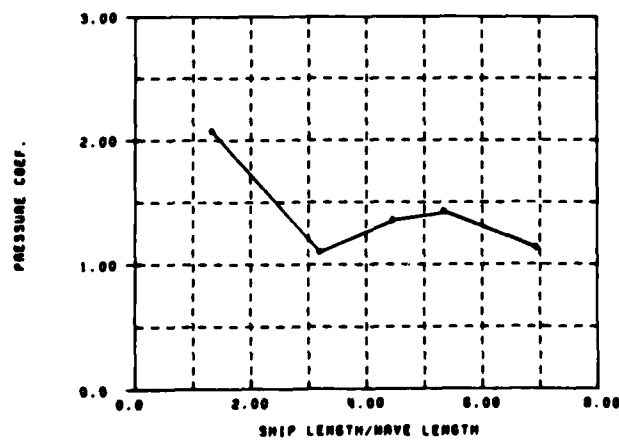


FIGURE 101: S-J. CORY PRESSURE RAO, FULL LOAD CONDITION,  $F_R=-100$ , TAP NO. 7

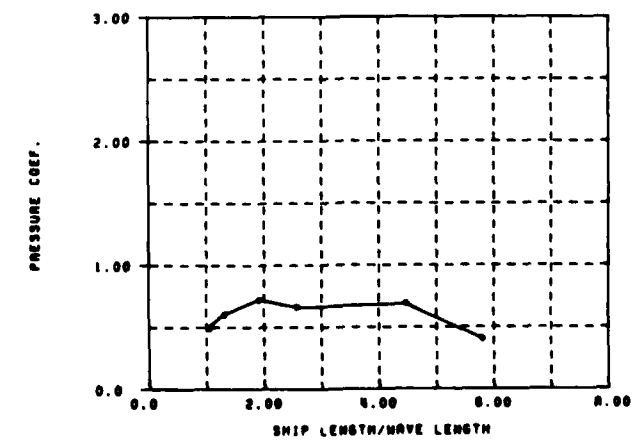


FIGURE 104: S-J. CORY PRESSURE RAO, FULL LOAD CONDITION,  $F_R=-100$ , TAP NO. 10

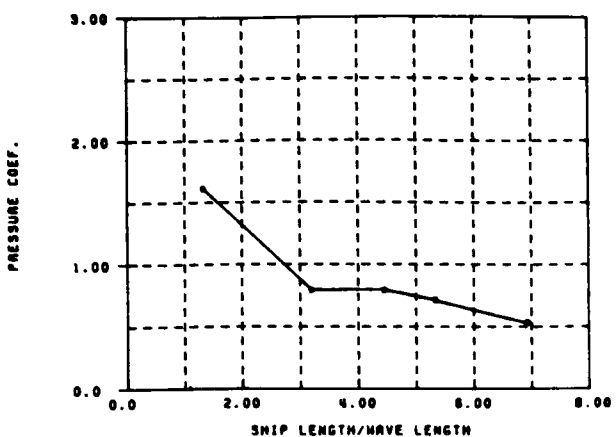


FIGURE 105: S.J. Coat Pressure RAO, FULL LOAD CONDITION,  $F_w=100$ , TAP NO. 11

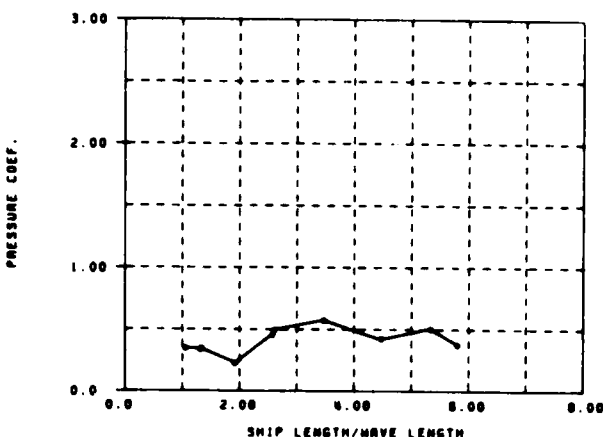


FIGURE 106: S.J. Coat Pressure RAO, FULL LOAD CONDITION,  $F_w=100$ , TAP NO. 14

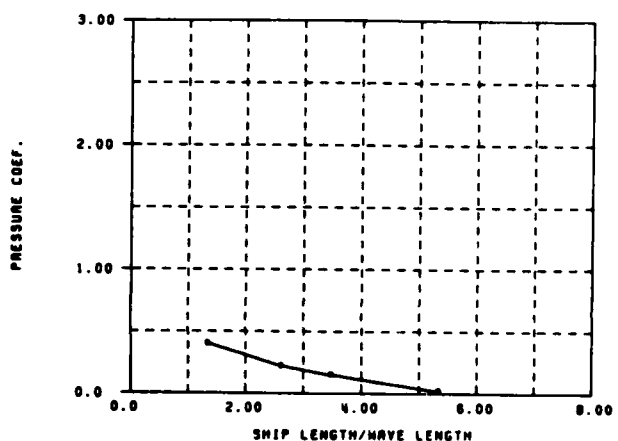


FIGURE 108: S.J. Coat Pressure RAO, FULL LOAD CONDITION,  $F_w=100$ , TAP NO. 12

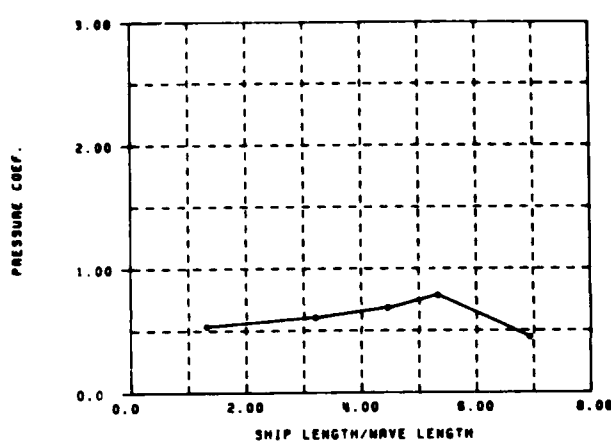


FIGURE 109: S.J. Coat Pressure RAO, FULL LOAD CONDITION,  $F_w=100$ , TAP NO. 15

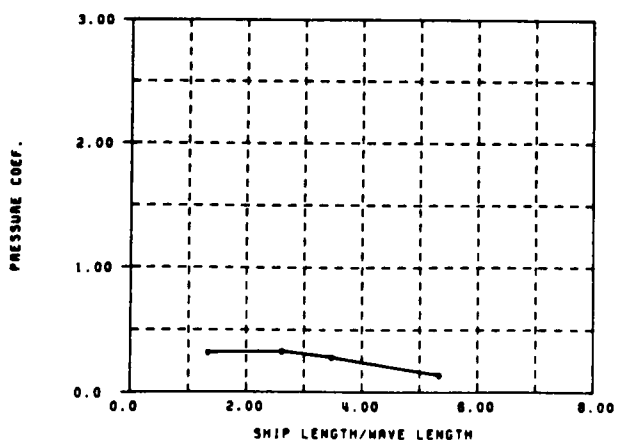


FIGURE 107: S.J. Coat Pressure RAO, FULL LOAD CONDITION,  $F_w=100$ , TAP NO. 13

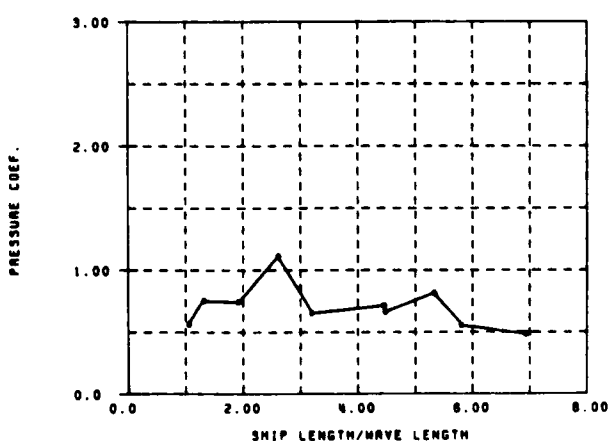


FIGURE 110: S.J. Coat Pressure RAO, FULL LOAD CONDITION,  $F_w=100$ , TAP NO. 16

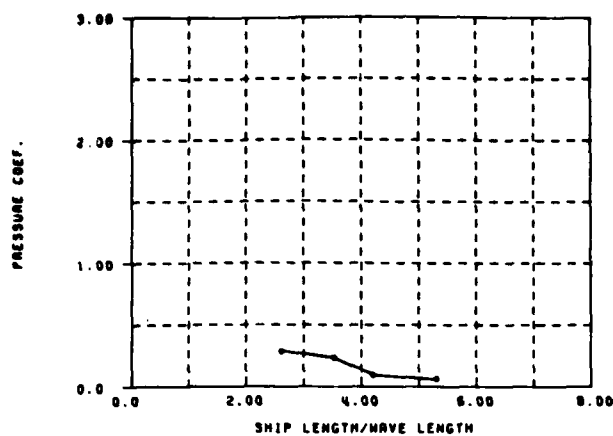


FIGURE 111: S.J. CORY PRESSURE RAO, FULL LOAD CONDITION,  $F_N=100$ , TAP NO. 17

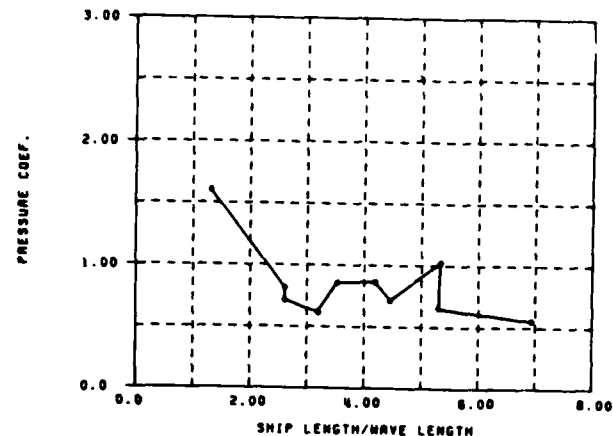


FIGURE 114: S.J. CORY PRESSURE RAO, FULL LOAD CONDITION,  $F_N=100$ , TAP NO. 20

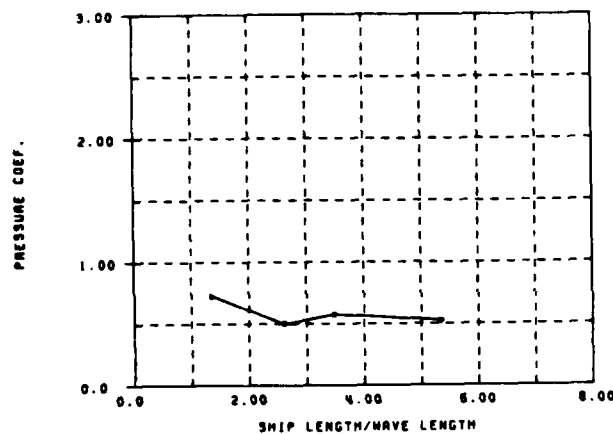


FIGURE 112: S.J. CORY PRESSURE RAO, FULL LOAD CONDITION,  $F_N=100$ , TAP NO. 18

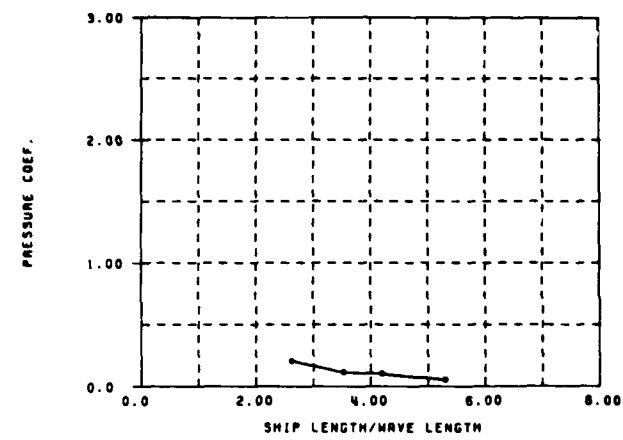


FIGURE 115: S.J. CORY PRESSURE RAO, FULL LOAD CONDITION,  $F_N=100$ , TAP NO. 21

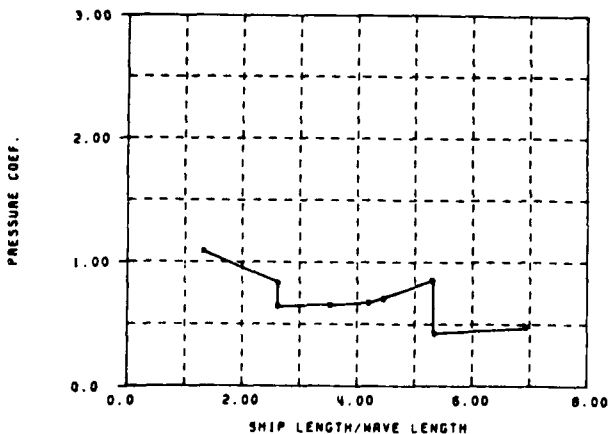


FIGURE 113: S.J. CORY PRESSURE RAO, FULL LOAD CONDITION,  $F_N=100$ , TAP NO. 19

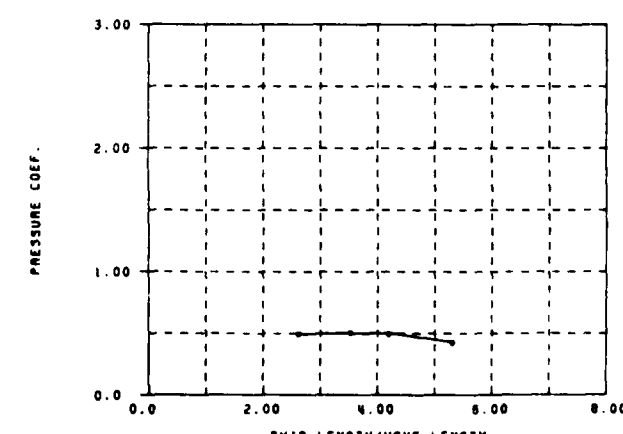


FIGURE 116: S.J. CORY PRESSURE RAO, FULL LOAD CONDITION,  $F_N=100$ , TAP NO. 22

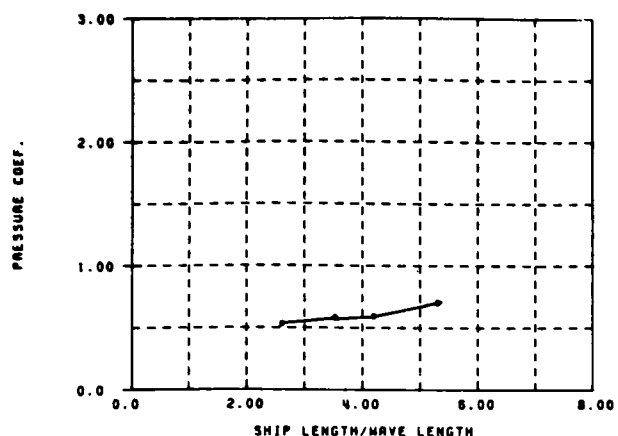


FIGURE 117: S-J. CORT PRESSURE RAO, FULL LOAD CONDITION,  $F_N=-100$ , TAP NO. 23

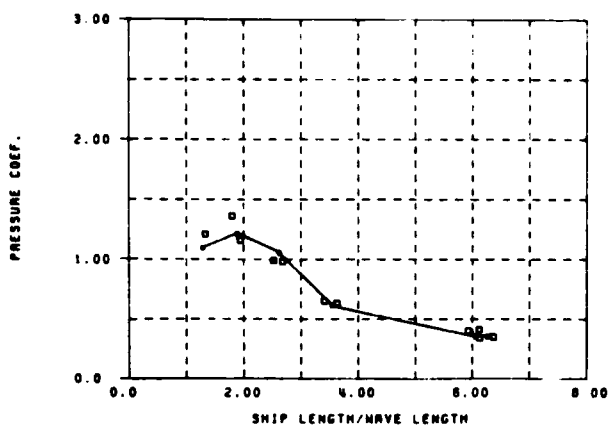


FIGURE 120: S-J. CORT PRESSURE RAO, FULL LOAD CONDITION,  $F_N=-132$ , TAP NO. 2

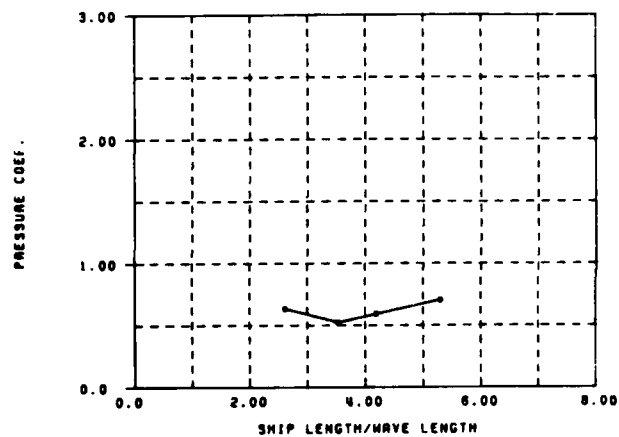


FIGURE 118: S-J. CORT PRESSURE RAO, FULL LOAD CONDITION,  $F_N=-100$ , TAP NO. 24

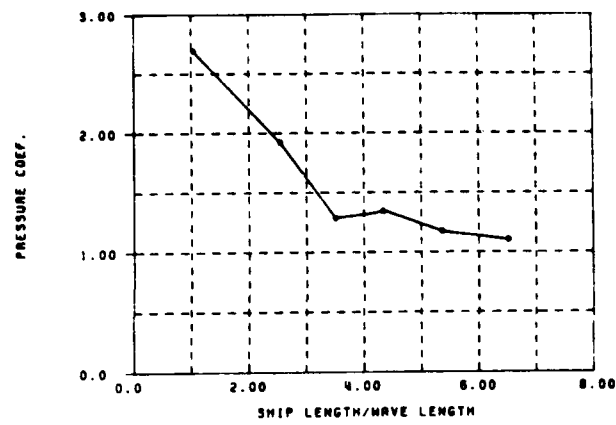


FIGURE 121: S-J. CORT PRESSURE RAO, FULL LOAD CONDITION,  $F_N=-132$ , TAP NO. 3

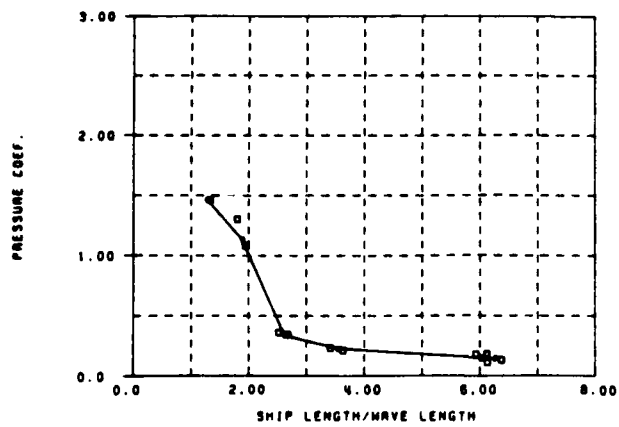


FIGURE 119: S-J. CORT PRESSURE RAO, FULL LOAD CONDITION,  $F_N=-132$ , TAP NO. 1

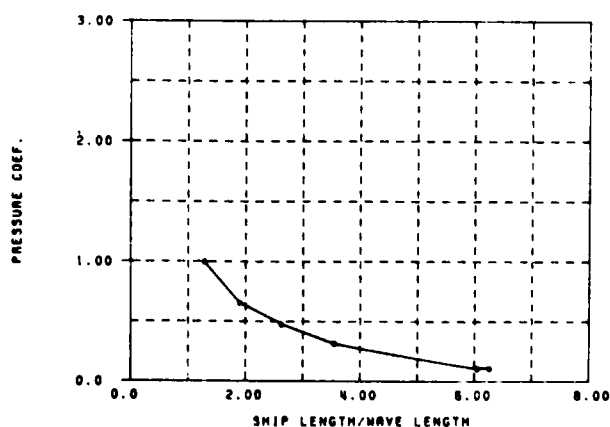


FIGURE 122: S-J. CORT PRESSURE RAO, FULL LOAD CONDITION,  $F_N=-132$ , TAP NO. 8

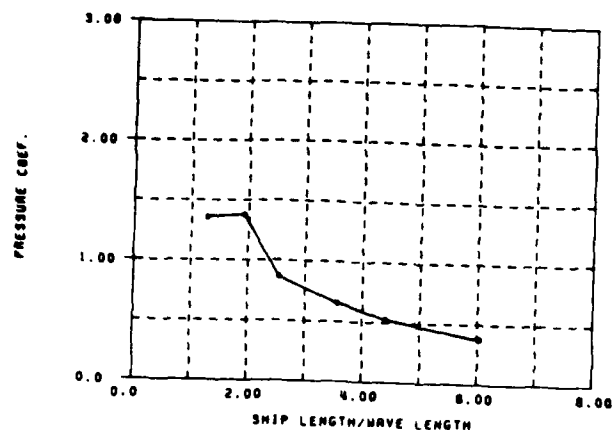


FIGURE 123: S.J. CORT PRESSURE RAO, FULL LOAD CONDITION,  $F_N=132$ , TAP NO. 5

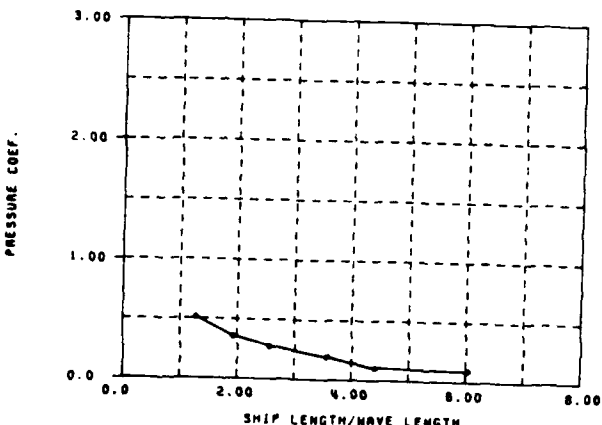


FIGURE 126: S.J. CORT PRESSURE RAO, FULL LOAD CONDITION,  $F_N=132$ , TAP NO. 8

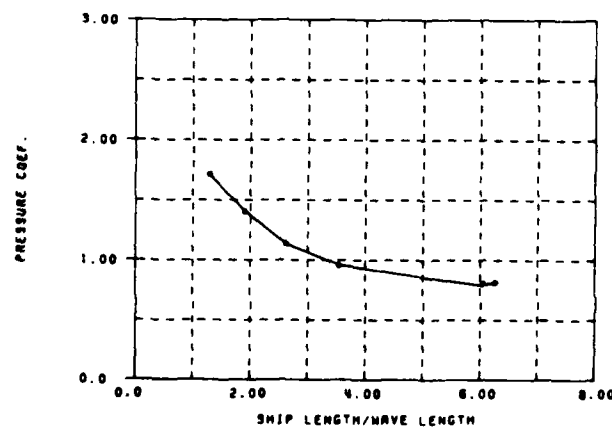


FIGURE 128: S.J. CORT PRESSURE RAO, FULL LOAD CONDITION,  $F_N=132$ , TAP NO. 6

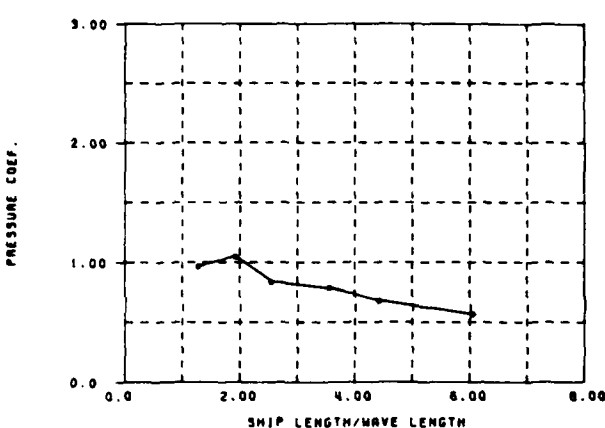


FIGURE 127: S.J. CORT PRESSURE RAO, FULL LOAD CONDITION,  $F_N=132$ , TAP NO. 9

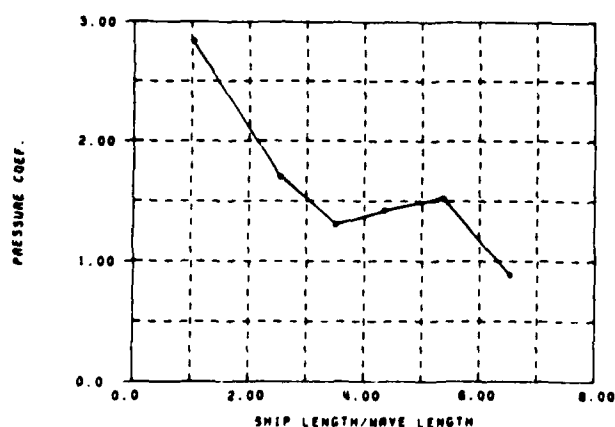


FIGURE 125: S.J. CORT PRESSURE RAO, FULL LOAD CONDITION,  $F_N=132$ , TAP NO. 7

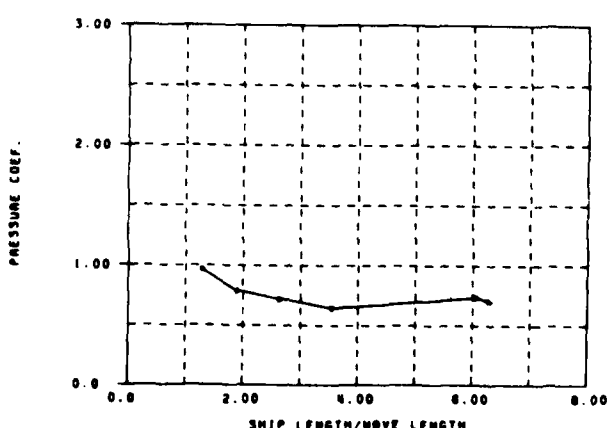


FIGURE 128: S.J. CORT PRESSURE RAO, FULL LOAD CONDITION,  $F_N=132$ , TAP NO. 10

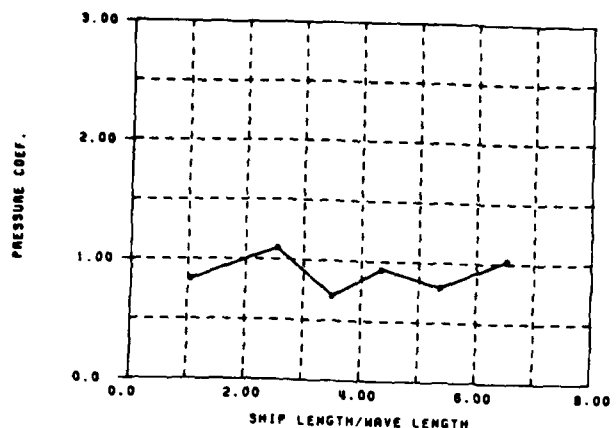


FIGURE 129: S.J. CORY PRESSURE RAO, FULL LOAD CONDITION,  $F_N=132$ , TAP NO. 11

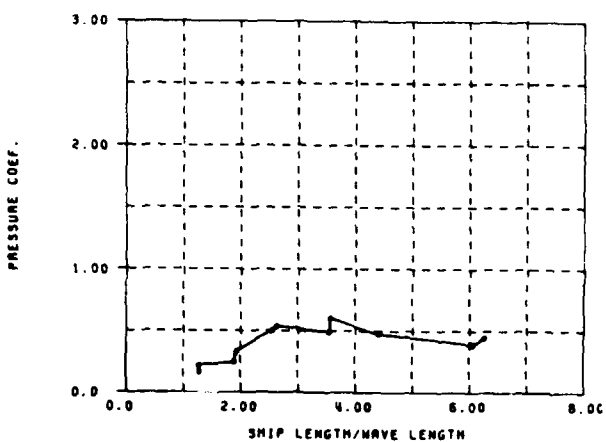


FIGURE 132: S.J. CORY PRESSURE RAO, FULL LOAD CONDITION,  $F_N=132$ , TAP NO. 14

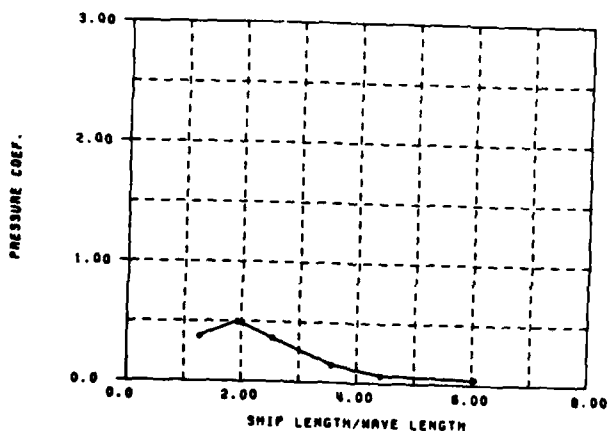


FIGURE 130: S.J. CORY PRESSURE RAO, FULL LOAD CONDITION,  $F_N=132$ , TAP NO. 12

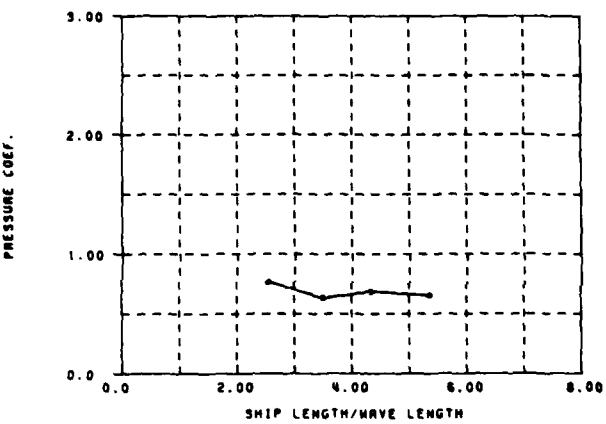


FIGURE 133: S.J. CORY PRESSURE RAO, FULL LOAD CONDITION,  $F_N=132$ , TAP NO. 15

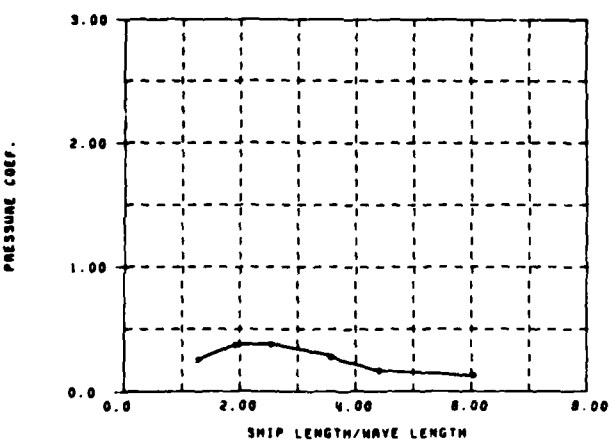


FIGURE 131: S.J. CORY PRESSURE RAO, FULL LOAD CONDITION,  $F_N=132$ , TAP NO. 13

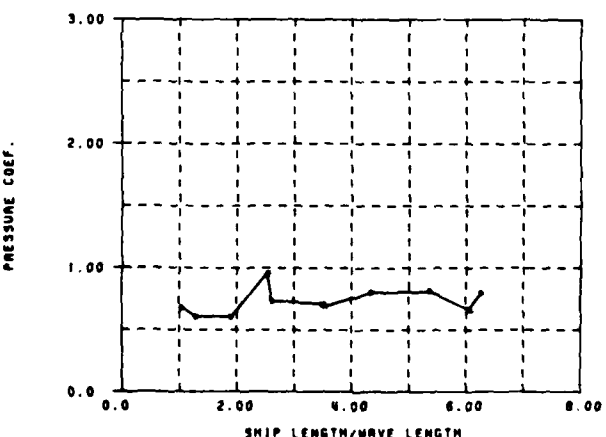


FIGURE 134: S.J. CORY PRESSURE RAO, FULL LOAD CONDITION,  $F_N=132$ , TAP NO. 16

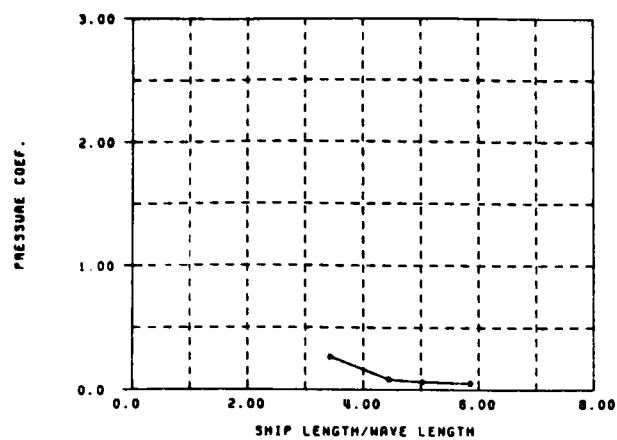


FIGURE 135: S.J. CORY PRESSURE RAO, FULL LOAD CONDITION,  $F_N=132$ , TAP NO. 17

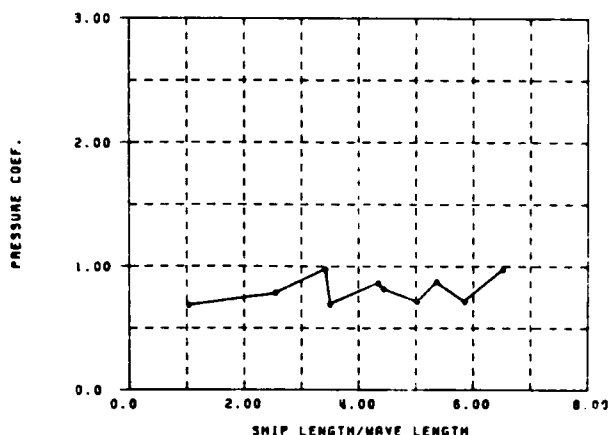


FIGURE 138: S.J. CORY PRESSURE RAO, FULL LOAD CONDITION,  $F_N=132$ , TAP NO. 20

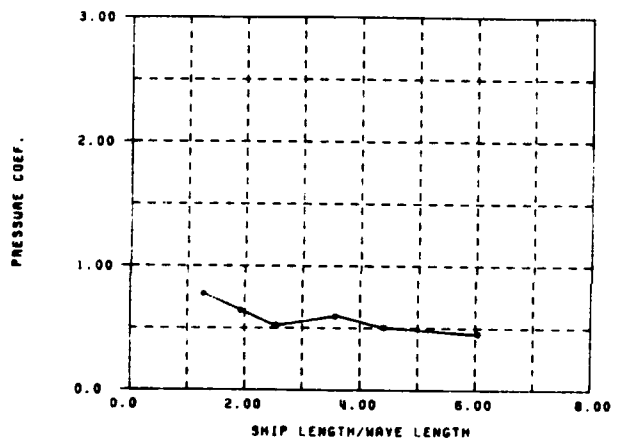


FIGURE 136: S.J. CORY PRESSURE RAO, FULL LOAD CONDITION,  $F_N=132$ , TAP NO. 18

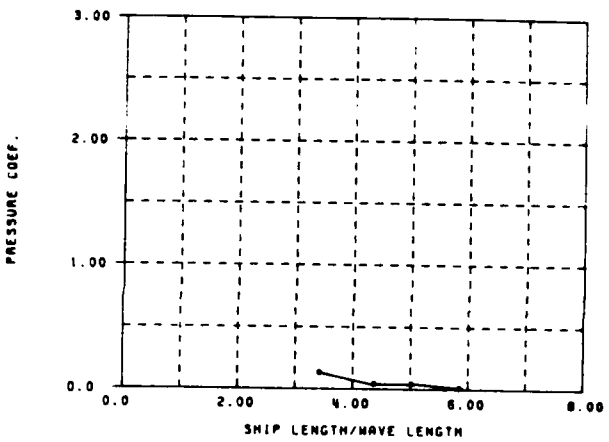


FIGURE 139: S.J. CORY PRESSURE RAO, FULL LOAD CONDITION,  $F_N=132$ , TAP NO. 21

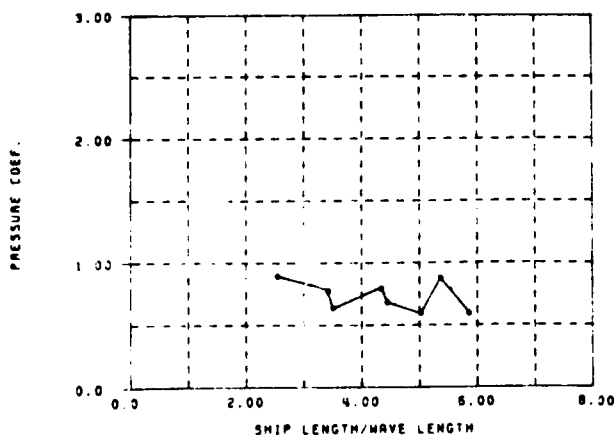


FIGURE 137: S.J. CORY PRESSURE RAO, FULL LOAD CONDITION,  $F_N=132$ , TAP NO. 19

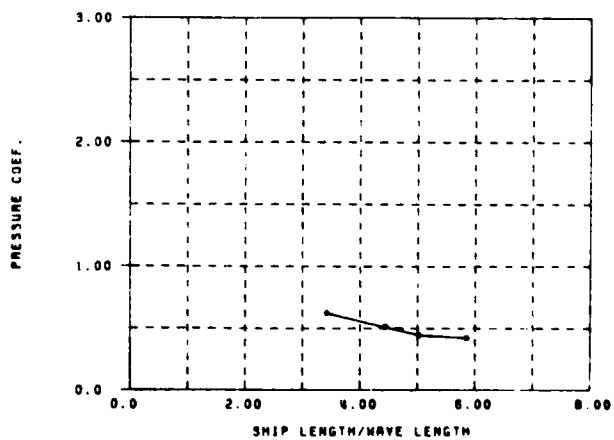


FIGURE 140: S.J. CORY PRESSURE RAO, FULL LOAD CONDITION,  $F_N=132$ , TAP NO. 22

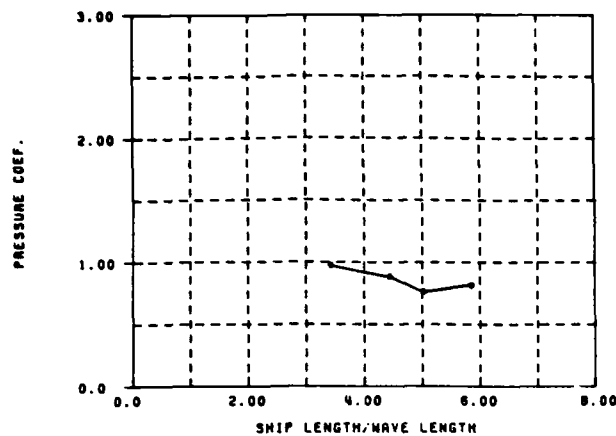


FIGURE 141: S.J. CORT PRESSURE RAO, FULL LOAD CONDITION,  $F_R=132$ , TAP NO. 23

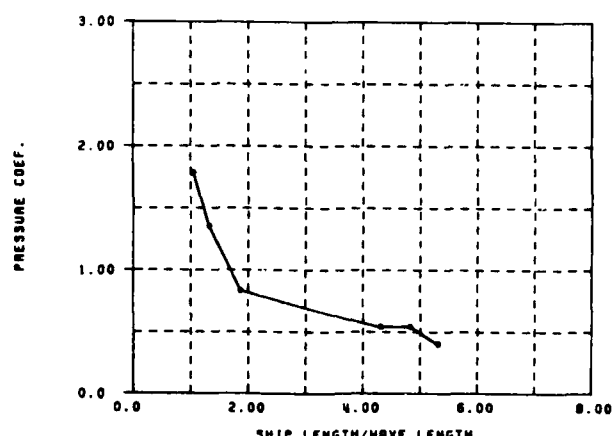


FIGURE 144: S.J. CORT PRESSURE RAO, BALLAST CONDITION,  $F_R=100$ , TAP NO. 4

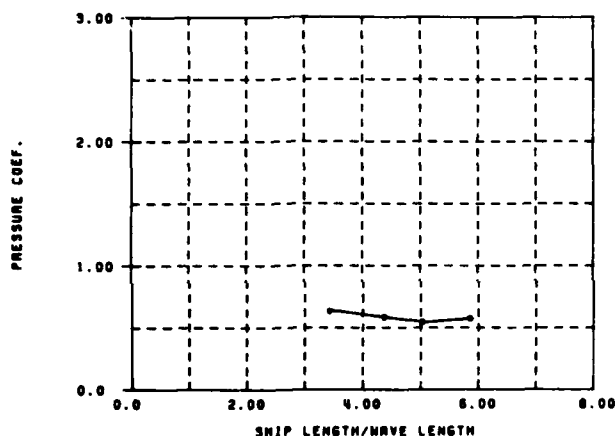


FIGURE 142: S.J. CORT PRESSURE RAO, FULL LOAD CONDITION,  $F_R=132$ , TAP NO. 24

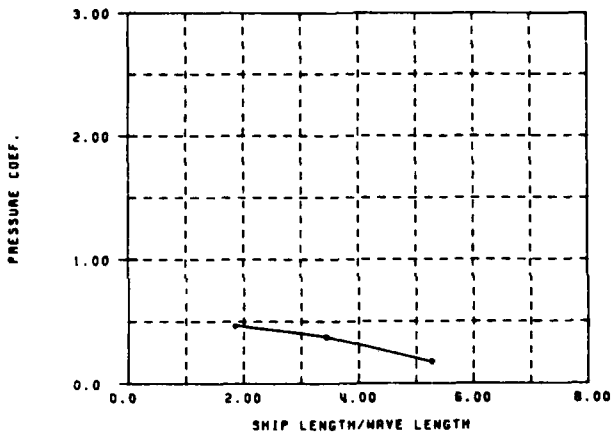


FIGURE 145: S.J. CORT PRESSURE RAO, BALLAST CONDITION,  $F_R=100$ , TAP NO. 8

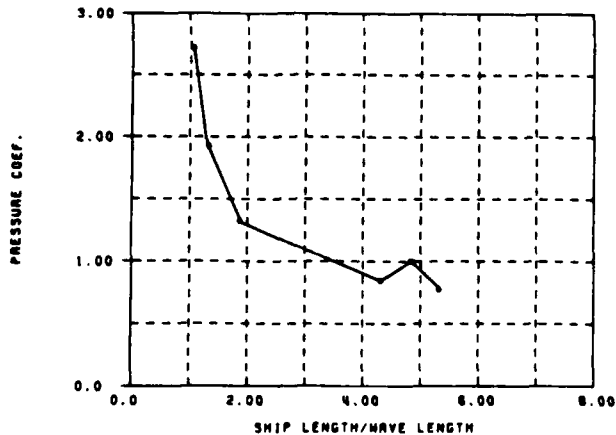


FIGURE 143: S.J. CORT PRESSURE RAO, BALLAST CONDITION,  $F_R=100$ , TAP NO. 1

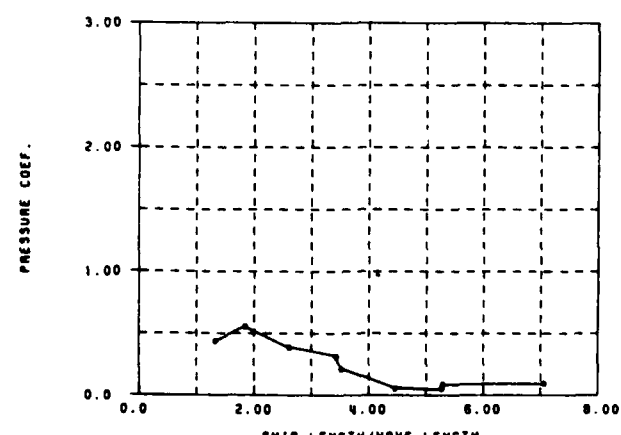


FIGURE 146: S.J. CORT PRESSURE RAO, BALLAST CONDITION,  $F_R=100$ , TAP NO. 12

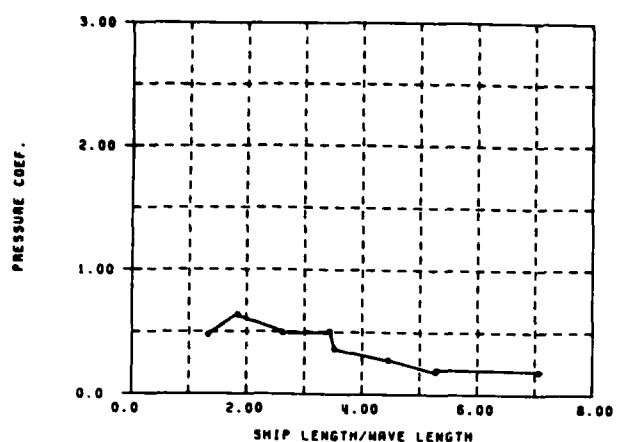


FIGURE 147: S.J. CORY PRESSURE RAO, BALLAST CONDITION,  $F_N=100$ , TAP NO. 13

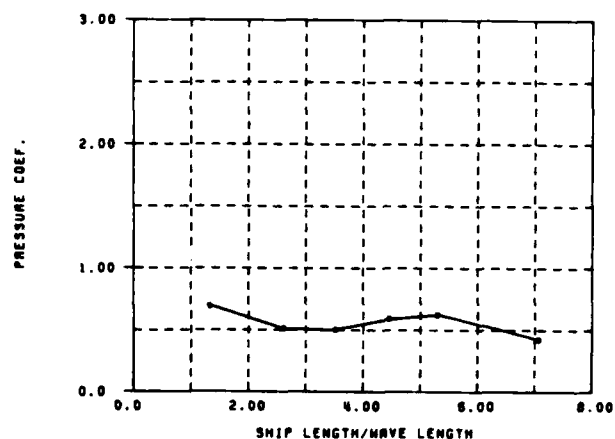


FIGURE 150: S.J. CORY PRESSURE RAO, BALLAST CONDITION,  $F_N=100$ , TAP NO. 18

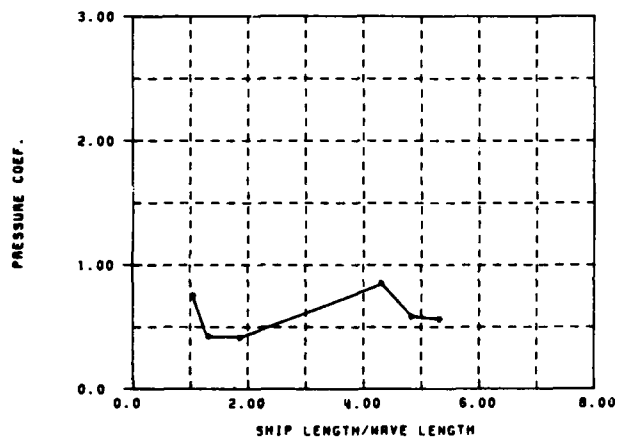


FIGURE 148: S.J. CORY PRESSURE RAO, BALLAST CONDITION,  $F_N=100$ , TAP NO. 14

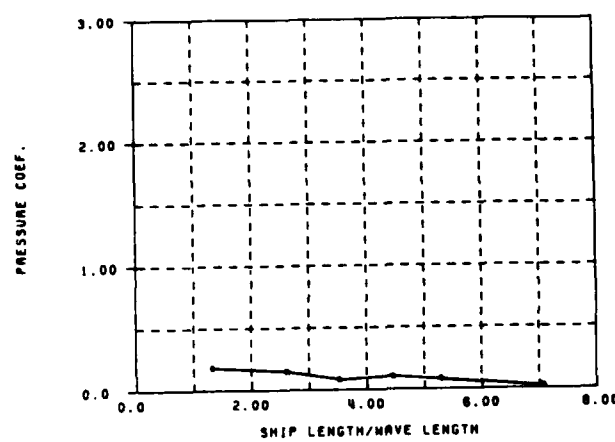


FIGURE 151: S.J. CORY PRESSURE RAO, BALLAST CONDITION,  $F_N=100$ , TAP NO. 21

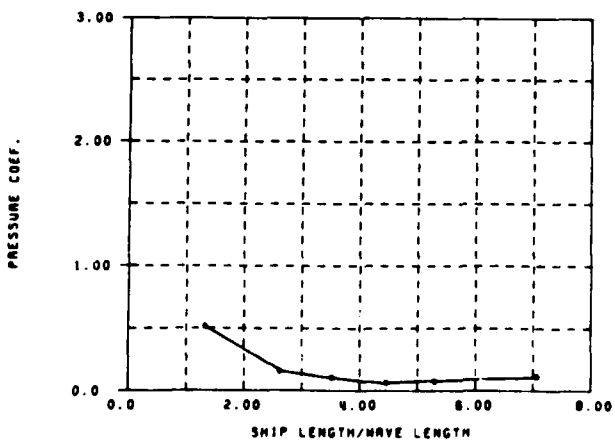


FIGURE 149: S.J. CORY PRESSURE RAO, BALLAST CONDITION,  $F_N=100$ , TAP NO. 17

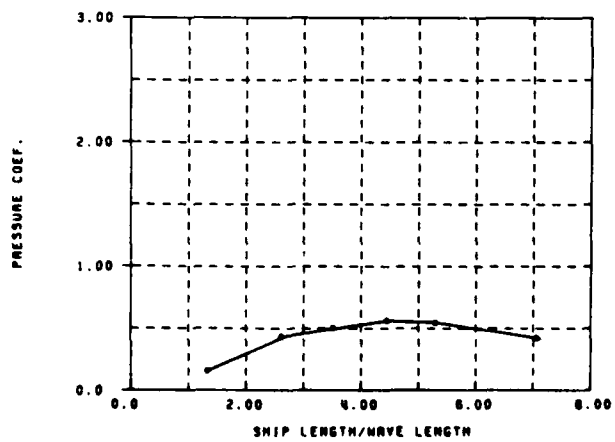


FIGURE 152: S.J. CORY PRESSURE RAO, BALLAST CONDITION,  $F_N=100$ , TAP NO. 22

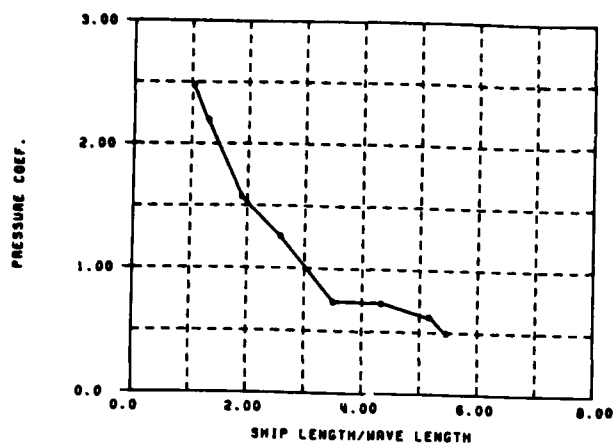


FIGURE 153: S-J. CORY PRESSURE RAO, BALLAST CONDITION,  $F_N=132$ , TAP NO. 1

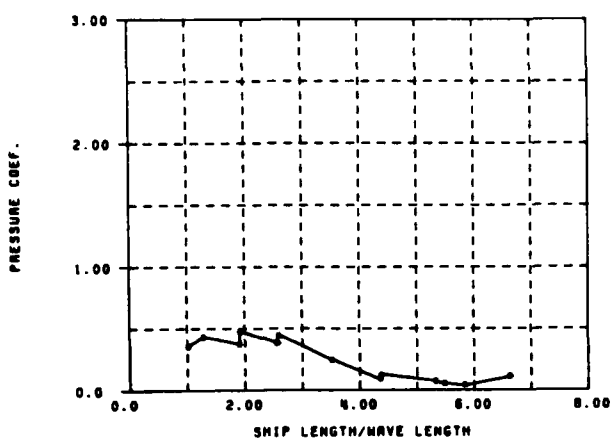


FIGURE 156: S-J. CORY PRESSURE RAO, BALLAST CONDITION,  $F_N=132$ , TAP NO. 12

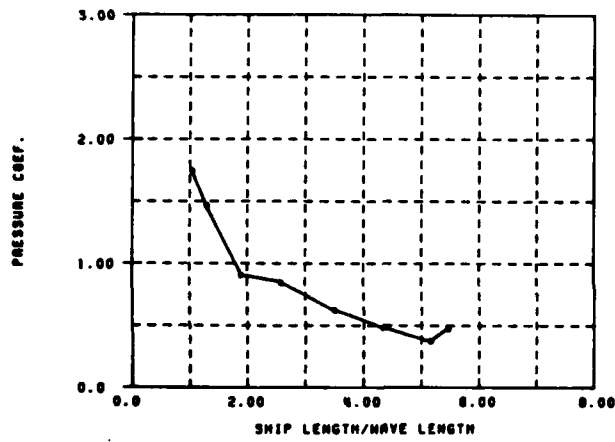


FIGURE 154: S-J. CORY PRESSURE RAO, BALLAST CONDITION,  $F_N=132$ , TAP NO. 8

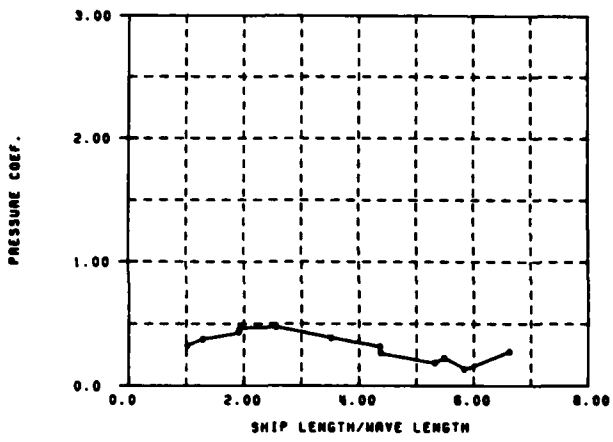


FIGURE 157: S-J. CORY PRESSURE RAO, BALLAST CONDITION,  $F_N=132$ , TAP NO. 13

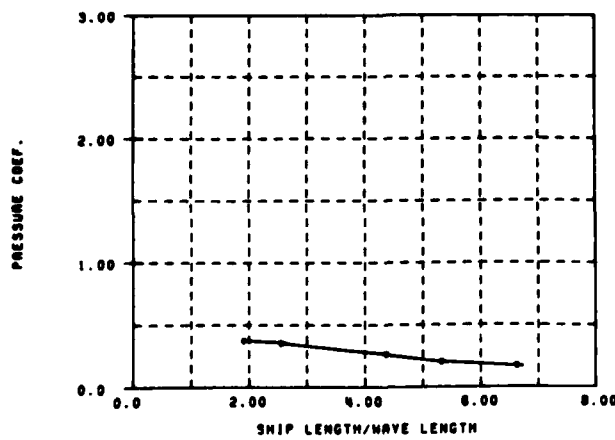


FIGURE 155: S-J. CORY PRESSURE RAO, BALLAST CONDITION,  $F_N=132$ , TAP NO. 9

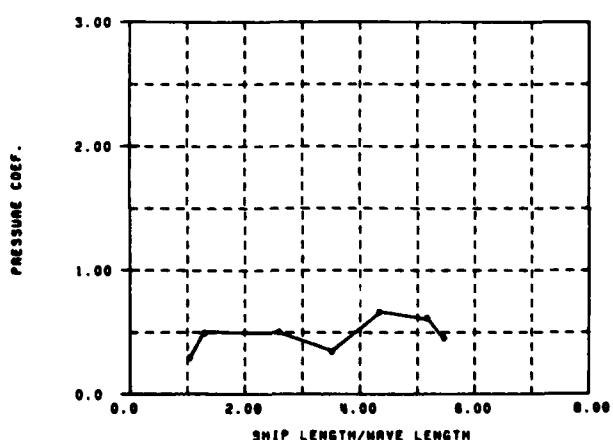


FIGURE 158: S-J. CORY PRESSURE RAO, BALLAST CONDITION,  $F_N=132$ , TAP NO. 14

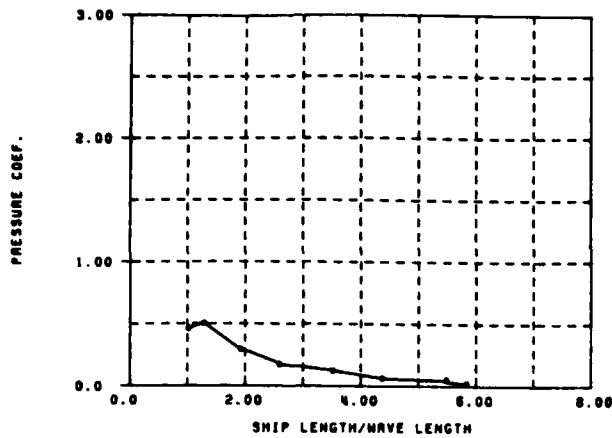


FIGURE 159: S-J. CORT PRESSURE RAO, BALLAST CONDITION,  $F_N=152$ , TAP NO. 17

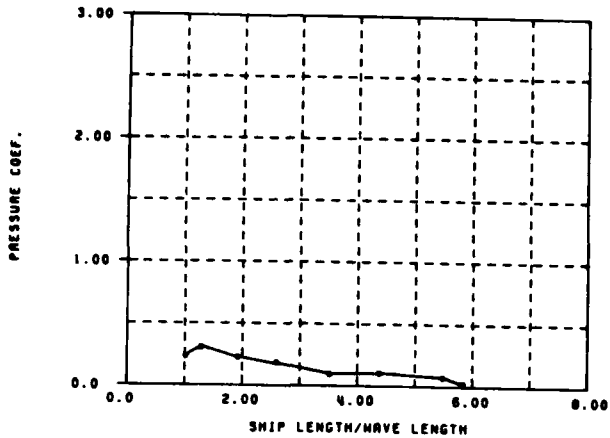


FIGURE 161: S-J. CORT PRESSURE RAO, BALLAST CONDITION,  $F_N=132$ , TAP NO. 21

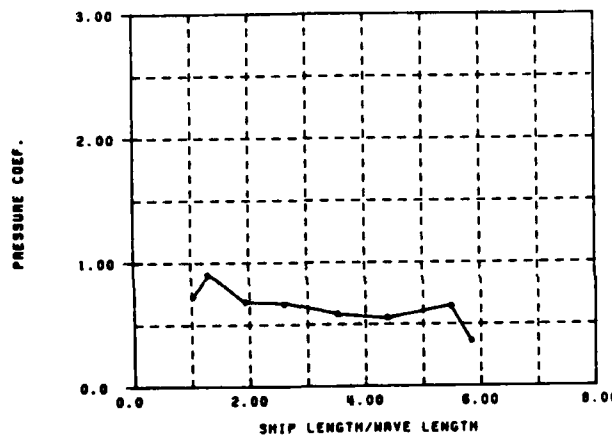


FIGURE 160: S-J. CORT PRESSURE RAO, BALLAST CONDITION,  $F_N=132$ , TAP NO. 18

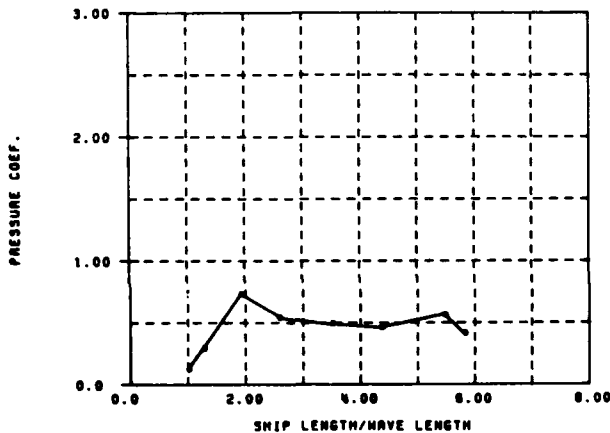


FIGURE 162: S-J. CORT PRESSURE RAO, BALLAST CONDITION,  $F_N=132$ , TAP NO. 22

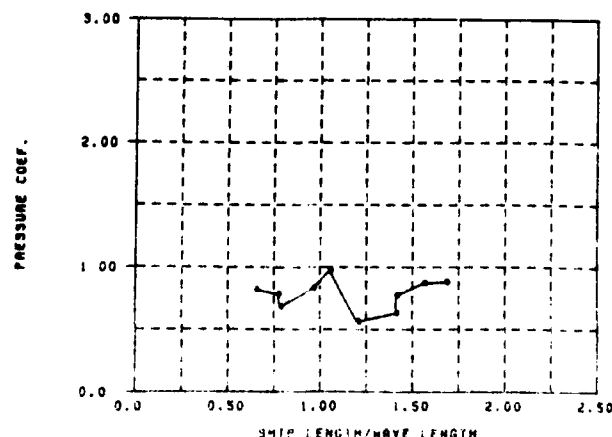


FIGURE 163: SL-7 PRESSURE RAO, RESTRAINED FROM MOTION,  $F_N=23$ , TAP NO. 1

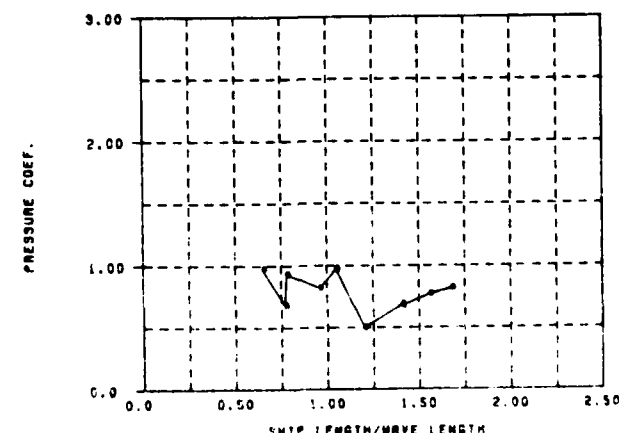


FIGURE 164: SL-7 PRESSURE RAO, RESTRAINED FROM MOTION,  $F_N=23$ , TAP NO. 2

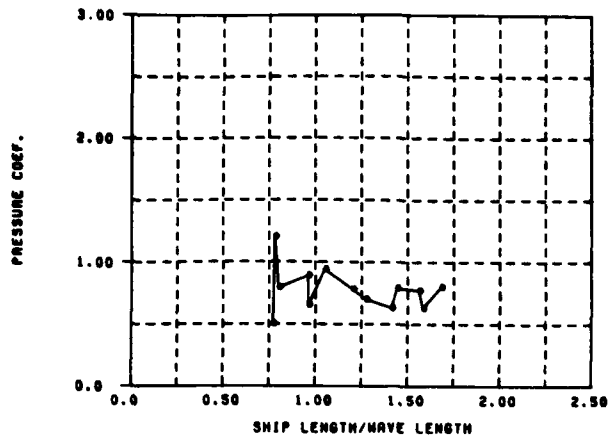


FIGURE 165: SL-7 PRESSURE RAO, RESTRAINED FROM MOTION,  $F_n=0.23$ , TAP NO. 3

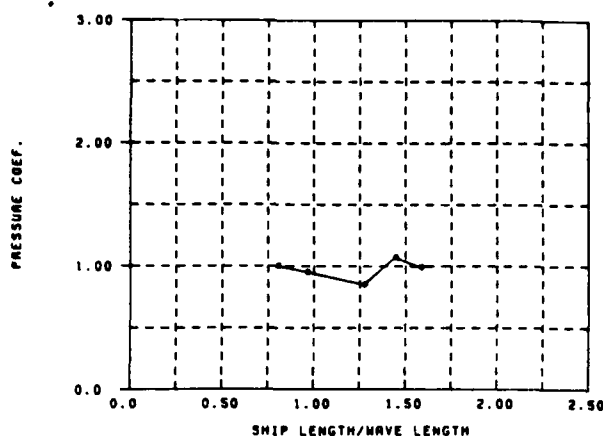


FIGURE 166: SL-7 PRESSURE RAO, RESTRAINED FROM MOTION,  $F_n=0.23$ , TAP NO. 7

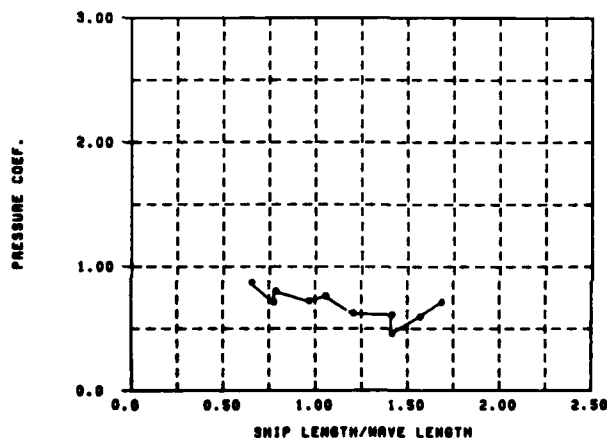


FIGURE 167: SL-7 PRESSURE RAO, RESTRAINED FROM MOTION,  $F_n=0.23$ , TAP NO. 4

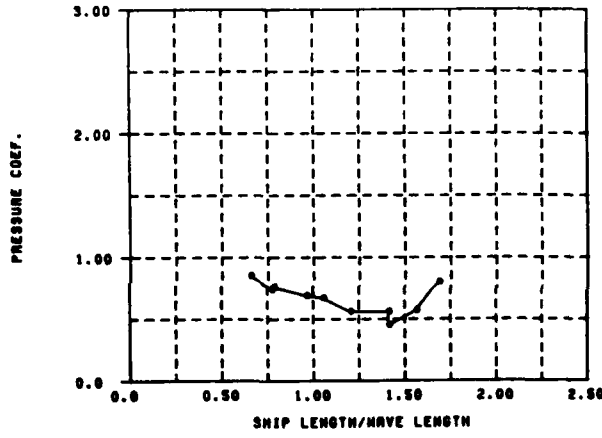


FIGURE 168: SL-7 PRESSURE RAO, RESTRAINED FROM MOTION,  $F_n=0.23$ , TAP NO. 8

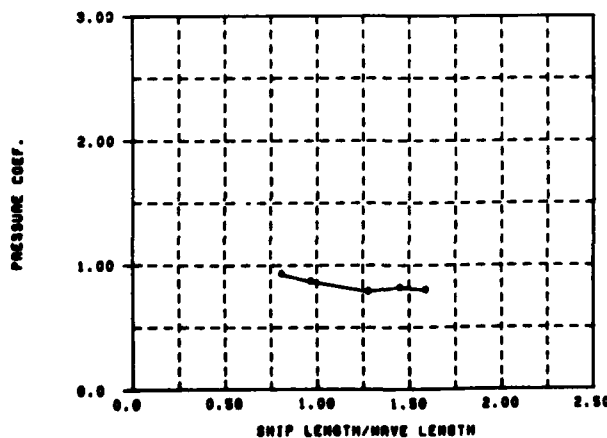


FIGURE 169: SL-7 PRESSURE RAO, RESTRAINED FROM MOTION,  $F_n=0.23$ , TAP NO. 5

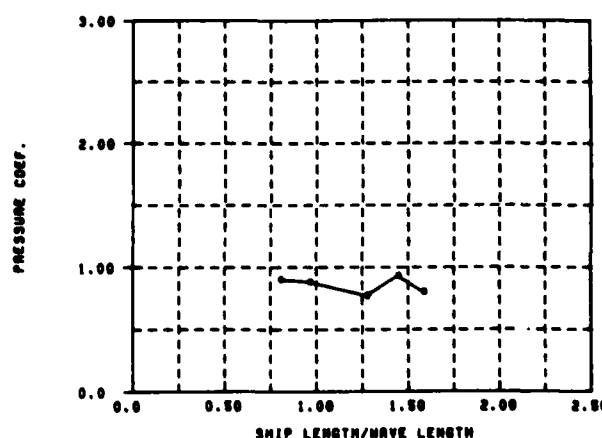


FIGURE 170: SL-7 PRESSURE RAO, RESTRAINED FROM MOTION,  $F_n=0.23$ , TAP NO. 9

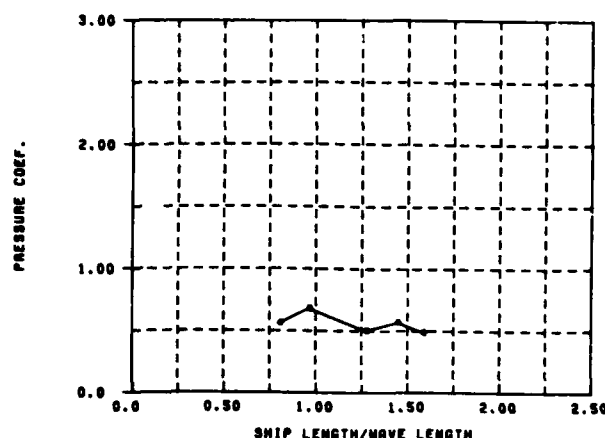


FIGURE 171: SL-7 PRESSURE RAO, RESTRAINED FROM MOTION,  $F_y=0.25$ , TAP NO. 10

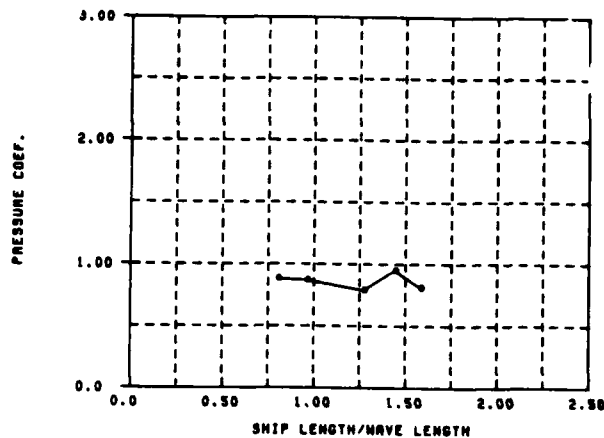


FIGURE 174: SL-7 PRESSURE RAO, RESTRAINED FROM MOTION,  $F_y=0.25$ , TAP NO. 13

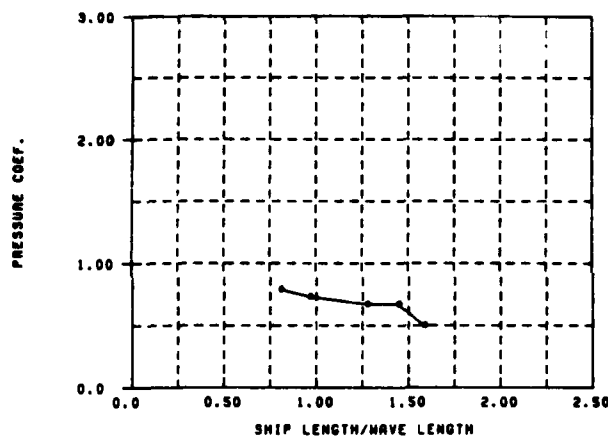


FIGURE 172: SL-7 PRESSURE RAO, RESTRAINED FROM MOTION,  $F_y=0.25$ , TAP NO. 11

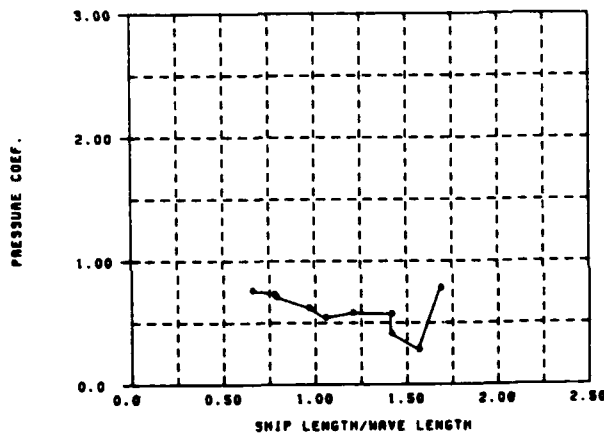


FIGURE 175: SL-7 PRESSURE RAO, RESTRAINED FROM MOTION,  $F_y=0.25$ , TAP NO. 14

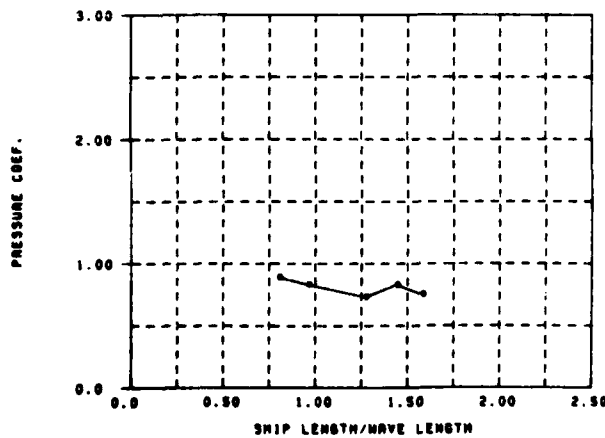


FIGURE 173: SL-7 PRESSURE RAO, RESTRAINED FROM MOTION,  $F_y=0.25$ , TAP NO. 12

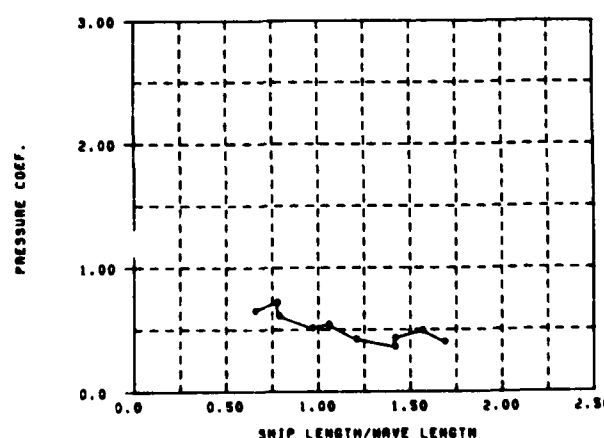


FIGURE 176: SL-7 PRESSURE RAO, RESTRAINED FROM MOTION,  $F_y=0.25$ , TAP NO. 15

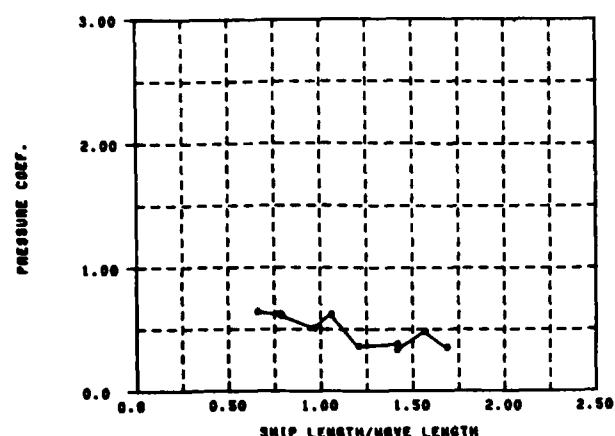


Figure 177: SL-7 Pressure RAO, RESTRAINED FROM MOTION,  $F_R=0.25$ , TAP NO. 21

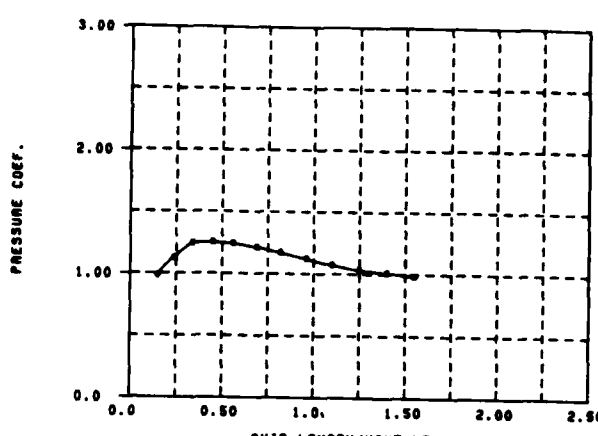


Figure 180: SL-7 PRESSURE RAO, FORCED HEAVE MOTION,  $F_R=0.25$ , TAP NO. 4

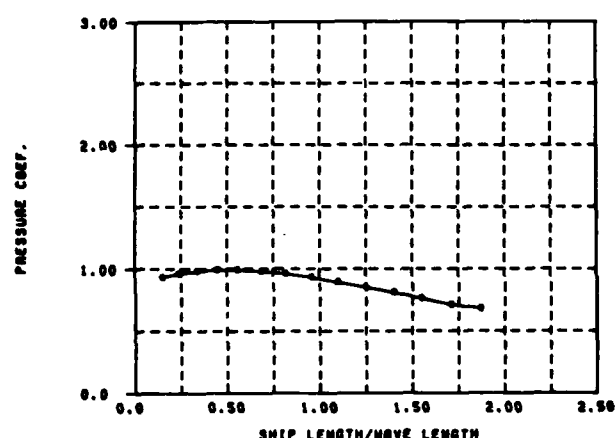


Figure 178: SL-7 PRESSURE RAO, FORCED HEAVE MOTION,  $F_R=0.25$ , TAP NO. 2

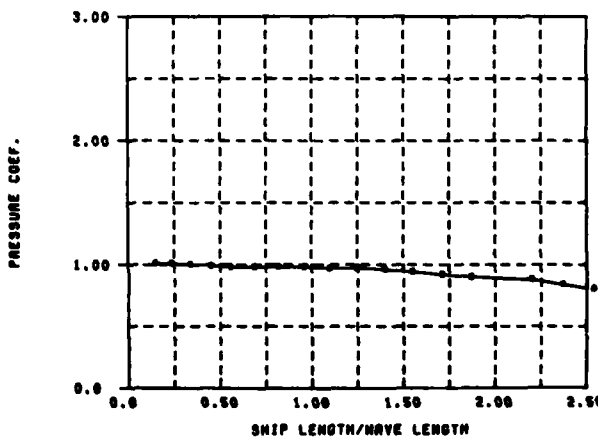


Figure 181: SL-7 PRESSURE RAO, FORCED HEAVE MOTION,  $F_R=0.25$ , TAP NO. 6

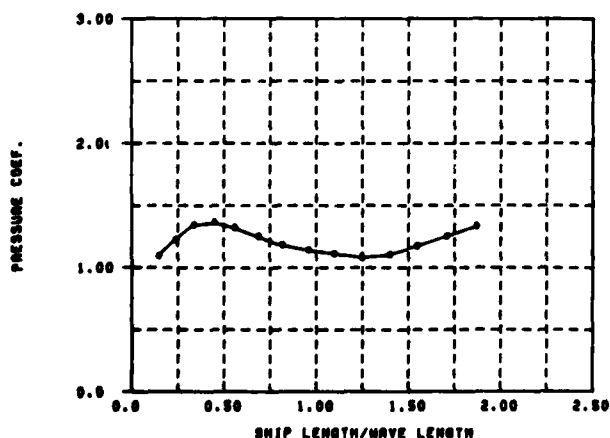


Figure 179: SL-7 PRESSURE RAO, FORCED HEAVE MOTION,  $F_R=0.25$ , TAP NO. 3

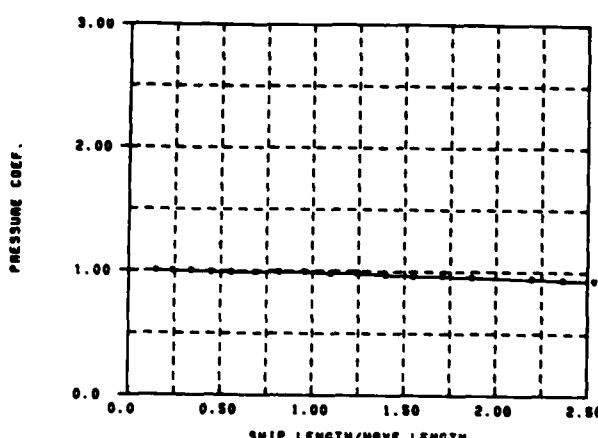


Figure 182: SL-7 PRESSURE RAO, FORCED HEAVE MOTION,  $F_R=0.25$ , TAP NO. 7

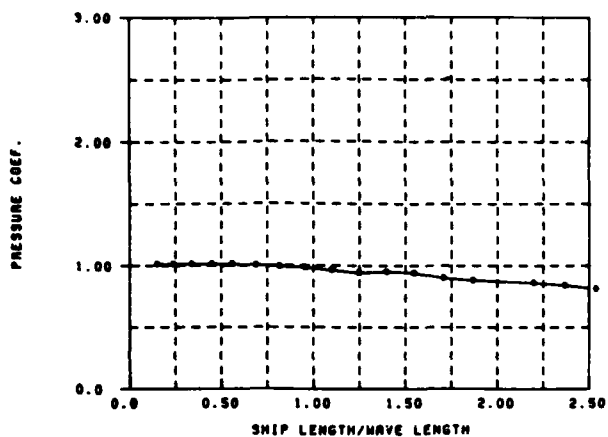


FIGURE 185: SL-7 PRESSURE RAO, FORCED HEAVE MOTION,  $F_N=0.23$ , TAP NO. 9

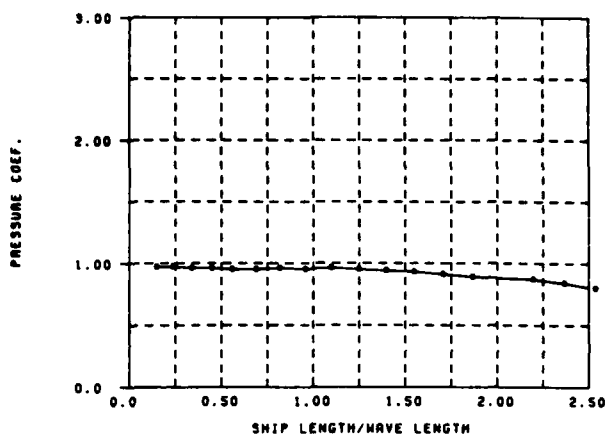


FIGURE 186: SL-7 PRESSURE RAO, FORCED HEAVE MOTION,  $F_N=0.23$ , TAP NO. 12

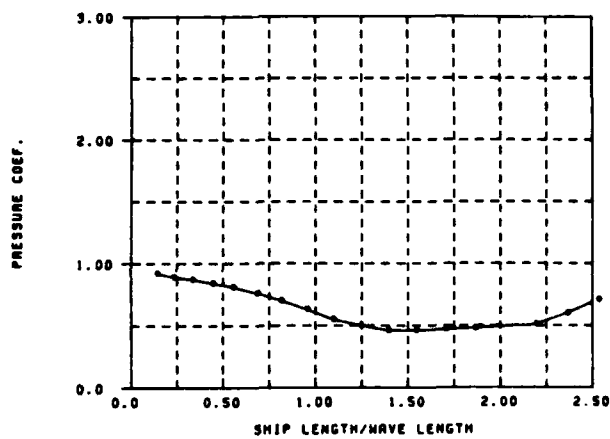


FIGURE 184: SL-7 PRESSURE RAO, FORCED HEAVE MOTION,  $F_N=0.23$ , TAP NO. 10

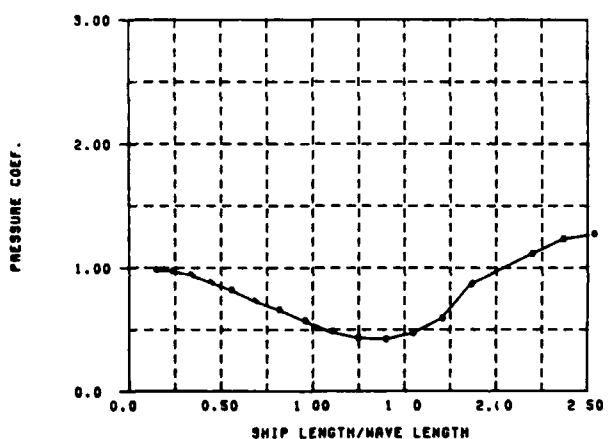


FIGURE 187: SL-7 PRESSURE RAO, FORCED HEAVE MOTION,  $F_N=0.23$ , TAP NO. 14

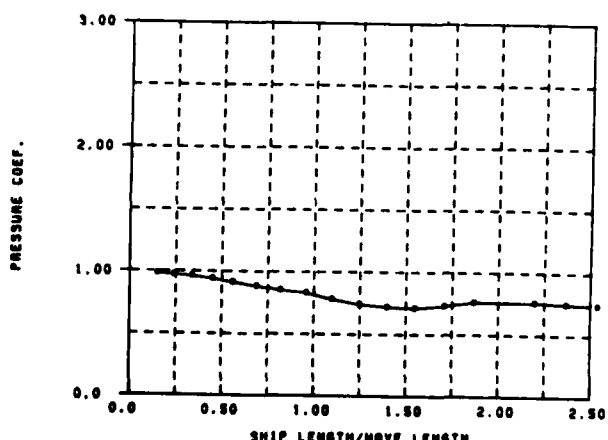


FIGURE 188: SL-7 PRESSURE RAO, FORCED HEAVE MOTION,  $F_N=0.23$ , TAP NO. 11

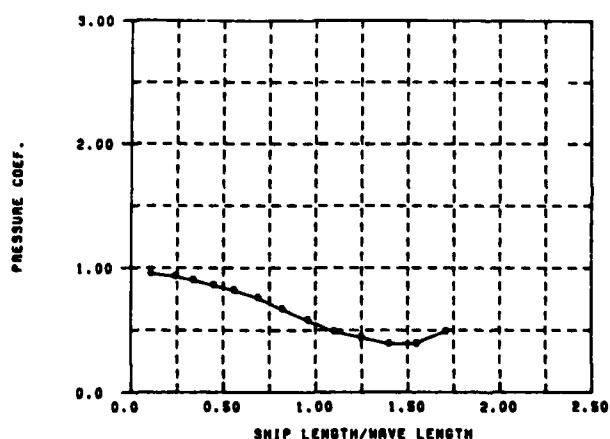


FIGURE 188: SL-7 PRESSURE RAO, FORCED HEAVE MOTION,  $F_N=0.23$ , TAP NO. 19

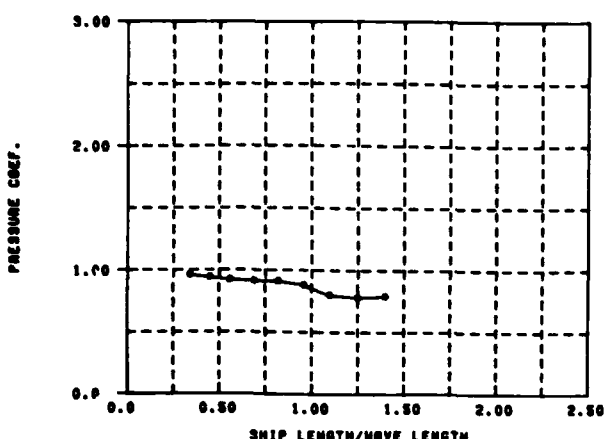


FIGURE 199: SL-7 PRESSURE RAO, FORCED PITCH MOTION,  $F_R=0.23$ , TAP NO. 1

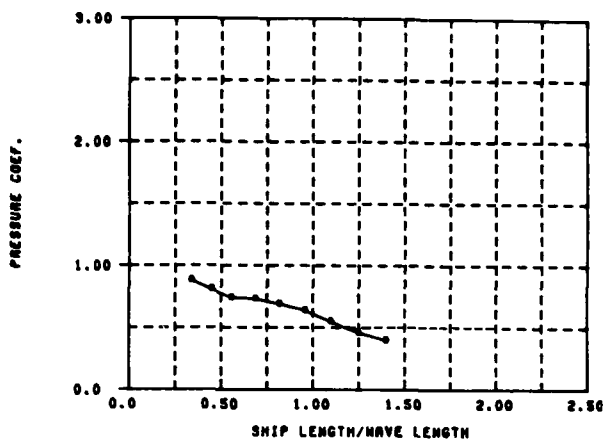


FIGURE 192: SL-7 PRESSURE RAO, FORCED PITCH MOTION,  $F_R=0.23$ , TAP NO. 4

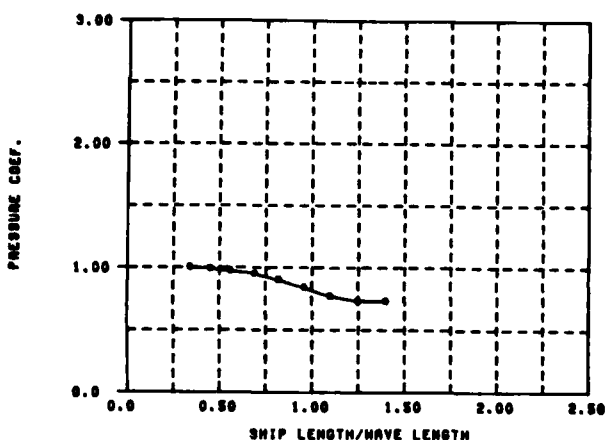


FIGURE 190: SL-7 PRESSURE RAO, FORCED PITCH MOTION,  $F_R=0.23$ , TAP NO. 2

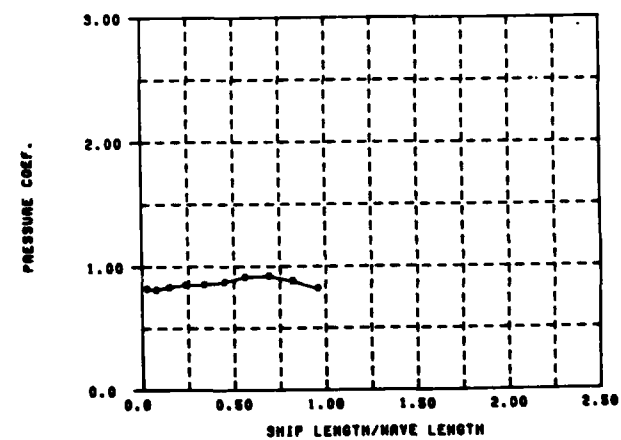


FIGURE 193: SL-7 PRESSURE RAO, FORCED PITCH MOTION,  $F_R=0.23$ , TAP NO. 6

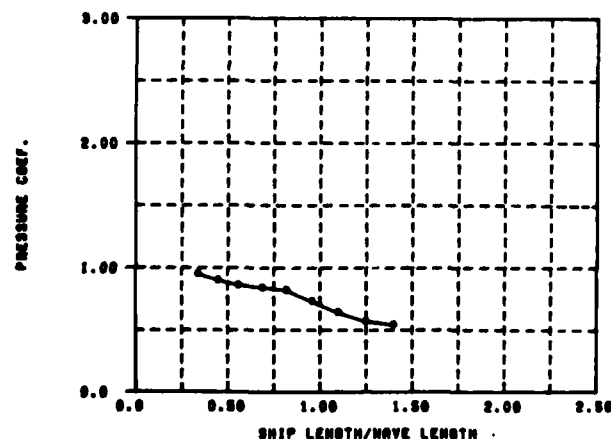


FIGURE 191: SL-7 PRESSURE RAO, FORCED PITCH MOTION,  $F_R=0.23$ , TAP NO. 5

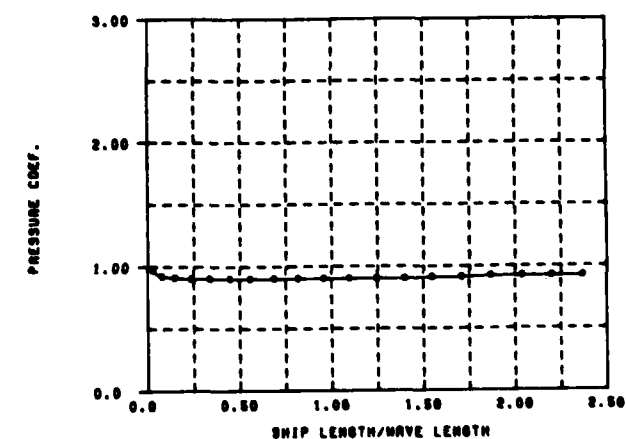


FIGURE 194: SL-7 PRESSURE RAO, FORCED PITCH MOTION,  $F_R=0.23$ , TAP NO. 7

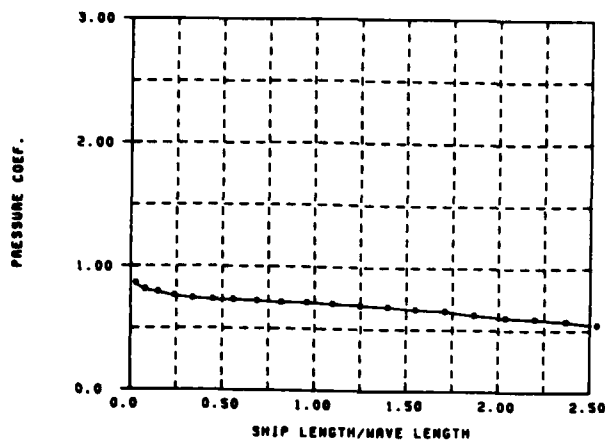


FIGURE 195: SL-7 PRESSURE RAO, FORCED PITCH MOTION,  $F_h=0.23$ , TAP NO. 9

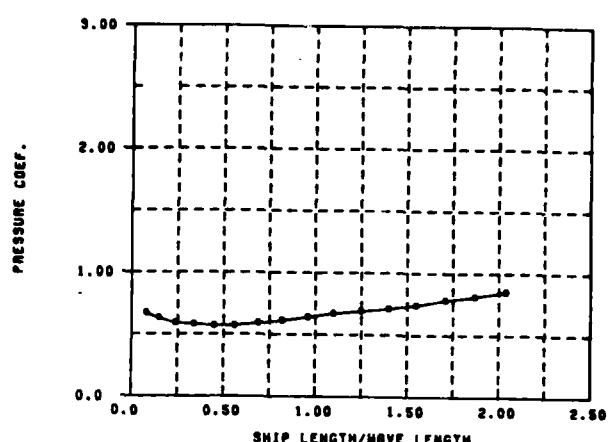


FIGURE 198: SL-7 PRESSURE RAO, FORCED PITCH MOTION,  $F_h=0.23$ , TAP NO. 14

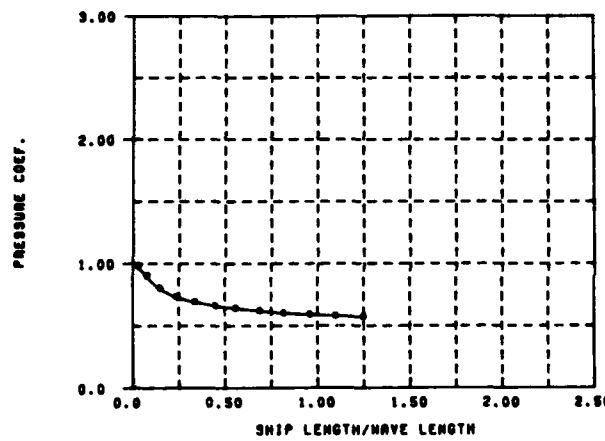


FIGURE 196: SL-7 PRESSURE RAO, FORCED PITCH MOTION,  $F_h=0.23$ , TAP NO. 11

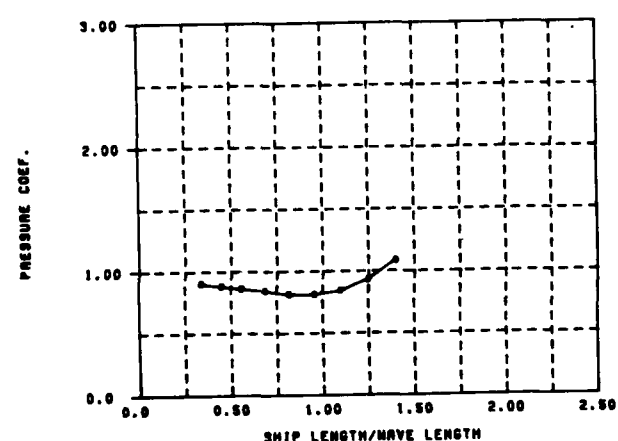


FIGURE 199: SL-7 PRESSURE RAO, FORCED PITCH MOTION,  $F_h=0.23$ , TAP NO. 19

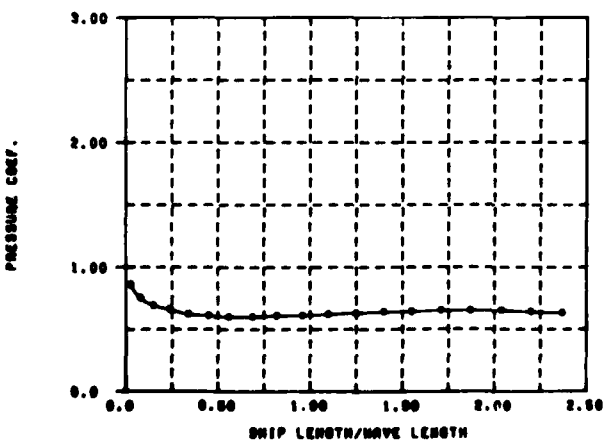


FIGURE 197: SL-7 PRESSURE RAO, FORCED PITCH MOTION,  $F_h=0.23$ , TAP NO. 12

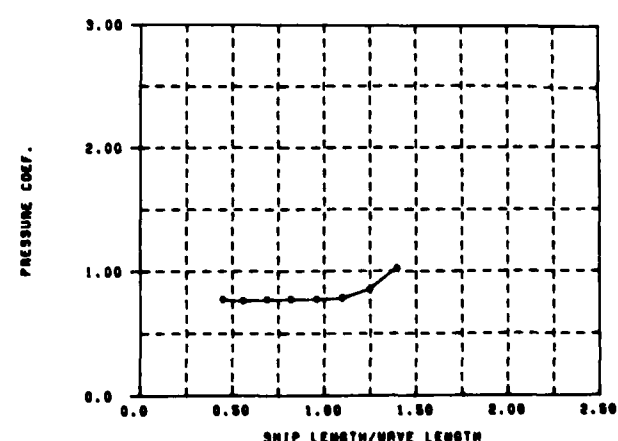


FIGURE 200: SL-7 PRESSURE RAO, FORCED PITCH MOTION,  $F_h=0.23$ , TAP NO. 21

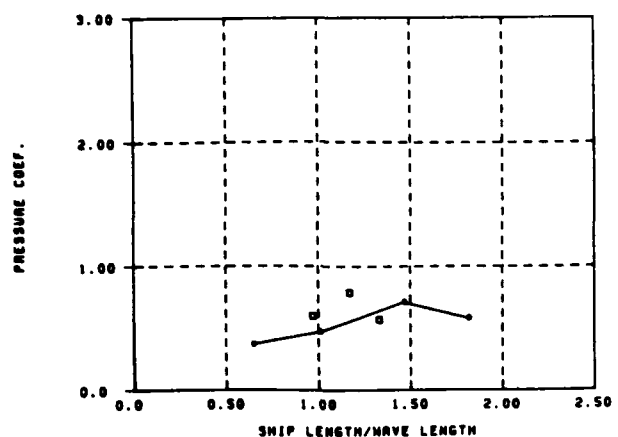


FIGURE 201: SL-7 LINEARITY CHECK, PRESSURE RAO,  $F_B=0.25$ , TAP NO. 4

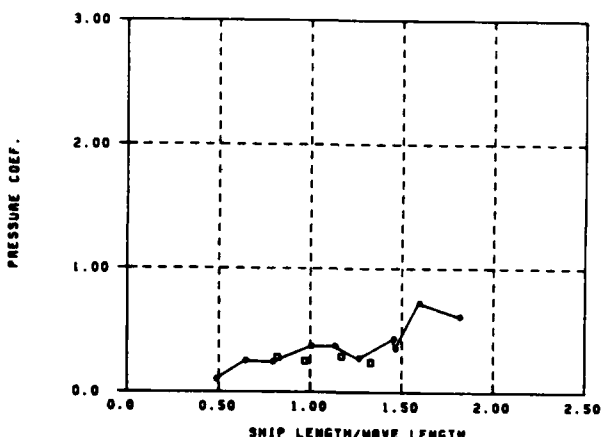


FIGURE 203: SL-7 LINEARITY CHECK, PRESSURE RAO,  $F_B=0.25$ , TAP NO. 16

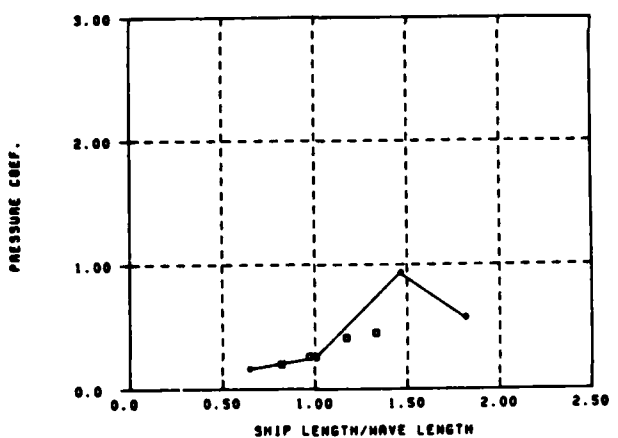


FIGURE 202: SL-7 LINEARITY CHECK, PRESSURE RAO,  $F_B=0.25$ , TAP NO. 14

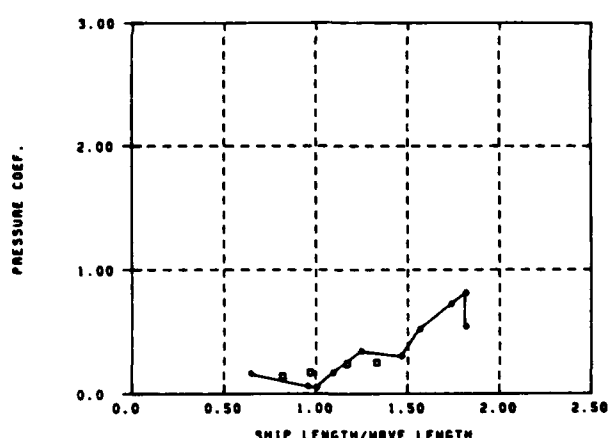


FIGURE 204: SL-7 LINEARITY CHECK, PRESSURE RAO,  $F_B=0.25$ , TAP NO. 24

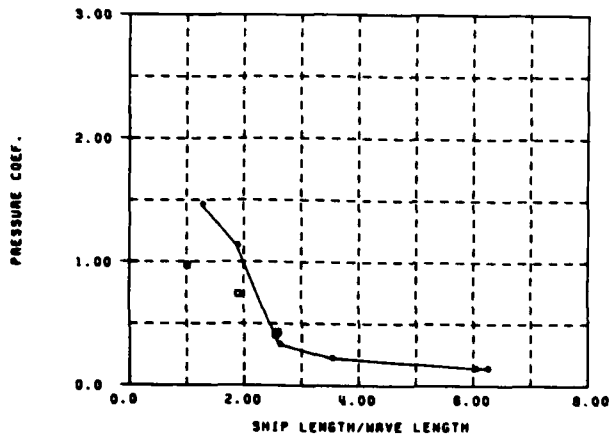


FIGURE 205: S.J. CORY LINEARITY CHECK, PRESSURE RAO,  $F_h=-132$ , TAP No. 1

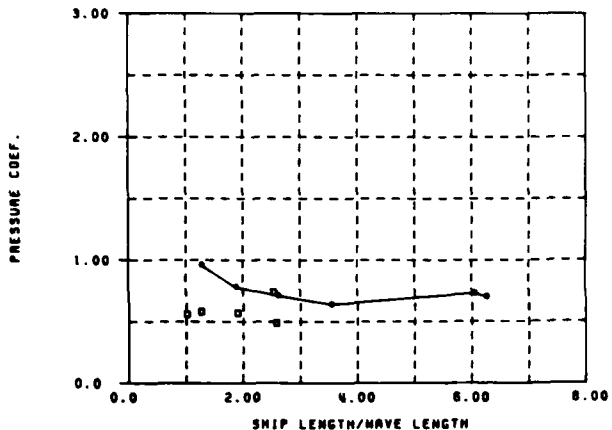


FIGURE 207: S.J. CORY LINEARITY CHECK, PRESSURE RAO,  $F_h=-132$ , TAP No. 10

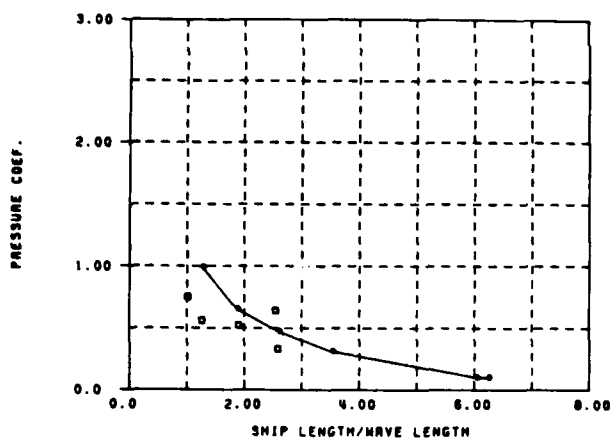


FIGURE 206: S.J. CORY LINEARITY CHECK, PRESSURE RAO,  $F_h=-132$ , TAP No. 4

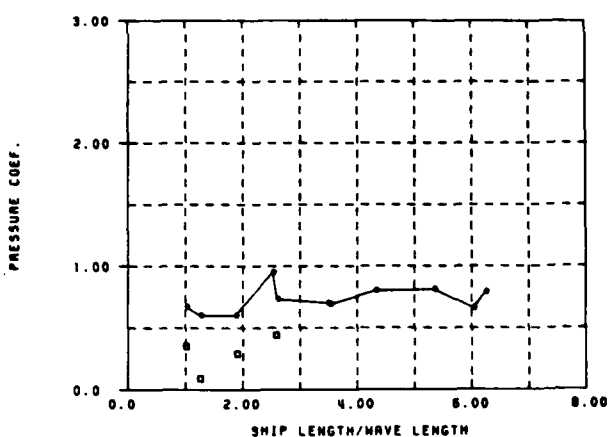


FIGURE 208: S.J. CORY LINEARITY CHECK, PRESSURE RAO,  $F_h=-132$ , TAP No. 16

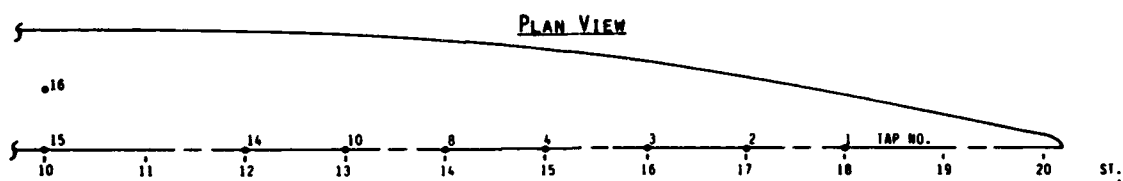
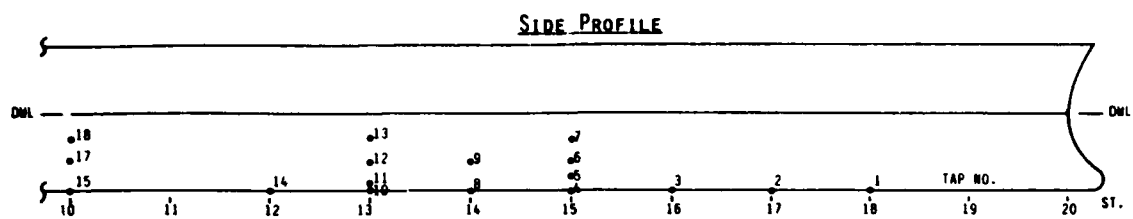


FIGURE 209: PRESSURE TAP LOCATIONS ON SL-7 (FOREBODY)

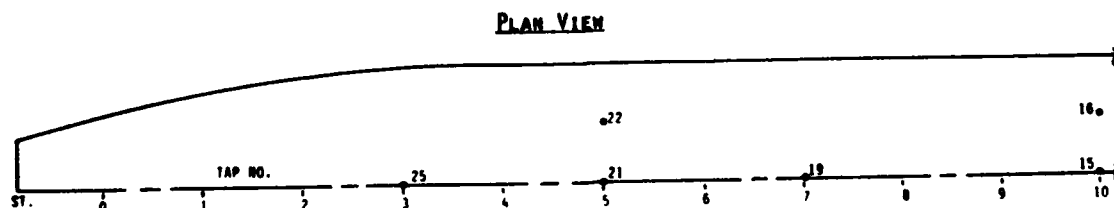
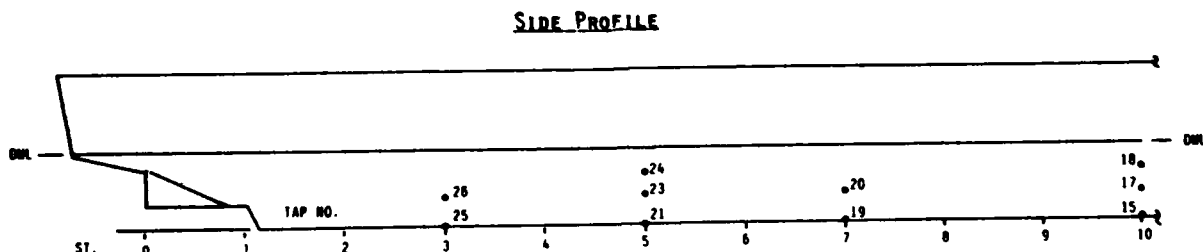
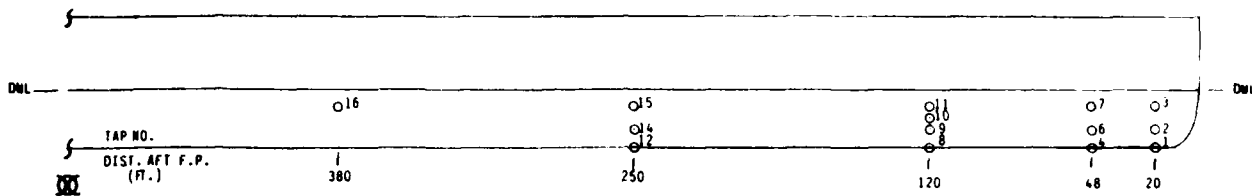


FIGURE 210: PRESSURE TAP LOCATIONS ON SL-7 (AFTERBODY)

SIDE PROFILE



PLAN VIEW

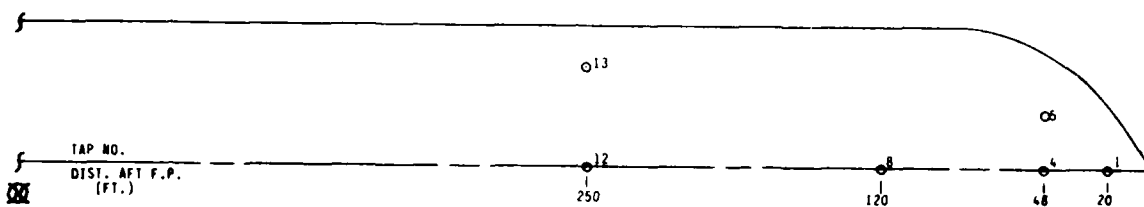
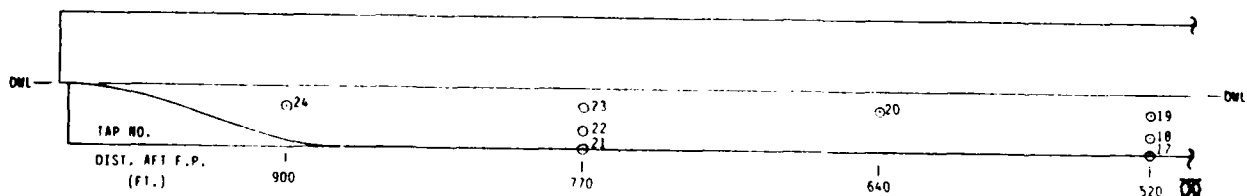


FIGURE 211: PRESSURE TAP LOCATIONS ON S.J. CORT (FOREBODY)

SIDE PROFILE



PLAN VIEW

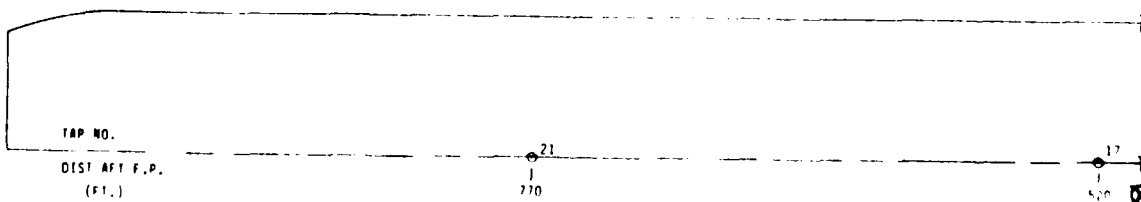


FIGURE 212: PRESSURE TAP LOCATIONS ON S.J. CORT (AFTERBODY)

SHIP RESEARCH COMMITTEE  
Maritime Transportation Research Board  
National Academy of Sciences-National Research Council

The Ship Research Committee has technical cognizance of the inter-  
agency Ship Structure Committee's research program.

John D. Hart, (BS), Chairman, Consultant, Annapolis, MD  
William H. Hsu, PhD, Dept. of Civil Engineering, Univ. of Illinois  
William A. Strommen, (BS), Research Director - Offshore Technology, Amoco  
Production Co., Tulsa, OK  
John P. Miller, (BS), Sr. Systems Analyst, National Ocean and Atmospheric Admin.,  
Rockville, MD  
John A. Sauer, (BS), Research & Technology, AMCO Inc., Middletown, OH  
John F. C. Dickey, (BS), Director of Engg., Analysis & Technology, Inc.,  
Norwalk, Connecticut, CT  
John J. Gosselink, (BS), Consultant, Quakertown, PA  
John R. Dunn, Executive Secretary, Ship Research Committee

The Ship Research Committee's Ship Design, Resistance, and Load Criteria Advisory Group pre-  
pared the specifications and reviewed the proposals for this project.

John D. Hart, Chairman, Consultant, Annapolis, MD  
William H. Hsu, Dept. of Civil Engineering, Univ. of Illinois  
William A. Strommen, Research Director - Offshore Technology, Dept. of  
Civil Engineering, Texas Tech Univ., Lubbock, TX  
John F. C. Dickey, Director of Engg., Analysis & Technology, Inc., Houston, TX  
John J. Gosselink, Consultant, Philadelphia, PA  
John R. Dunn, Executive Secretary, Ship Research Committee, Bethlehem  
Steel Corp., Sparrows Point, MD

The 1971 Ad Hoc Project Advisory Committee provided the liaison  
between the investigators and reviewed the project reports with the investigator.

John D. Hart, Chairman, Consultant, Baltimore, MD  
William H. Hsu, Vice President for Academic Affairs, State Univ. of New York  
Maritime College, Bronx, NY  
John J. Gosselink, Consultant, Quakertown, PA

END

FILED

5-84